

THE UNIVERSITY OF CALGARY

The Theoretical Simulation of Near
Infrared Atmospheric Extinction

by

Kevin Michael Volk

A THESIS

SUBMITTED TO THE FACULTY OF GRADUATE STUDIES
IN PARTIAL FULFILLMENT OF THE REQUIREMENTS FOR THE
DEGREE OF MASTER OF SCIENCE

DEPARTMENT OF PHYSICS

CALGARY, ALBERTA

SEPTEMBER, 1983

© Kevin Volk 1983

THE UNIVERSITY OF CALGARY

FACULTY OF GRADUATE STUDIES

The undersigned certify that they have read, and recommend to the Faculty of Graduate Studies for acceptance, a thesis entitled, "The Theoretical Simulation of Near Infrared Atmospheric Extinction" submitted by Kevin Michael Volk in partial fulfillment of the requirements for the degree of Master of Science.



Supervisor T.A. Clark (Physics)



S. Kwok (Physics)



R.A. Kydd (Chemistry)



E.F. Milone (Physics)

Date Oct. 6. 1983.

Abstract

The process which is used to correct infrared photometric observations for the effects of atmospheric absorption is examined in light of the work of Manduca and Bell (1979). This atmospheric extinction at J, H and K wavelengths is generally assumed to follow a linear magnitude/air mass relationship which, upon extrapolation to zero air mass should give the magnitude of the observed object as it would be measured above the atmosphere. Using a numerical simulation of atmospheric absorption, Manduca and Bell demonstrated that this procedure leads to significant errors in the zero point magnitude. In view of the importance of this result to infrared astronomical observations, this approach was repeated, with some small variations in technique, in this thesis, and subsequently extended to a multiple layer approximation to the atmosphere rather than the single layer approach of Manduca and Bell.

Calculations were carried out for 3 infrared observing sites in addition to Calgary-Mauna Kea, Hawaii (4.20 km), Mount Lemmon, Arizona (2.79 km) and Kitt Peak National Observatory, Arizona (2.06 km). The majority of the calculations were performed for Kitt Peak, over a range of H₂O column density values

since it was expected that the results would be sensitive to this factor. The qualitative features of the present results are the same as for those of Manduca and Bell; the magnitude/air mass relation shows little curvature over the observable range of air mass, yet the extrapolated zero point values have large systematic errors with these being greatest for the J filter and smallest for the K filter. The atmospheric extinction is shown to have a slight dependence upon the type of object which is observed. The single layer and multiple layer calculations carried out here predict significantly less atmospheric extinction than the analogous Manduca and Bell calculations. Possible sources of systematic error are examined and it is concluded that the discrepancy is mainly due to improvement in the standard filters.

An attempt was made to analyse the magnitude/air mass relation based upon the expected air mass dependence of the major sources of atmospheric extinction. Although the errors in the zero point magnitudes are substantially reduced, they are not eliminated. The alternative, calculating those zero point errors for each site as a function of H_2O column density, is difficult to carry out. It is concluded that at present there is no simple and accurate method of correcting for atmospheric extinction.

Acknowledgements

Like all of the works of men, this thesis is not solely the result of one person's work. I would like to briefly thank the following individuals and organizations for their contributions to the project which resulted in this thesis or to producing this thesis. Without this assistance the thesis would still be far from completion.

First and foremost my thanks goes to Dr. T.A. Clark, my supervisor, for his invaluable advice and assistance during every phase of the work which underlies this thesis. His efforts to obtain time at Mount Lemmon Observatory and at Kitt Peak National Observatory in order to experimentally test the results presented here, although in the event poor weather prevented any useful data from being obtained, are also much appreciated.

My thanks also go to Rita Boreiko for her help in dealing with the computer system and for providing me with the spectral synthesis program used in the project, thereby saving me endless hours of frustration; to the Natural Science and Engineering Research Council for financial support over the period in which this work was done; and to Wendy Amero for typing this thesis.

Table of Contents

Title Page	i
Approval Sheet	ii
Abstract	iii
Acknowledgements	v
Table of Contents	vi
List of Tables	vii
List of Figures	ix
Chapter One - Introduction and Basic Theory	1
Chapter Two - Survey of the Results of Manduca and Bell (1979)	29
Chapter Three - The Curtis-Godson Approximation	59
Chapter Four - The Single Layer Model Calculations	77
Chapter Five - The Multiple Layer Model Calculations	106
Chapter Six - Conclusions	151
List of References	178

List of Tables

Table		
1	Summary of the Manduca and Bell (1979) results for the Johnson JKL and KPNO JHK filters.	51
2	Narrow-band filter results from Manduca and Bell (1979).	54
3	Results of the single layer Kitt Peak summer calculations.	92
4	Description of the atmospheric layers for the multiple layer model.	110
5	Linear segment fit for the mean USSA H ₂ O mass mixing ratio.	113
6	Layer by layer H ₂ O column density values.	117
7	Final H ₂ O parameters for the atmospheric layers in the multiple layer model.	122
8	Linear segment fit to the USSA mean O ₃ abundance profile.	124
9	O ₃ parameters for the atmospheric layers in the multiple layer model.	129
10	Normal (sea-level) dry air composition from USSA (1976).	130
11	Column density values, in cm ⁻² , for the uniformly mixed molecules.	130
12	Pressure and temperature parameters for the uniformly mixed molecules.	131
13	Multiple layer model results for the four sites.	133
14	Aerosol extinction values for subtraction from the extinction curves.	154
15	Square-root law zero point errors, using the aerosol correction.	155

16	Square-root law zero point errors, in magnitudes, for the multiple layer models when the aerosol correction is ignored.	162
----	---	-----

List of Figures

Figure 1	A typical atmospheric transmittance profile.	4
2	Demonstration of scaling in a plane-parallel atmosphere.	12
3	Extinction curves for "Kitt Peak" summer from Manduca and Bell (1979).	49
4a	The extinction between $X = 1.00$ and $X = 2.00$ plotted against the extinction between $X = 0.00$ and $X = 1.00$ for the Manduca and Bell (1979) Kitt Peak calculations.	55
4b	The extinction between $X = 1.00$ and $X = 2.00$ plotted against the extinction between $X = 0.00$ and $X = 1.00$ for the Manduca and Bell (1979) Mauna Kea calculations.	56
5	The filter response profile as a function of wavelength for the new (post 1979) Kitt Peak J filter (Joyce, 1982).	87
6	The filter response profile as a function of wavelength for the new (post 1979) Kitt Peak H filter (Joyce, 1982).	88
7	The filter response profile as a function of wavelength for the new (post 1979) Kitt Peak K filter (Joyce, 1982).	89
8a	Single layer results for Kitt Peak. H_2O column density - 2.50 PMM.	93
8b	Single layer results for Kitt Peak. H_2O column density - 2.50 PMM.	94
8c	Single layer results for Kitt Peak. H_2O column density - 5.05 PMM.	95
8d	Single layer results for Kitt Peak. H_2O column density - 5.05 PMM.	96
8e	Single layer results for Kitt Peak. H_2O column density - 7.54 PMM.	97

8f	Single layer results for Kitt Peak. H ₂ O column density - 7.54 PMM.	98
8g	Single layer results for Kitt Peak. H ₂ O column density - 10.1 PMM.	99
8h	Single layer results for Kitt Peak. H ₂ O column density - 10.1 PMM.	100
9	Comparison of the cool giant results of Manduca and Bell (1979) with the equivalent 4000 K model results for Kitt Peak summer.	101
10	The mean mid-latitude water vapour mass mixing ratio as a function of altitude.	114
11	The water vapour mass mixing ratio as a function of pressure.	116
12	The mean mid-latitude ozone mass mixing ratio as a function of altitude.	123
13	C(P) and PC(P) as a function of pressure for ozone in layer 8.	125
14a	Multiple layer results for Mauna Kea.	134
14b	Multiple layer results for Mauna Kea.	135
14c	Multiple layer results for Mount Lemmon.	136
14d	Multiple layer results for Mount Lemmon.	137
14e	Multiple layer results for Kitt Peak.	138
14f	Multiple layer results for Kitt Peak.	139
14g	Multiple layer results for Calgary.	140
14h	Multiple layer results for Calgary.	141
15	The magnitude difference as a function of air mass.	143
16	Plot of E against $\Delta + E$ for the J filter results.	148
17	Plot of E against $\Delta + E$ for the H and K filter results.	149
18	Comparison of the theoretical extinction curve with observational data for the J filter.	166

19	Comparison of the theoretical extinction curve with observational data for the H filter.	167
20	Comparison of the theoretical extinction curve with observational data for the K filter.	168

Chapter One

Introduction and Basic Theory

Medium-band photometry, which may be defined as photometry done with filters for which the ratio of the filter width $\Delta\lambda$ to the filter center wavelength λ is of the order of 0.2, is of tremendous importance to modern astronomy. In the wavelength range from the visible to the far infrared such medium-band photometry [hereafter simply "photometry" unless otherwise noted] is perhaps the most common technique used in stellar astronomy. The key role played by such photometry is somewhat surprising when it is remembered that modern photometry is just over 30 years old. The UBV filter system which is standard for visible observations was established in the early 1950's, while the extension to longer wavelengths came later.

Infrared photometry in the $1\mu\text{m}$ to $3\mu\text{m}$ wavelength range, known as the near infrared, will be of primary concern here. In many ways the establishment of photometry in the near infrared was simply a direct adaptation of the techniques which had been developed to deal with the UBV filters. Over the past few years it has become apparent that several incorrect assumptions were made in this process, leading to errors which must be corrected. These errors arise because of certain fundamental differences in the

physical processes at work in the infrared as compared with the visible wavelengths. In this first chapter the data reduction methods which are used in photometry, both in the visible wavelengths and in the near infrared, will be described and the resulting problems encountered in the near infrared will be considered.

In moving to the near infrared region of the spectrum a problem appears which has no direct counterpart in visible photometry; there is thermal radiation from objects at ordinary temperatures. The very air is always a bright source of infrared radiation. It is as if visible observations were made by day, and had to contend with the brightness of the sky. To be able to make observations in spite of this sky background required the development of methods which could overcome this problem.

Johnson (1962) was the first to report modern style photometry in the infrared wavelengths. To remove the sky background flux it was arranged that the secondary telescope mirror would rock slightly at a fairly high frequency. In one position the telescope was looking at the object of interest, while in a second position an "empty" sky comparison field was in view. Using appropriate electronics, the outputs from these two fields of view were subtracted to remove the sky background flux. This process allows a signal to

background ratio of 10^{-4} to 10^{-6} to be overcome. Subsequently some refinements were made in this "chopping" process, but the basic idea remains the same.

Another innovation was the cooling of the detector to 77 K, using a liquid N₂ cooling system. This served to reduce the infrared background from surfaces within the photometer itself, and also increased the detector sensitivity by reducing the thermal "shot" noise inherent in all semiconductor detectors. Slight changes in telescope design served to ensure that the superstructure of the telescope did not contribute significantly to the background radiation.

Johnson established a series of infrared filters for use in the near to middle infrared. These filters were assigned letter designations in order of wavelength, starting with the J filter at $1.25\mu\text{m}$. The set of filters was eventually extended out to the N filter at $10.2\mu\text{m}$. Setting up these filters was more difficult than at visible wavelengths because of the nature of infrared atmospheric absorption. A typical near infrared absorption profile is given in Figure 1. There are areas of good transmittance interspaced with areas of strong line absorption. The filters must be carefully made to fit the relatively transparent areas, called atmospheric windows. The lines are due to molecular vibrational and rotational transitions. Also shown in Figure 1 are the filter profiles for the

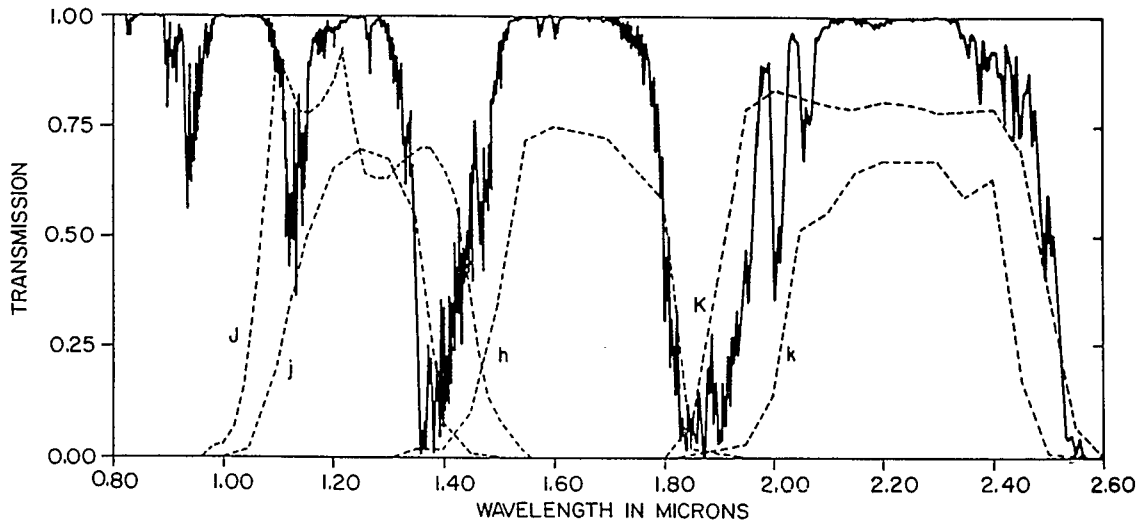


Figure 1- A typical atmospheric transmission profile plotted as a function of wavelength. The filter response functions for the original Johnson J and K filters (Johnson, 1965c) as well as the Kitt Peak J, H and K filters which were used prior to 1979 [denoted as j, h and k] are plotted.

From Manduca and Bell (1979).

Johnson J and K filters and it can be seen that these filters overlap areas of strong absorption at $1.40\mu\text{m}$ and beyond $2.00\mu\text{m}$. This led to the adoption of a second set of filters which were narrower. The newer J and K filters, which were used at Kitt Peak National Observatory from the early 1970's until 1979, are also illustrated in Figure 1.

The original Johnson filter set did not take advantage of the atmospheric window around $1.55\mu\text{m}$ to $1.80\mu\text{m}$. In the late 1960's a new filter was introduced to fit this atmospheric window, by a California Institute of Technology group (Becklin and Neugebauer, 1968). This filter became known as the H filter. The Kitt Peak H filter which was used until 1979 is also illustrated in Figure 1.

In 1979 a new set of JHK filters were adopted at Kitt Peak and several other observatories as part of a bulk purchase from the manufacturers. This served to standardize the filters and also to further tighten the filter bandpasses. The latest filters will be taken as standard here. The filter profiles for these JHK filters are given in Figures 5 to 7, in Chapter 4. There are also various independent filter sets developed by different infrared astronomy groups, which hampers standardization. The alternate systems are slowly being abandoned and replaced by the JHK filter sequence; even so, it will be some time before

reasonable standardization of infrared filters is achieved.

The fundamental quantity which is measured by photometry is the absolute radiation flux of an object as a function of wavelength. In order to relate the measured object magnitudes to the absolute radiation flux, a three step process is required:

- 1) the observed magnitudes must be corrected for the effects of atmospheric absorption along the line of sight (the atmospheric extinction correction);

- 2) the observed magnitudes must be corrected for any discrepancies in the filter response or the photometer response compared to the standards, or any other systematic instrumental effects. In particular, the photometer sensitivity often fluctuates slowly over time. This step is known as the transformation to the standard system;

- 3) the "standard" magnitudes which have been corrected for atmospheric effects must be related to the absolute radiative flux at particular wavelengths. This turns out to require assumptions about the nature of the object's spectrum.

In what follows step (2) will be ignored, as it would be extremely difficult to carry out in a numerical simulation. This is normally done by observing a number of bright stars which have been carefully observed with the standard equipment and

assigned standard magnitude values. These standard stars are then used to match up the magnitudes from any particular telescope to the standard magnitudes. To do this for a numerical simulation would require knowledge of the absolute radiative flux of a set of these stars so that simulated magnitudes could be produced for them. This data is simply not available. The only available infrared data which was taken outside the atmosphere is from rocket-borne instruments - the AFGL infrared sky survey (Kleinman, et. al., 1979). This data is not suitable because it starts at $4.2\mu\text{m}$, which is too far into the infrared to be useful here, and because the accuracy is only $\pm 10\%$ in absolute flux values. The new IRAS satellite will yield better data, but this data will still be too far in the infrared to apply to the JHK filters.

It is odd, in view of the importance of the extinction corrections in the reduction of photometric data, that the extinction problem is rarely the subject of overt discussion in the literature of astronomy; this applies to both the theoretical justification of the methods used to make extinction corrections and the correction methods themselves. The best general discussion of the extinction and transformation methods for data reduction is Hardie (1962), while as far as the author is aware there is no available paper which gives the justification of the empirical approach used

by Hardie or discusses the limitations of this approach. This lack of information is rather unfortunate because it can easily lead to the application of the extinction corrections in circumstances in which systematic errors result from their use.

The theoretical development of the extinction law starts from the monochromatic case. Let $I_\lambda d\lambda$ be the incident radiative flux between λ and $\lambda + d\lambda$. For a ray of radiation incident upon some absorbing material

$$\frac{dI_\lambda}{dx} = -k_\lambda I_\lambda \quad (1.1)$$

where k_λ is the absorption coefficient at wavelength λ and x is a measure of the thickness of absorbing material. This equation holds when I_λ is small enough that non-linear absorption effects do not arise and the radiation from the material can be neglected. In astronomy I_λ is always far below the threshold for non-linear effects, and reradiation is generally negligible. The infrared sky background is not of concern because it is assumed to be removed by the chopping.

Equation (1) may be re-arranged slightly to

$$\frac{1}{I_\lambda} \frac{dI_\lambda}{dx} = -k_\lambda \quad (1.2)$$

which can then be integrated with respect to x . The x integral takes place over the ray path from some $x = 0$ where the absorption commences, to $x = x_0$ where, it is

assumed, the radiation is measured. the integration is

$$\int_0^{x_0} \frac{1}{I_\lambda} \frac{dI_\lambda}{dx} dx = - \int_0^{x_0} k_\lambda dx \quad (1.3)$$

k_λ is a function of x because it depends upon the state of the absorbing material.

Defining a mean absorption coefficient for the path

$$\bar{k}_\lambda = \frac{\int_0^{x_0} k_\lambda(x) dx}{\int_0^{x_0} dx} = \frac{1}{x_0} \int_0^{x_0} k_\lambda(x) dx \quad (1.4)$$

equation (1.3) becomes

$$\ln(I_\lambda(x_0)) - \ln(I_\lambda(0)) = - \bar{k}_\lambda x_0 \quad (1.5)$$

Exponentiation gives the familiar form

$$I_\lambda(x_0) = I_\lambda(0) e^{-\bar{k}_\lambda x_0} \quad (1.6)$$

This equation is sometimes known as Beer's law. Under the assumptions noted above it applies to any path, any medium, any type of absorption and any wavelength.

The monochromatic magnitude corresponding to I_λ is defined by

$$m_\lambda = -2.5 \log_{10}(I_\lambda/I_{\lambda_0}) \quad (1.7a)$$

or, equivalently,

$$m_\lambda = - \frac{2.5}{\ln(10)} \ln(I_\lambda) + C_\lambda \quad (1.7b)$$

where I_{λ_0} and C_λ are arbitrary constants which set the zero point of the magnitude scale. Using equation (1.7 b) in equation (1.5) gives the magnitude extinction law

$$m_{\lambda}(x_0) = m_{\lambda}(0) + \frac{2.5}{\ln(10)} \bar{k}_{\lambda} x_0 \quad (1.8)$$

This equation is not very useful as it stands, because measuring m_{λ} at various x values does not allow $m_{\lambda}(0)$ to be found. If, however, k_{λ} is the same for two paths, one of length x_0 and one of length Xx_0 where X is known, then

$$m_{\lambda}(Xx_0) = m_{\lambda}(0) + \left[\frac{2.5}{\ln(10)} x_0 \bar{k}_{\lambda} \right] X$$

$$m_{\lambda}(x_0) = m_{\lambda}(0) + \left[\frac{2.5}{\ln(10)} x_0 \bar{k}_{\lambda} \right] \quad (1.9)$$

so knowing X , $m_{\lambda}(x_0)$ and $m_{\lambda}(Xx_0)$ gives $m_{\lambda}(0)$. If a series of paths have the same \bar{k}_{λ} , the result is a linear magnitude/path length relation. The problem is to find a situation in which \bar{k}_{λ} is the same for different paths.

One obvious case in which \bar{k}_{λ} is the same for different paths is when the absorbing medium is homogeneous. In this case k_{λ} is not a function of x and applies to any path through the material. This is often useful for measuring k_{λ} , but it does not apply to the atmosphere. Another case in which \bar{k}_{λ} is the same for different paths is when the paths differ only in an overall scale factor. If for a path $0 \leq Y \leq Y_0$ and a path $0 \leq x \leq x_0$ conditions are such that $k_{\lambda}(y) = k_{\lambda}(x)$ for $Y = \frac{Y_0}{x_0} x$ the \bar{k}_{λ} values will be the same.

As is illustrated in Figure 2, all the paths through a horizontally stratified plane parallel

atmosphere differ from the zenith path only by a scale factor of $\sec\theta$, when refraction is ignored, where θ is the zenith angle. The real atmosphere has a slight curvature, which precludes the scaling; this curvature is small enough compared to the thickness of the atmosphere that the use of a scale factor introduces only a very small error, so all atmospheric paths are described by their length ratio to the zenith path. This ratio is denoted as the air mass, and is generally symbolized as X . X is a function of θ only, but is slightly more complicated than $\sec\theta$. A useful formula is

$$X = \sec\theta(1.0012 - 0.0012 \sec^2\theta) \quad (1.10)$$

which applies out to $X \approx 3$ (Young, 1974). Using this X equations (1.9) may be summed up as

$$m_\lambda(X) = m_\lambda(0) + K_\lambda X \quad (1.11)$$

where

$$K_\lambda = \frac{2.5}{\ln(10)} \bar{k}_\lambda x_0 \quad (1.12)$$

The assumption of a horizontally stratified atmosphere is not strictly true. However, considering that most of the weather occurs in the troposphere, up to roughly 10 km above sea level, and that horizontal changes in the weather occur over scales of hundreds of kilometers this assumption is more realistic than it appears. Under good observing conditions this

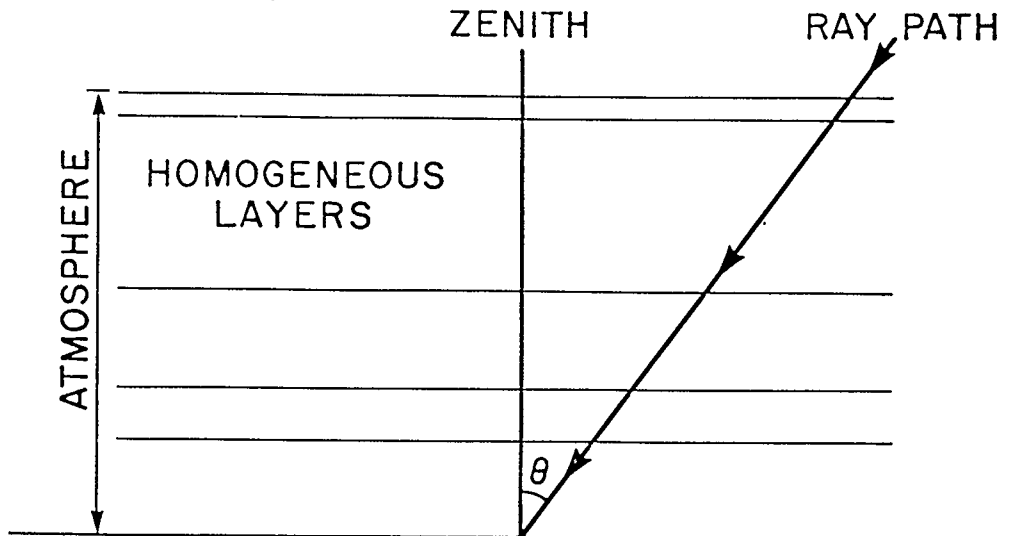


Figure 2- In a plane parallel atmosphere made up of a set of homogeneous horizontal layers, the ray path through the atmosphere at an angle θ to the zenith differs from the zenith path by a scale factor of $\sec\theta$. For a given total atmospheric thickness this relation holds as the number of layers becomes very large, and hence it holds for an arbitrary horizontally stratified atmosphere. This ignores the slight refraction of rays as they pass through the atmosphere.

assumption is well warranted. When the horizontal stratification assumption breaks down this produces variable extinction over regions of the sky, which is generally apparent to the observer. Weather fronts are also of concern as they represent a relatively rapid transition between very different conditions.

So far only monochromatic radiation has been considered. Once a filter of finite width is introduced, the problem becomes much more complex. Let $\phi(\lambda)$ be a function which describes the filter transmittance as a function of wavelength. The measured quantity is no longer I_λ but I , where

$$I = \int_0^{\infty} \phi(\lambda) I_\lambda d\lambda \quad (1.13)$$

Consider some particular point in the atmosphere, where I is being measured. Equation (1.1) applies at each wavelength, so it can be multiplied by $\phi(\lambda)$ and then integrated over all λ .

$$\int_0^{\infty} \frac{dI_\lambda}{dx} \phi(\lambda) d\lambda = - \int_0^{\infty} k_\lambda I_\lambda \phi(\lambda) d\lambda \quad (1.14)$$

$$\frac{d}{dx} \left[\int_0^{\infty} I_\lambda(x) \phi(\lambda) d\lambda \right] = - \int_0^{\infty} k_\lambda(x) I_\lambda(x) \phi(\lambda) d\lambda \quad (1.15)$$

Defining a new k by the relation

$$\bar{k} = \frac{\int_0^{\infty} k_{\lambda}(x) I_{\lambda}(x) \phi(\lambda) d\lambda}{\int_0^{\infty} I_{\lambda}(x) \phi(\lambda) d\lambda} \quad (1.16)$$

equation (1.15) becomes

$$\frac{dI}{dx} = -\bar{k}x \quad (1.17)$$

It must be stressed that \bar{k} is quite different than the \bar{k}_{λ} which appeared in the monochromatic case. \bar{k} is a weighted wavelength average, which depends upon $\phi(\lambda)$ and I_{λ} , rather than an average of k_{λ} along a ray path at a specific wavelength. In the formal sense equation (1.17) is much like equation (1.1), so with

$$\bar{k} = \frac{1}{x_0} \int_0^{x_0} \bar{k}(x) dx \quad (1.18)$$

there follows a Beer's law type of result

$$I(x_0) = I(0) e^{-\bar{k}x_0} \quad (1.19)$$

If a filter magnitude is defined in terms of I the result is

$$m(x_0) = m(0) + \frac{2.5}{\ln(10)} \bar{k} x_0 \quad (1.20)$$

and once again the problem is to find conditions in which k is common to a series of paths.

In all this the distinction between \bar{k} and \bar{k}_{λ} must be kept in mind. Writing out \bar{k} explicitly,

$$\bar{k} = \int_0^{x_0} \frac{\int_0^{\infty} k_{\lambda}(x) I_{\lambda}(x) \phi(\lambda) d\lambda}{\int_0^{\infty} I_{\lambda}(x) \phi(\lambda) d\lambda} dx \quad (1.21)$$

several features can be seen. \bar{k} is a function of I_{λ} , so it will depend somewhat upon the spectrum of the object under consideration. Also, whereas \bar{k}_{λ} was obtained by integrating a state function along a path the \bar{k} quantity which is integrated to give \bar{k} is not a state function. \bar{k} is dependent upon the entire previous path to point x because $I_{\lambda}(x)$ depends upon the whole path to point x . This is equivalent to saying that \bar{k} is a function of the column density so even for a homogeneous layer \bar{k} is path dependent.

Under these circumstances, even with a horizontally stratified atmosphere, the linear magnitude/air mass relation will apply only when \bar{k} is linear with column density. This is made clear by recasting the linear extinction law in the following form: the change in absorption which is observed when θ is increased so X changes by 1.00 is the same as the change in absorption which occurs over a path through the atmosphere at the zenith. If the extinction is proportional to the column density, as is the case for Rayleigh scattering by molecules for example, the magnitude/air mass relation will be linear, subject to the assumptions discussed above.

In the visible wavelengths the main sources of extinction are molecular Rayleigh scattering and aerosol particle scattering. The Rayleigh scattering is dominant under clear sky conditions, and is well known to be the cause of the daytime blue sky. It is proportional to the total molecular column density. The aerosols scatter by a much more complicated process and they show considerable temporal and geographical variation. Even so, if the aerosols are horizontally stratified and no intermittent sources of aerosol are present near the site of observation this contribution to the extinction will give the same type of linear extinction law. The slope may vary from night to night due to fluctuations in the aerosol population. Thus the UVB filters show a linear magnitude/air mass relation and can easily be corrected for atmospheric extinction.

The general method of dealing with extinction which is described in Hardie (1962) and is known as the Hardie method may now be outlined. Assume that a series of magnitudes m_i form a photometric system. From pairs of magnitude values a set of colour indices $C_{ij} \equiv m_i - m_j$ are derived. As found above, it is assumed that

$$m_i(X) = m_i(0) + k_i X \quad (1.22)$$

which implies that

$$C_{ij}(X) = C_{ij}(0) + k_{cij} X \quad (1.23)$$

The k 's will depend upon the spectral characteristics of the source. In the Hardie method one particular colour index C_{kl} is used to parameterize this dependence; further, the basic dependence is assumed to be linear. Thus,

$$\begin{aligned} k_i &= k'_i + C_{kl} k''_i \\ k_{cij} &= k'_{cij} + C_{kl} k''_{cij} \end{aligned} \quad (1.24)$$

The k' values are called the primary extinction coefficients, and the k'' values are called the secondary extinction coefficients.

The Hardie method proceeds in the following way. First, pairs of stars with very different C_{kl} values but nearly the same X values are observed. Forming difference equations

$$\begin{aligned} \Delta m_i(X) &= \Delta m_i(0) + k''_i X \Delta C_{kl} \\ \Delta C_{ij}(X) &= \Delta C_{ij}(0) + k''_{cij} X \Delta C_{kl} \end{aligned} \quad (1.25)$$

the $\Delta m_i(0)$ and $\Delta C_{ij}(0)$ values are assumed from the standard magnitude system so that the secondary extinction coefficients can be found. Once that is done, the same data can be used to solve for the primary extinction coefficients using

$$\begin{aligned} m_i(X) - C_{kl} X k''_i &= m_i(0) + k'_i X \\ C_{ij}(X) - C_{kl} X k''_{cij} &= C_{ij}(0) + k'_{cij} X \end{aligned} \quad (1.26)$$

The solution process can be made iterative if desired. Usually least squares fits are used to derive the coefficients.

Once the photometric system is established, this

approach is designed to obtain the extinction coefficients relatively quickly. This is why the $m_i(0)$ values are assumed to be known. When a system is just being set up this method cannot be used. Instead, observations of standard stars must be made under stable atmospheric conditions in order to obtain good $m_i(0)$ values for later use.

Experience with the UBV extinction coefficients shows that the k'' values are nearly constant over a single night, but that the k' values can show short term fluctuations. As a result, the usual approach is to observe star pairs at the beginning of the night and then observe individual stars at regular intervals to check the k' values. At the end of the night more star pairs can be observed to check the k'' values.

The main problem with this method, aside from the question of the validity of the linear extinction law, is the assumption that k is linear in $C_{k\lambda}$. This must be checked by plotting the fit residuals as a function of $C_{k\lambda}$, in order that any systematic trends can be found. For the UBV filter set, the B-V colour index is chosen as the parameterization variable and it is found that k_{U-B} is non-linear in B-V. This causes problems with the $(U-B)_0$ colours, so it is difficult to reproduce the standard U-B colours. Various papers discuss this problem, and propose some sort of semi-empirical correction method. For further discussion see Gutierrez-Moreno, Moreno and Cortes (1981).

In the past decade, a few papers have proposed alternate data reduction methods, generally making more use of computers (Young, 1974; Harris, Fitzgerald and Reed, 1981). These approaches have not yet been accepted by astronomers in general so they will not be dealt with here.

Before considering the specific problems that result from using the Hardie method for the infrared filter system, some comments should be made about the absolute calibration of photometric systems. This requires finding the equivalent to $I_{\lambda 0}$ in equation (1.7a) for each filter in the system. The magnitude zero points, equivalent to C_{λ} in equation (1.7b), are related to the I_0 values but unless the detector system has been very carefully calibrated these values by themselves do not allow the I_0 values to be found.

The absolute calibration may be considered as occurring in two steps. The relative values of the zero points can be set by assuming colour values for a known type of object spectrum. This will hold independent of the overall intensity calibration. The relative zero points are chosen so that a particular type of star has colour indices equal to 0.00, which ensures that most types of stars and other objects will have reasonable colour values. As well, the zero points for the UBV set of filters are constrained by the desire that the V magnitudes should match the old

style photographic magnitudes fairly closely.

For many years the relative zero points were set by assuming that an average A0V star has the same magnitude in all the filters, and that such a star radiates as a 10 000 K blackbody. The two assumptions allow the magnitude systems to be set up, and are sufficient to allow both effective temperatures and bolometric corrections to be deduced. The A0V stars were chosen because they are reasonably common, include several bright northern stars, and have a very simple spectrum. This was how the UBV filter system was set up (Johnson and Morgan, 1953) with Vega chosen as the primary standard. Vega is now known to be slightly different from an average A0V star; on the H-R diagram Vega is just above the mean A0 main sequence in a position which implies that it is late in its main sequence life. Vega was eventually assigned $m_v = 0.02$.

Many attempts have been made to provide an absolute flux calibration for Vega over the range of the UBV filters from ground based observations (see Hayes and Latham, 1975, and the references listed therein). Calibration observations have been done at Mt. Palomar (Oke and Schild, 1970), Mt. Hopkins (Hayes, Latham and Hayes, 1975) and the Lick Observatory (Hayes, 1970), but no single standard calibration has emerged from them. The usual method was to use a

blackbody comparison source for direct absolute flux calibrations. The type of blackbody source used was usually a cavity held at the melting point of a metal- platinum for the near ultraviolet because its melting point is high (2045 K), and copper beyond about 6000A because it melts at 1357.6 K which is very near the standard of 1337.5 K for the melting point of gold. Sometimes tungsten lamps were also used. The precision of these measurements is limited by several factors. The melting point blackbodies have the drawback that, in spite of the relative inertness of gold, platinum and copper, after a brief period of use impurities begin to effect the melting point as oxides form in the material. As well, the atmospheric extinction corrections must be carefully made not only for Vega but also for the telescope to comparison source path. The comparison source must be far enough away that the telescope focus need not be altered between observations.

The absolute flux calibration which results is expressed in terms of the object flux I_λ at a particular λ value. The value chosen, called the effective wavelength, is calculated from the filter response function

$$\lambda_{\text{EFF}} = \frac{\int_0^{\infty} \lambda \phi(\lambda) d\lambda}{\int_0^{\infty} \phi(\lambda) d\lambda} \quad (1.27)$$

The I_{λ} value at λ_{EFF} for a source of magnitude 0.00 will depend somewhat upon what type of object is being observed, for if the object spectral distribution is altered for a given I_{λ} at λ_{EFF} the magnitude will also be slightly changed. To be truly accurate the absolute calibration would have to be separately done for each spectral type, but this has never been attempted. At present the various Vega calibrations disagree by a few percent, corresponding to a range of 0.035 magnitudes at 5556 Å, λ_{EFF} for the V filter.

The absolute flux calibration of infrared filter systems is generally done in a similar manner to that for the UVB filters, save that the absolute flux measurements from the ground are more difficult so various models are used instead. Either Vega or a 10 000 K blackbody of the same size and distance as Vega is used as the primary standard. In some systems, a 10 000 K blackbody star in the place of Vega is assumed to have zero magnitude in all the filters, then from this and an atmospheric model for Vega the magnitudes of Vega are set (see, for example, Gehrz, Hackwell and Jones, 1974). In other systems, Vega is assumed to have zero magnitude in all the filters and

the absolute calibration is done from a Vega model (see, for example, Stecker, Erickson and Witteborn, 1979). The different methods cause discrepancies of the order of 0.02 magnitudes between the various systems.

The absolute calibration of infrared filter systems is usually assumed to be independent of the type of source observed, because all objects are assumed to follow a Rayleigh-Jeans flux law. The usual blackbody law for a source of temperature T is

$$I_{\lambda} \propto \frac{1}{\lambda^5} \frac{1}{e^{C_2/\lambda T} - 1} \quad (1.28)$$

where C_2 is the second radiation constant, $\frac{hc}{k}$ in terms of the fundamental constants, which has a value of 14 388 μmK . If $\frac{C_2}{\lambda T}$ is small then $e^{C_2/\lambda T} \approx 1 + C_2/\lambda T$ so

$$I_{\lambda} \propto \frac{T}{\lambda^4} \quad (1.29)$$

which is the classical Rayleigh-Jeans law. To the extent that this law is followed for sources in the infrared, the absolute calibration is independent of T . Actually, for $\lambda \sim 2\mu\text{m}$ and T in the range 2 000 K to 30 000 K, which covers the main sequence for stars, the approximation is poor except for right at the upper end of the temperature range. Thus, the assumption does not hold for the JHK filters and most types of stars, although it is a good assumption for $\lambda > 20\mu\text{m}$, in the far infrared. In spite of this, the Rayleigh-Jeans law

is often assumed for stars in the near infrared.

It is rather unfortunate that Vega has become the primary photometric standard for both the UBV and infrared filter sets, because Vega is now known to be slightly variable (Ferne, 1981). Vega shows variability at irregular intervals. When active the V magnitude varies by about 0.02 magnitudes over a period of hours.

In view of the preceding discussion, it is surprising that Johnson's calibration of his JKLMN filter set was not based upon either Vega or a 10 000 K blackbody source, nor even upon AOV stars. Instead, Johnson (1965 b) used the sun to calibrate his filters in a somewhat indirect manner. The absolute spectrum of the sun was assumed to follow the tabulation of Allen (1963). If the solar magnitudes were known the absolute calibration would be directly obtained. However, observing the sun with a photometer which was designed for stellar observations is subject to various problems. The extreme brightness of the sun could cause non-linearities in the photometer response, if it did not simply burn out the detector. The sun is not a point source like other stars, which could also cause some problems. Finally, daytime observations are subject to different extinction than the usual night-time observations because of the changes in atmospheric structure due to solar heating. These

factors make it nearly impossible to use a standard photometer to obtain solar magnitudes.

To obtain data for the sun Johnson worked indirectly. In the years around 1960 several groups had measured the solar V magnitude. Johnson used these results to obtain a weighted mean value of $m_V = -26.74$ for the sun. The solar colour indices were not measured, but instead were assumed from a study of 14 stars which are quite similar to the sun. Oddly, only 2 of these stars were of type G2V, while 7 of them were of type G0V. From m_V and the assumed colours the absolute calibration was carried out. Johnson clearly considered the results to be only accurate to about $\pm 10\%$.

This calibration has remained standard, in spite of the changes in the filters which have taken place in the last 20 years. For example, Johnson's values are given in Allen (1981). This calibration could be redone much more accurately today, but this has never been attempted.

When infrared photometry was first being done, extinction observations showed $m(X)$ to be linear in X within the errors of observation. For this reason the Hardie method was adopted for use in the infrared. Considering the causes of infrared extinction, this result is surprising. The aerosol and molecular scattering which cause the visible extinction are still

present, although the latter has become very small by the time the J filter has been reached, but another source of extinction has become important; the molecular absorption lines contribute strongly to k . Unlike the other two sources of absorption, strong lines do not show a linear growth of mean absorption with column density. Once the line core becomes saturated, which occurs high in the atmosphere for strong CO_2 lines, the mean line absorption increases roughly as the square-root of the column density. Under such conditions the linear extinction law must be in error.

The effect of this may readily be deduced. Between $X = 1.00$ and $X = 2.00$ the strong lines will increase in mean absorption by about 40% as the column density increases by a factor of 2. Extrapolating back to what is formally equivalent to $X = 0.00$ will result in an underestimate of the correction, leaving $m(0)$ too large. This error will depend upon the type of object being observed and upon the atmospheric conditions, meaning that systematic errors will be present in both relative and absolute photometry.

The strongly saturated lines will introduce a different type of extinction law, causing the $m(X)$ relation to curve. If the $X = 1.00$ and $X = 2.00$ points are used to define a line, then the $m(X)$ will curve upwards at large X as compared with the line because of

this. This effect must be small enough that it is not obvious from extinction data. It is difficult to tell what effect this has upon the Hardie method if no tests are made for higher order X dependencies.

This whole question was examined by Johnson (1965 a). Using a simple model combining sources of linear extinction with the type of extinction which results from fully saturated non-overlapping lines,

$$I(X) = I(0)[1 - \gamma\sqrt{X}] \quad (1.30)$$

where γ is an average band extinction for the strong lines, Johnson assessed the zero point errors which result from the linear extinction law. Sinton and Strong (1960) proposed the above type of extinction law for use at somewhat longer wavelengths than are of concern here, 8 μm to 14 μm , but such an equation might apply to the JHK filters as well. The results Johnson obtained indicated that the linear extinction law gives more accurate results than the "square-root" law, even though some non-linearity is present. Johnson recommended an extra correction amounting to 15% - 30% of k in order to allow for the non-linearity. Such a correction can easily be done by extrapolating $m(X)$ to $X = -0.15$ or $X = -0.30$. This correction is rather ad-hoc, but Johnson carried the day and the square-root law was discredited.

The problem with this correction, aside from whether it is accurate, is that there is no way to be sure if it was used or not because the extinction

correction process is rarely discussed in scientific papers. For purely relative photometry, which is quite often done, this is not of importance. For any sort of absolute photometry this ambiguity is serious because it represents an uncertainty of around 0.03 magnitudes between different observers. At the present time, the accuracy of photometry is reaching 0.001 magnitudes under very good conditions so such an uncertainty is too large to let stand. It was many years before the whole extinction problem came to light again. The new study of infrared extinction will be considered in the next chapter.

Chapter Two

Survey of the Results of Manduca and Bell (1979)

Very little interest was shown in the non-linearity problem for infrared extinction in the period following the work of Johnson (1965a). Photometric data taken at this time did not show appreciable curvature in the $m(X)$ versus X plots, so there seemed to be no cause for concern. It was 14 years before the problem was examined again. Manduca and Bell (1979) [hereafter abbreviated MB] published the results of a numerical simulation of atmospheric extinction, originally carried out to lay the groundwork for a comparison of the colours from stellar models to the actual observed colours, which showed the non-linearity problem to be much worse than was indicated by the simple models used in Johnson (1965a). As MB serves as the starting point for the work presented in this thesis, the paper will be examined in detail here.

In principle, equation (1.20)

$$m(x_0) = m(0) + \frac{2.5}{\ln(10)} \bar{k} x_0 \quad (2.1)$$

can be evaluated for any specified atmospheric path by numerical integration provided that $\phi(\lambda)$, I_λ and k_λ are known. This procedure turns out to be far too complicated to carry out completely. k_λ will be a

very complicated function of pressure, temperature and composition because of the molecular lines which occur in the infrared. Rather than being any sort of reasonable continuous function, k_λ would have to be expressed as the sum of a large number of spectral line functions. The spectral line functions will vary along the atmospheric path in a complex manner which will be slightly different for each line. When the total number of lines to be included is in the tens of thousands, the problem of calculating k is clearly too large to be done without significant approximation. In fact, several approximations must be made in order that the problem can be dealt with.

In the consideration of extinction as it applies to photometry given in Chapter 1, the basic approach was to imagine the telescope system to be observing at various points in the atmosphere; that was why the λ integration was carried out before the x integration. An alternative conceptual approach is to use the monochromatic result, equation (1.6), and

$$I_\lambda(x_0) = I_\lambda(0)e^{-\bar{k}_\lambda x_0} \quad (2.2)$$

then include the system response. Multiplying equation (1.2) by $\phi(\lambda)$ and integrating over λ gives

$$\int_0^\infty \phi(\lambda) I_\lambda(x_0) d\lambda = \int_0^\infty \phi(\lambda) I_\lambda(0) e^{-\bar{k}_\lambda(x_0)x_0} d\lambda \quad (2.3)$$

or

$$I(x_0) = \int_0^{\infty} \phi(\lambda) I_{\lambda}(0) e^{-\bar{k}_{\lambda}(x_0)x_0} d\lambda \quad (2.4)$$

This equation can also be converted to a magnitude/air mass relation by defining a \bar{k} from the weighted mean of $e^{-\bar{k}_{\lambda}(x_0)x_0}$, but the result is less clear than the other approach. Equation (2.4) is useful for numerical calculations because k_{λ} is independent of I_{λ} , and so need not be re-calculated for each object which is considered.

Under the assumptions given in Chapter 1, the monochromatic extinction law may be written as

$$\begin{aligned} I_{\lambda}(X) &= I_{\lambda}(0) e^{-\bar{k}_{\lambda}(x_0)x_0 X} \\ &= I_{\lambda}(0) [e^{-\bar{k}_{\lambda}(x_0)x_0}]^X \end{aligned} \quad (2.5)$$

where now x_0 denotes the zenith path. With

$$I_{\lambda}(X = 1.00) = I_{\lambda}(0) e^{-\bar{k}_{\lambda}(x_0)x_0} \quad (2.6)$$

equation (2.5) shows that once the atmospheric transmittance $t(\lambda, X)$ is found for X equal to 1.00 it can be calculated for all $X > 1.00$ via

$$t(\lambda, X) = [t(\lambda, 1.00)]^X \quad (2.7)$$

Once again $X = 0.00$ corresponds to $x_0 = 0$, the above atmosphere case.

This is advantageous because $t(\lambda, X)$ need only be calculated for $X = 1.00$ to allow the calculation of $I(X)$ for $X \geq 1.00$, which then converts directly into $m(X)$ for $X \geq 1.00$. Setting $X = 0.00$ gives $m(0)$. The calculation of $\bar{k}_{\lambda}(x_0)$ remains a major problem, but once it is obtained the other quantities then follow routinely.

Equation (2.7) is another form of the linear magnitude/air mass relation for the monochromatic case. In the formal sense this equation may be considered to apply for all X , or for $X \geq 0.00$. If the equation is used for $X \geq 0.00$ then a continuous extinction curve can be defined. This is often done for the real filters as well, and such $m(X)$ curves will be given in this thesis. However, it must be stressed that there is no physical meaning to $X < 1.00$ in the atmosphere except for $X = 0.00$. $X \geq 1.00$ is based upon the zenith angle, and is specific to each site. Unless the circumstances are such that k is constant or strictly a function of the total column density along the ray path, $X = 1.00$ at one altitude or location can not be set as equivalent to an X value at another altitude or location. In the atmosphere, this is not possible.

The above equations hold in the monochromatic limit, and obviously no computer can work at that limit. MB and all others doing work on the atmospheric transmittance must work at a finite resolution. When the finite set of $t(\lambda, X)$ values are used to approximate the continuous $t(\lambda, X)$ function, small errors occur which produce small errors in $I(X)$. These errors increase as X increases because the exponentiation of the set of $t(\lambda, X = 1.00)$ points to give $t(\lambda, X)$ increases the difference between adjacent t values. The error naturally decreases as the

resolution of the calculation is increased. A compromise must be reached between the accuracy and the amount of computer time and resources which are available.

MB do not discuss the overall accuracy of their results. No definitive statements can be made about the accuracy because of certain features of the computer program they used. Kyle (1968) discusses the accuracy of numerical grid calculations of a spectral line profile under various assumptions, which should serve as a guideline to what sort of factors influence the accuracy of the calculations.

If a spectral line is centered at ν_0 , where $\nu \equiv \frac{1}{\lambda}$ is called the wavenumber, and this line is to be approximated by values at a series of grid points ν_i spaced by $\Delta\nu$ with the grid point nearest to ν_0 displaced by $\delta\nu$, Kyle found that three factors determine the mean error in the numerical absorption profile. The factors are the line shape, the grid spacing and $\delta\nu$. Oddly enough, $\delta\nu$ was found to play a critical role in determining the overall error of the numerical simulation. It was found that, for a Lorentz line shape, the error was larger for larger $\Delta\nu$ values but also that for a given $\Delta\nu$ the error was the greatest when $\delta\nu$ was zero. Kyle's results showed that for a line of half-width α the error is

smallest for $\delta\nu \approx \frac{1}{4} \alpha$. The difference between $\delta\nu = 0$ and $\delta\nu = \frac{1}{4} \alpha$ is quite dramatic. $\Delta\nu$ should be chosen to be about equal to α , but with the optimum $\delta\nu$ even $\Delta\nu = 2\alpha$ gives a reasonably accurate result.

The reason for this is that in a Lorentz line the line center falls away quite steeply within about $\pm 2 \alpha$ of ν_0 , and then flattens out to blend into the very broad line wings. A better estimate of the core contribution is obtained with a small offset because then two points or more fall within the line core, whereas with no offset only the ν_0 point falls in the core for $\Delta\nu \approx \alpha$. For very small (or very large) $\frac{\Delta\nu}{\alpha}$ values this makes little difference, but when $\frac{\Delta\nu}{\alpha}$ is between 1 and 2 the overall error may be increased by an order of magnitude if $\delta\nu$ is not properly chosen. This is of key importance because some atmospheric transmittance programs put the spectral lines on the grid points to use the line symmetry to save computer time.

The general approach used to calculate k_λ is as follows. Dealing with the real atmosphere would be very difficult because of its inhomogeneity, so the atmosphere is approximated by a suitable homogeneous layer. The pressure, temperature and column density for whatever molecules are of importance in the gas are all that are needed to calculate k_λ for a homogeneous path, provided that the proper line-parameter data is

available for these molecules. There are several approximation methods which yield the parameters for a homogeneous path which gives nearly the same transmittance as a specified inhomogeneous path. The Curtis-Godson approximation is the most useful of these methods. Discussion of these approximation methods will be deferred until Chapter 3. In MB the atmosphere was modelled as a single homogeneous layer using the Curtis-Godson technique. For each spectral line in the wavelength interval of interest, four quantities must be specified - the line shape, the line strength expressed as the contribution per molecule to k_λ , the line width and the line wavelength. The first three of these can vary along the path, for they are functions of temperature, pressure, or both. If the line strength is symbolized as S , the column density as N and the line profile function as $F(\nu)$, then for each line

$$k_\lambda(\nu) = SN F(\nu) \quad (2.8)$$

$F(\nu)$ is normalized in such a way that

$$\int_0^\infty F(\nu) d\nu = 1 \quad (2.9)$$

Numerous line shapes have been proposed, but none have been shown to fit spectral lines exactly. A single line shape is usually chosen, and then assumed to fit all the lines, rather than trying to use different line shapes for different lines. In some cases two line

shapes are used when one is a limiting case of the other, especially when a large range of conditions are being considered.

The spectral line data required for this calculation process is available in the form of a computer compilation produced by the Air Force Cambridge Research Laboratory (McClatchey, et. al., 1973). This lists the line parameters for nearly 110 000 spectral lines of the molecules H₂O, CO₂, CO, O₃, CH₄ and N₂O which fall in the range 0.76 μ m to 3.20mm. The results of both theoretical calculations and experimental studies were used to obtain the line parameters in this compilation. The approach varied from molecule to molecule depending upon the state of the theoretical treatment of each specific molecule and upon the available experimental data. Lines below a certain line strength threshold were omitted from the compilation. The selection process is discussed at length in McClatchey, et. al., (1973) and so will not be described here. The compilation is thought to be fairly complete in the near infrared, the region of interest in the present project and MB.

Considering that N₂ and O₂ make up 99% of the atmosphere by number, it might be expected that these molecules would be the dominant absorbers of infrared radiation. However, each of these two elements is

composed of one dominant isotope, which means in turn that almost all the N_2 and O_2 molecules are formed from identical atoms. This makes the normal dipole vibrational and rotational transitions for a diatomic molecule impossible due to the added degree of molecular symmetry (for discussion of this matter, see, for example, Goody (1964)). Thus N_2 contributes very little to infrared line absorption in spite of making up just under 80% of all the molecules in the atmosphere. O_2 contributes some line absorption, often through magnetic dipole transitions due to its unusual magnetic moment, but it is not a major source of line absorption in the near infrared. H_2O and CO_2 turn out to be the dominant absorbing molecules over much of the infrared. At wavelengths beyond $4\mu m$ N_2 begins to contribute a kind of continuum absorption due to collisionally induced transitions which would otherwise be forbidden (Wing and Rinsland, 1979). This may be of marginal importance in the L filter, but appears to be completely negligible at shorter wavelengths. Such absorption apparently was ignored by MB.

Save for O_2 , all of the molecules in the McClatchey line compilation are variable constituents of the atmosphere. This is particularly true for H_2O and O_3 , which undergo enormous fluctuations with position and time. It will be assumed that the other

molecules are uniformly mixed over the whole atmosphere. This is not so, but at a site removed from man-made sources of CO_2 , CO and N_2O it is an acceptable assumption. The abundance of some of these molecules is reduced at very high altitudes while for others, especially CO , there is an enhancement. This is a minor effect because only a small part of the atmosphere is present at high altitudes. Over most of the atmosphere the compositional fluctuations are relatively small.

The program which was used by MB to calculate $t(\lambda, X = 1.00)$ was named IRTRANS. This program was first described in Traub and Stier (1976), having been developed by M. Stier and subsequently refined by W. Traub and later MB. For each of the seven molecules included in the McClatchey line parameter compilation the program is given a pressure value, a temperature value and a column density value as input parameters. Thereafter the calculations proceed under the assumption of homogeneity. For each run of IRTRANS the grid spacing $\Delta\nu$ and the range of wavenumber values which is to be covered are also input as parameters. If the wavenumber range is greater than 10 000 times $\Delta\nu$, the program breaks the range into smaller sections.

Once a grid section is set up, a region beyond the end points of the grid out to a set maximum range is searched for any lines which are strong enough to

effect the grid interval. IRTRANS also retrieves the parameters for those lines which fall within the grid. Each of these lines is shifted to the nearest grid point, to save time by taking advantage of the line symmetry. Any line which contributes less than 0.0005 to k_λ at line center, when calculated from the line strength, line half-width and the column density, is left out by IRTRANS.

When all the necessary data has been compiled, the program proceeds to calculate each line's contribution to k_λ at all the grid points. The line profiles are followed until their contribution to k_λ falls below 0.0005, after which they are ignored. Eventually the contributions from all of the lines will have been included, and IRTRANS then includes the effects of aerosol scattering and molecular Rayleigh scattering at each grid point. From the total k_λ value, exponentiation gives the fractional transmittance.

One of the most important features of such a program is the assumed line profile which is used. The most widely used line profile has been the simple Lorentz profile, whose line shape function is

$$F_L(\nu) = \frac{\alpha}{\pi[(\nu - \nu_0)^2 + \alpha^2]} \quad (2.10)$$

for a line of frequency ν_0 . α is the half-width of the line. This line profile applies to the case of the undisturbed radiation of a molecule, producing what is

called the natural line shape, and also to the case in which intermolecular collisions trigger the radiation. In the second case α is directly proportional to the pressure, and is usually assumed to be inversely proportional to the square root of the temperature. There has been some concern about how closely the Lorentz profile is actually followed by collisionally broadened lines, especially in the far wings where there is some indication of a much faster decline than equation (2.10) indicates (see, for example, Burch, et al., (1969)).

Strictly speaking, this type of line profile will only be observed in the rest frame of the emitting molecules. The thermal motions of gas molecules along the line of sight will cause Doppler broadening, as the observer will see the superposition of numerous Lorentz line profiles at slightly different central wavelengths. For a monochromatic transition the Doppler line profile would be

$$F_D(\nu) = \frac{1}{\sqrt{\pi} \beta} e^{-\frac{(\nu-\nu_0)^2}{\beta^2}} \quad (2.11)$$

where β is related to the mean component of molecular velocity along the line of sight. For a molecule of mass M in atomic mass units, and a temperature T , β is given by

$$\beta = 4.30 \times 10^{-7} \nu_0 \left(\frac{T}{M}\right)^{\frac{1}{2}} \quad (2.12)$$

The actual profile which results from the Doppler

broadening of a Lorentz profile is called a Voigt profile, and is obtained by the convolution of F_D and F_L . This function, $F_V(\nu)$, is not one which can be expressed in closed form, although tabulations do exist.

In IRTRANS the Voigt line profile was generally used, with the convolution evaluated by a special subroutine. This was a relatively slow process, so some shortcuts were used at little cost in accuracy.

If $\frac{\alpha}{\beta} > 10^{-7}$ and $|\frac{\nu-\nu_0}{\beta}| > 12$, corresponding to the wings of most lines, $F_V(\nu)$ is within 1% of $F_L(\nu)$; in this limit the Lorentz profile was substituted for the Voigt profile. Further, when $\frac{\alpha}{\beta} > 2$ the whole Voigt profile is closely approximated by the Lorentz profile so $F_L(\nu)$ was used in this case. In that range the pressure broadening becomes dominant.

As noted in Kyle (1968) the line core is not handled properly when a spectral line is centered exactly on a grid point. To combat this problem IRTRANS uses a further set of approximations to describe each line's contribution to its own grid point. The line wings are assumed to be properly allowed for, so only the line core contribution need be adjusted to obtain overall accuracy. For those lines whose cores are described by a Voigt profile, the adopted line core contribution to k_λ is the value found $\frac{1}{4}\Delta\nu$ from line center. There is no explanation of why this particular value is used, although it does match

the optimum offset of Kyle (1968). For those lines which are always treated by using the Lorentz profile, the core contribution to k_λ is found by averaging between $\nu_0 - \frac{1}{2}\Delta\nu$ and $\nu + \frac{1}{2}\Delta\nu$. The averaging is done by integrating over k_λ , as $F_L(\nu)$ is exactly integrable. As

$$\int_{\nu_0 - \frac{1}{2}\Delta\nu}^{\nu_0 + \frac{1}{2}\Delta\nu} F_L(\nu) d\nu = \frac{2}{\pi} \tan^{-1} \left(\frac{\Delta\nu}{2\alpha} \right) \quad (2.13)$$

the result is

$$k = \frac{2SN}{\pi\Delta\nu} \tan^{-1} \frac{\Delta\nu}{2\alpha} \quad (2.14)$$

for the central grid point.

Traub and Stier (1976) call this process an exact integration. In actuality this is misleading, because although the integration is exactly done the quantity which should be averaged is not k_λ but rather e^{-k_λ} .

Their approach is to put

$$e^{-\bar{k}_\lambda} = e^{-\frac{1}{\Delta\nu} \int_{\Delta\nu} k_\lambda d\lambda} \quad (2.15)$$

instead of

$$e^{-\bar{k}_\lambda} = \frac{1}{\Delta\nu} \int_{\Delta\nu} e^{-k_\lambda} d\lambda \quad (2.16)$$

The second form is the exact form, but apparently this integration cannot be evaluated in closed form for the Lorentz line profile. The equation (2.14) result is nearly exact in the weak line limit where $e^{-k_\lambda} \approx 1 - k_\lambda$ and $e^{-\bar{k}} \approx 1 - \bar{k}$. Otherwise the \bar{k} value found from this equation is in error in a somewhat complicated manner.

As originally used, IRTANS performed calculations at a grid spacing of 0.05 cm^{-1} or less; such a grid spacing gives $\frac{\Delta\nu}{\alpha} \approx 1$ for most lines under standard temp-

erature and pressure. MB use a larger spacing of 0.20 cm^{-1} , typically, so $\frac{\Delta\nu}{\alpha} \approx 4$. This grid spacing is somewhat larger than is desirable, considering that the calculations are carried out for high altitude sites, but this is necessary for reasons of cost. The key question in assessing the overall accuracy of the results is the effect of the core integration. For strong lines the practical effect is small simply because the core is strongly saturated. The difference between $k = 50$ (say) and $k = 60$ is small in relation to the total flux from areas with little absorption. For intermediate lines the approximation will tend to cause an overestimate of the total absorption, because averaging k_λ gives weight to large k_λ values whereas the averaging of e^{-k_λ} will give weight to small k_λ values. This effect is worse in cases where there is a large range of k_λ over the range of integration.

The formulae for Rayleigh scattering and aerosol scattering are taken from Hayes and Latham (1975). Expressed in magnitudes per air mass, with λ in μm and ν in μm^{-1} , the formula for aerosol extinction is

$$A_{\text{AER}}(\lambda, h) = \alpha \nu^\beta e^{-h/H} \quad (2.17)$$

where h is the altitude of the observation site, $H = 1.5$ km, $\beta = 0.80$ and $\alpha = 0.084$. The aerosols present in the atmosphere come from numerous sources, and their size distribution and number density show considerable fluctuations with time. This means that equation (2.17)

is a reflection of average conditions and may not apply at any given time. The aerosol scattering contributes roughly 0.018 magnitudes per air mass for the J filter, roughly 0.014 magnitudes per air mass for the H filter and 0.011 magnitudes per air mass for the K filter at Kitt Peak (2.06 km).

The Rayleigh extinction in magnitudes per air mass is given by

$$A_{\text{RAY}}(\lambda, h) = 9.4977 \times 10^{-3} \nu^4 \left[0.23465 + \frac{107.6}{146 - \nu^2} + \frac{0.93161}{41 - \nu^2} \right]^2 \times e^{-\frac{h}{7.996 \text{ km}}} \quad (2.18)$$

For Kitt Peak, the Rayleigh extinction amounts to 0.003 magnitudes per air mass for the J filter, 0.001 magnitudes per air mass for the H filter and 0.0004 magnitudes per air mass for the K filter. The Rayleigh extinction values show that this is a very small factor in the infrared, even compared to the aerosol extinction. These sources of extinction, especially the aerosol extinction, do not change too much over the filter bandwidths. This means that the contribution from these sources is approximated closely by the values at λ_{EFF} , given above for Kitt Peak.

MB adopted parameters to correspond to the Kitt Peak site in summer and winter and to the Mauna Kea site. It was felt that these two sites are fairly representative of infrared facilities in general. The basic atmospheric models which they used were taken

from the standard midlatitude models for summer and winter conditions presented in McClatchey, et. al., (1972). These models are part of a supplemental series of models produced as extensions of the U.S. Standard Atmosphere (1962), calculated by assuming a temperature profile produced out of a series of layers which have a constant temperature gradient. Once the temperature as a function of height is fixed, the pressure and composition profiles for a hydrostatically stable atmosphere can be calculated. MB presumably used the 30°N supplemental atmospheric models for Kitt Peak (latitude 31°57'N) and the single 15°N supplemental model for Mauna Kea (latitude 19°50'N).

The only significant alteration made by MB was to reduce the H₂O column density in the atmospheric models by 50%, to fit observations carried out at the Catalina mountain site by Johnson, et. al., (1968), for the Kitt Peak calculations. This seems reasonable, for Arizona is probably dry compared to an average midlatitude site. The pressure values for each molecule were obtained from the Curtis-Godson approach, and then the temperature values chosen to be those which occur at P_{EFF} in the atmospheric model. MB give no details of how they obtained their P_{EFF} values for H₂O and O₃, which depend somewhat upon the vertical distribution which is assumed for these molecules. No such problem arises for the other five molecules because they are

assumed to be uniformly mixed. The results are not as sensitive to the P_{EFF} and T_{EFF} values, which primarily effect the half-widths of the lines, as they are to the column density values. T_{EFF} does influence the line strength values, but the column density values are far more uncertain for H_2O and O_3 than are the T_{EFF} values. After the initial runs, MB performed additional calculations with the H_2O column density first increased and then decreased by a factor of 2 from the initial runs to get some idea of how the results change when the water vapour content of the atmosphere changes.

The extinction calculations were carried out for two sources. A Vega model and a cool giant model were used in order that the colour dependence of the extinction could be assessed. Published filter response profiles for the original Johnson J, K and L filters as well as the Kitt Peak J, H and K filters which were in use around 1978 were chosen for the calculations. MB then used the output from IRTRANS to calculate the apparent magnitude of the source every 0.5 air masses from $X = 0.00$ to $X = 3.00$. As has been discussed, the $X = 0.50$ point is of dubious significance, so the shape of the numerically simulated extinction curve below $X = 1.00$ has no real use. Nevertheless MB present the data as a continuous curve from $X = 0.00$ to $X = 3.00$.

As MB comment, the results do not necessarily correspond to any real site or set of conditions. Just how closely the adopted parameters actually come to the real conditions at Kitt Peak or Mauna Kea during any time of the year is an open question. Further, as has been seen, the approximations used in setting up IRTRANS and obtaining the input parameters are sometimes rather uncertain. The major importance of the results is in their qualitative features, although there is some hope that the numerical values themselves will be useful.

The initial set of results are presented in the greatest detail in MB. The total H₂O column density values were 5.04, 1.69 and 1.2 precipitable millimeters (Pmm) of H₂O for Kitt Peak summer, Kitt Peak winter and Mauna Kea respectively. The conversion factors for Pmm are 1 Pmm = 3.3428×10^{21} molecules per cm² and 1 Pmm = 1 Kgm⁻² assuming water to have a density of exactly 1000 Kgm⁻³. Subsequent results were obtained by changing the H₂O column abundance without altering any other data values, which is permissible because H₂O makes up only a tiny fraction of the gases in the atmosphere.

MB used the response function of an InSb detector working at 77 K for the detector function. Some trials were also run using the response function of a PbS detector, with no significant alteration of the

results. The L filter results were only preliminary and so must be viewed with caution.

Figure 3, taken from MB, shows the calculated extinction curves for the cool giant model under Kitt Peak summer conditions, plus one curve for the Vega model for comparison. The Kitt Peak filter results are labelled j, h and k, with J, K and L referring to the older Johnson filters. The cool giant model has $T_{\text{EFF}} = 4000$ K, solar abundances and $\log_{10} g = 1.5$, corresponding to spectral class K4III. This model was taken from Bell and Gustafsson (1979). The Vega model is described as having solar abundances, $T_{\text{EFF}} = 9650$ K and $\log_{10} g = 4.0$. In all the curves in Figure 3 the qualitative features are the same. The extinction curves have a continuously decreasing slope over $X = 0.00$ to $X = 3.00$, with a much sharper change of slope below $X = 1.00$.

In each case, the $X = 1.00$ and $X = 2.00$ points were used to define a straight line with slope E magnitudes per air mass. The extrapolation of this line to $X = 0.00$ produces a zero point value which is too low by an amount Δ magnitudes, with a slight difference δ in the Δ values for the red giant model and the Vega model. δ is defined as $\Delta(\text{cool giant}) - \Delta(\text{Vega})$. The amount of curvature beyond $X = 1.00$ is relatively small, much less than the curvature to $X = 0.00$. This is regrettable because the curves

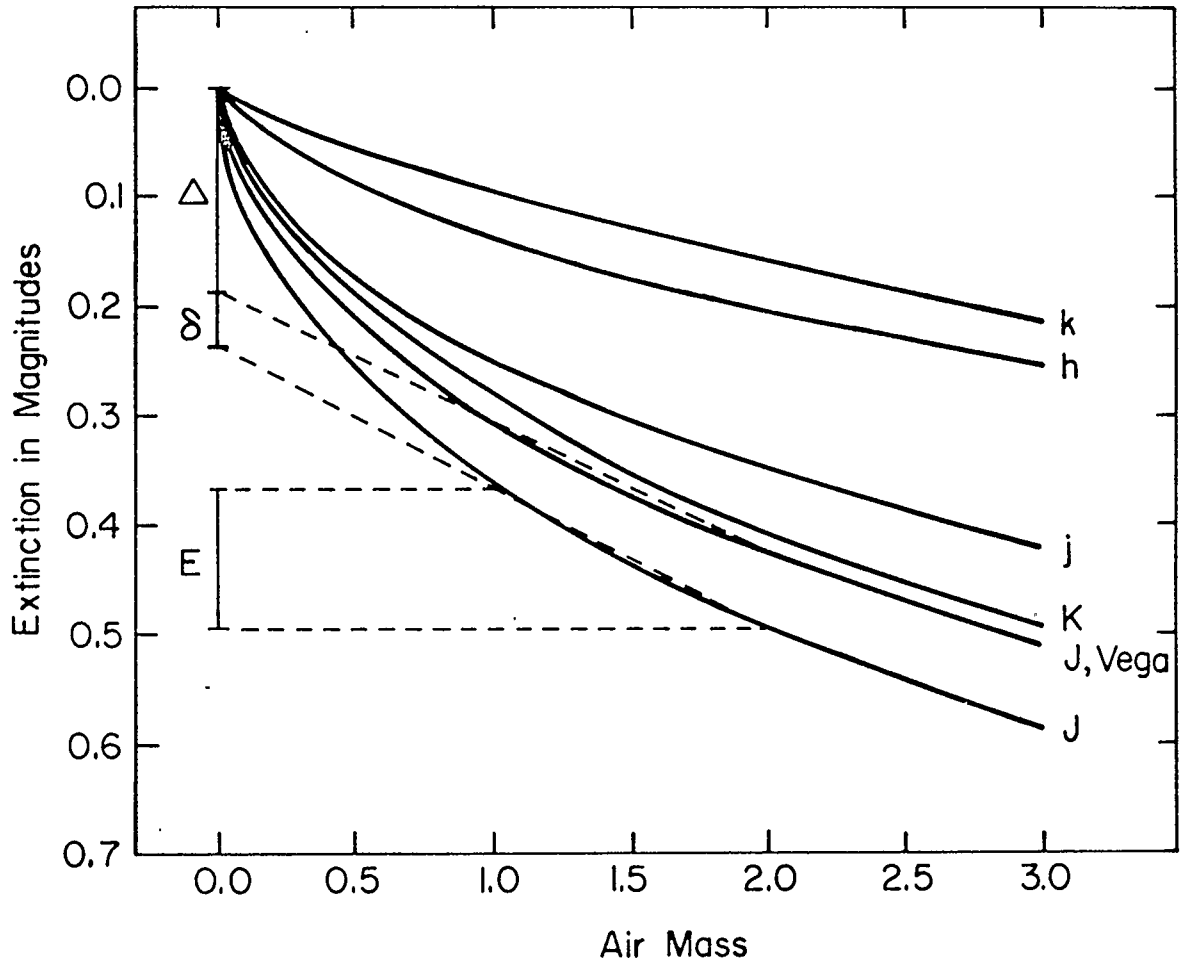


Figure 3- The extinction curves for the cool giant model in the Johnson J and K filters and the Kitt Peak pre-1979 J, H and K filters [denoted as j, h and k] under the 'Kitt Peak summer' conditions as obtained by Manduca and Bell(1979). The curve marked J,Vega is included to illustrate the effect of stellar type upon extinction. The definitions of Δ , E and δ are illustrated.

From Manduca and Bell (1979).

are not symmetrical about $X = 1.5$ and so observations for $X \geq 1.00$ may not be sufficient to deduce a zero point correction. MB do not give any type of analytical description of their curves.

The quantitative features of the results are presented in Table 1. The most important result is that the ratio $\frac{\Delta}{E}$ is much larger than the 0.15 - 0.30 figure that Johnson (1965a) deduced from his work. The mean $\frac{\Delta}{E}$ ratio from Table 1 is 0.946 for the red giant model and 0.876 for the Vega model. In terms of the individual filters, the mean $\frac{\Delta}{E}$ ratios are 1.349 for J, 0.944 for K, 0.641 for L, 1.195 for j, 0.827 for h and 0.420 for k. In the worst case the correction of Johnson (1965a) still leaves an error of 0.198 magnitudes in the zero point value. It appears that the simple models used in Johnson (1965a) were too unrealistic and so do not produce reasonable results.

The Δ values are largest for the J and j filters, declining markedly at longer wavelengths. It is not clear whether this is a definite trend or is the result of better atmospheric windows for the other filters. The new filters cause a reduction in Δ , especially for the K and k pair, which probably is a direct result of the reduction in filter band-widths to conform more closely to the atmospheric windows. The $\frac{\Delta}{E}$ ratio also falls more steeply in the case of the K and k pair than in the case of the J and j pair. The

TABLE 1

SITE	FILTER	E	VEGA		E	COOL GIANT		δ	
			Δ	Δ/E		Δ	Δ/E		
KITTE PEAK "SUMMER "	JOHNSON	J	0.117	0.187	1.598	0.129	0.237	1.837	0.050
		K	0.126	0.155	1.230	0.125	0.157	1.256	0.002
		L	0.195	0.141	0.723	0.194	0.141	0.727	0.000
	KPNO	J	0.096	0.130	1.354	0.098	0.154	1.571	0.024
		H	0.066	0.072	1.091	0.066	0.073	1.106	0.001
		K	0.066	0.029	0.439	0.065	0.029	0.446	0.000
KITTE PEAK "WINTER "	JOHNSON	J	0.093	0.107	1.151	0.106	0.136	1.283	0.029
		K	0.109	0.094	0.862	0.110	0.097	0.882	0.003
		L	0.153	0.085	0.556	0.153	0.085	0.556	0.000
	KPNO	J	0.075	0.074	0.987	0.080	0.088	1.100	0.014
		H	0.053	0.037	0.685	0.053	0.038	0.717	0.001
		K	0.054	0.020	0.370	0.053	0.021	0.396	0.001
MAUNA KEA	JOHNSON	J	0.079	0.078	0.987	0.081	0.100	1.235	0.022
		K	0.092	0.064	0.696	0.088	0.065	0.739	0.001
		L	-	-	-	-	-	-	-
	KPNO	J	0.053	0.054	1.019	0.057	0.065	1.140	0.011
		H	0.036	0.024	0.667	0.036	0.025	0.694	0.001
		K	0.027	0.013	0.481	0.036	0.014	0.389	0.001

E - MAGNITUDES/AIR MASS Δ - MAGNITUDES δ - MAGNITUDES
SOURCE: MANDUCA AND BELL (1979)

SUMMARY OF THE MANDUCA AND BELL (1979) RESULTS FOR THE JOHNSON JKL AND KPNO
JHK FILTERS.

colour dependence of Δ is negligible for all the filters except the J and j pair. It is interesting to note that δ is essentially cut in half by going to the newer filters, although E and Δ show no such simple change. δ should be a very complex function of the filter profile.

The colour dependence of Δ for the j filter is large enough that it could be detected from the V-J colours in stars. A model atmosphere fit to the other colours should show discrepancies in the V-J colour. Analysis for a number of stars of different types could, in principle, allow this effect to be observed. However, the effect is very small compared to the range of V-J colours, so detecting this effect would be an exacting task.

The results for other values of the H₂O column density are not tabulated in MB. Instead, E is plotted against E + Δ for the range of column density. These graphs are presented in Figure 4a and Figure 4b. The curves are not linear, and the Mauna Kea results do not lie on the same curve as the Kitt Peak results. This dashes any hope of having a fairly easy correction for variations in the H₂O column density, at least in this approach. E + Δ is somewhat sensitive to the value of E, especially for the j filter, so the Δ correction may not be accurately obtained from the E value even with a curve of this sort.

More calculations, for a set of narrow-band filters, are briefly presented in MB. Those results are presented in Table 2, which is taken directly from MB. It is worth noting that even here significant Δ values occur in a few cases. MB do not say whether these results are for Vega or for the cool giant. The worst case is for the 2.0 μm filter of Cohen, Frogel and Persson (1978). This filter was designed to measure stellar H_2O lines near 2.0 μm by comparison with the other filters. It runs into very heavy extinction because of atmospheric H_2O , which means that the results obtained may be misleading because of fluctuations in the atmospheric H_2O column density.

Although the shape of the extinction curves is similar to what would be expected from the square-root law, MB say that "...In general, no simple rule-of-thumb such as the 'square-root law' is adequate for estimating the true extinction...".

In summary, the results of MB show a large zero-point error occurring when infrared atmospheric extinction corrections are made in the usual manner. Despite showing very little curvature from $X = 1.00$ to $X = 3.00$ the magnitude/air mass relation from the numerical simulation is definitely non-linear. The linear extrapolation to $X = 0.00$ results in a zero point error which is slightly dependent upon the colour

Extinction for the filters of Pilachowski (1978)

<u>air mass</u>	Kitt Peak summer		Kitt Peak winter		Mauna Kea	
	<u>2.2</u>	<u>2.4</u>	<u>2.2</u>	<u>2.4</u>	<u>2.2</u>	<u>2.4</u>
0.5	0 ^m .012	0 ^m .086	0 ^m .008	0 ^m .046	0 ^m .003	0 ^m .030
1.0	.024	.159	.016	.088	.006	.058
1.5	.036	.223	.024	.126	.009	.083
2.0	.047	.281	.033	.162	.012	.108
2.5	.059	.334	.041	.196	.015	.130
3.0	.070	.383	.049	.227	.018	.152
Δ	.001	.037	.000	.014	.000	.008

Extinction for the filters of Cohen, Frogel
and Persson (1978)

<u>air mass</u>	Kitt Peak summer			Kitt Peak winter			Mauna Kea		
	<u>2.0</u>	<u>2.2</u>	<u>2.4</u>	<u>2.0</u>	<u>2.2</u>	<u>2.4</u>	<u>2.0</u>	<u>2.2</u>	<u>2.4</u>
0.5	0 ^m .250	0 ^m .012	0 ^m .043	0 ^m .191	0 ^m .009	0 ^m .029	0 ^m .135	0 ^m .003	0 ^m .019
1.0	.448	.023	.083	.349	.017	.057	.252	.006	.036
1.5	.611	.034	.121	.483	.025	.083	.355	.009	.053
2.0	.750	.045	.156	.598	.033	.108	.445	.013	.069
2.5	.869	.056	.189	.699	.041	.133	.526	.016	.085
3.0	.974	.066	.220	.787	.049	.156	.599	.019	.100
Δ	.146	.001	.010	.100	.001	.006	.059	.000	.003

Table 2- The narrow-band filter results of Manduca and Bell (1979). All values in magnitudes.

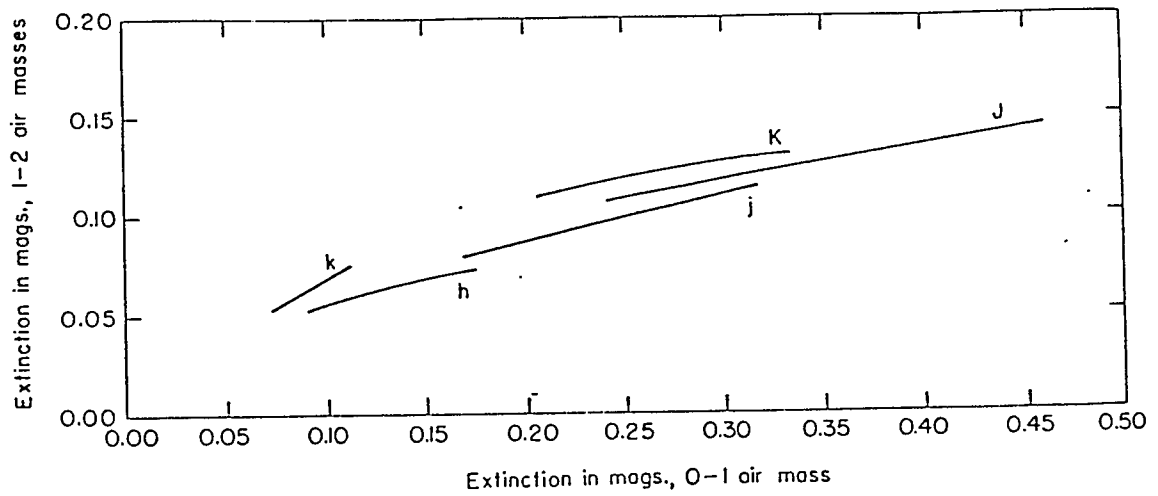


Figure 4a- The extinction between $X=1.00$ and $X=2.00$ plotted against the extinction between $X=0.00$ and $X=1.00$ for the Manduca and Bell (1979) Kitt Peak calculations. Figure symbols are as in Figure 1. From Manduca and Bell (1979).

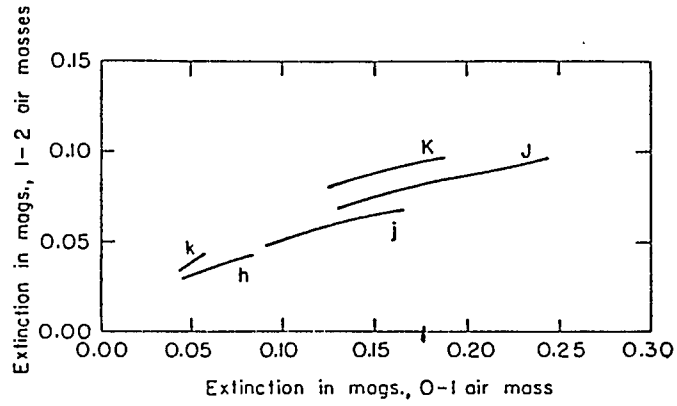


Figure 4b- The extinction between $X=1.00$ and $X=2.00$ plotted against the extinction between $X=0.00$ and $X=1.00$ for the Manduca and Bell (1979) Kitt Peak calculations. Figure symbols are as in Figure 1. From Manduca and Bell (1979).

of the object and critically dependent upon the H_2O column density. The zero-point error may be as large as 0.25 magnitudes, but decreases for the longer wavelength filters in the JHK sequence. It is not known whether this trend continues to the LMN filters. The correction proposed by Johnson (1965a) is much too small to be useful according to these results. MB did not find a relatively simple correction algorithm for atmospheric extinction corrections.

The implication of these results is that the whole process of atmospheric extinction correction must be reconsidered, and perhaps a totally new approach found. This is not surprising in view of the discussion in Chapter 1, but it is unfortunate because for 20 years infrared extinction corrections appear to have been done incorrectly. To the extent that Δ varies over time, due to changes in atmospheric conditions, or with the type of object being observed, systematic errors must be present in the observations. For purely relative photometry over short periods of time at the same X value no significant errors result provided that the stars which are observed are of nearly the same type. Variable star studies, for example, should not be subject to systematic errors for this reason provided comparison stars of the same type are used. Any process which uses the $m(0)$ values will be subject to errors if Δ changes. Any process which uses absolute

flux values derived from $m(0)$ will have, potentially, significant errors because of Δ . Infrared magnitudes can be measured to an accuracy of less than 0.01 magnitudes under good conditions, so variations of the order of 0.05 magnitudes in Δ over the year and δ values of the order of 0.02 magnitudes are large enough to be a serious problem now and will be more serious in the future when the accuracy of photometry is increased.

Chapter Three

The Curtis-Godson Approximation

Numerical simulation of atmospheric absorption must be carried out in some sort of approximate manner. In particular, to avoid the problems which would accompany the integration of k_ν over an atmospheric path along which the temperature, pressure and composition change in a complex manner, an approximation to replace the inhomogeneous path with a homogeneous path that yields the same absorption would be very useful because of the resulting saving in computer resources. The method of approximation must be carefully chosen because any errors which occur at this stage of the simulation procedure can effect the end result very strongly. This chapter discusses the Curtis-Godson approximation, which is the most useful method for relating an inhomogeneous path to an equivalent homogeneous path. The presentation here follows that of Jamieson, et. al., (1967) and Goody (1964).

Consider first the case of a homogeneous layer of gas, which contains one particular absorbing molecule. Let the column density of this absorbing molecule be expressed in the units Kgm^{-2} , denoted as μ_a , so that

$$\mu_a = \int \rho_a dx \quad (3.1)$$

where ρ_a is the density of the absorbing molecule.

The integral is taken along the path being considered.

As the gas is homogeneous, ρ_a is a constant. Further, ρ_a is a constant fraction of the total gas density ρ . The integral definition of μ_a becomes necessary when the inhomogeneous path is under consideration.

Over some interval $\Delta\nu$, in wavenumber, the mean fractional absorption A is defined by

$$A = \frac{1}{\Delta\nu} \int_{\Delta\nu} [1 - e^{-k_\nu \mu_a}] d\nu \quad (3.2)$$

If k_ν were constant over the interval $\Delta\nu$, A would show an exponential behaviour with μ . This is not generally the case in the infrared, because k_ν varies rapidly over small intervals in ν due to the spectral lines. For line absorption, A shows a very different functional relation to μ_a .

The Lorentz line shape will be assumed for all atmospheric conditions. As was noted in Chapter 2, this line shape results from pressure broadening. It may also be used to represent the natural line shape, although this is not observed under ordinary conditions. The program IRTRANS uses the Voigt line shape because Traub and Stier (1976) performed calculations for altitudes of up to 41 km; Doppler broadening is important at high altitudes where the gas density is low and thus the collisions which lead to pressure broadening become much less important. When carrying out calculations for ground sites the Lorentz profile is dominant because most of the absorbing molecules are

present below the area in which Doppler broadening is important.

With the same notation as in Chapter 2, equations (2.8) and (2.10), for a spectral line within an interval $\Delta\nu$

$$A = \frac{1}{\Delta\nu} \int_{\Delta\nu} \left[1 - e^{-\frac{S\alpha\mu_a}{\pi([\nu-\nu_0]^2+\alpha^2)}} \right] d\nu \quad (3.3)$$

Let the interval $\Delta\nu$ be large enough that the line under consideration contributes negligibly to the absorption outside this interval. Under this assumption, the limits of integration may be extended beyond the interval without altering the value of A . Taking the full range of ν ,

$$A = \frac{1}{\Delta\nu} \int_0^\infty \left[1 - e^{-\frac{S\alpha\mu_a}{\pi([\nu-\nu_0]^2+\alpha^2)}} \right] d\nu \quad (3.4)$$

Dividing numerator and denominator in the exponential by α^2 gives

$$A = \frac{1}{\Delta\nu} \int_0^\infty \left[1 - e^{-\frac{S\mu_a}{\pi\alpha} \frac{1}{[(\nu-\nu_0)/\alpha]^2+1}} \right] d\nu \quad (3.5)$$

Let $x \equiv \frac{S\mu_a}{2\pi\alpha}$ and $\nu' = \frac{\nu-\nu_0}{\alpha}$; $d\nu' = \frac{1}{\alpha} d\nu$ so

$$A = \frac{\alpha}{\Delta\nu} \int_{-\nu_0/\alpha}^\infty \left[1 - e^{-2x/(1+\nu'^2)} \right] d\nu' \quad (3.6)$$

If ν_0/α is a large number, $1 - e^{-2x/(1+\nu'^2)}$ will be

very close to zero for $v' < -v_0/\alpha$ provided that x is not too large. v_0/α is of the order of 10^4 for lines in the near infrared, so for $x \geq 10^6$ the lower limit may be extended to $-\infty$, and then

$$\begin{aligned} A &= \frac{\alpha}{\Delta v} \int_{-\infty}^{\infty} 1 - e^{-2x/(1+v'^2)} dv' \\ &= \frac{2}{\Delta v} \int_0^{\infty} 1 - e^{-2x/(1+v'^2)} dv' \end{aligned} \quad (3.7)$$

as the integrand is an even function of v' .

The integral can be evaluated exactly by substituting $v' = \tan\theta$ and eliminating the $\cos^2\theta$ terms which result by using $\cos^2\theta = 1/2(1+\cos 2\theta)$. The new form of the integral can then be related to Bessel functions. It is simpler to consider two limits in which the integral takes an elementary form. If the line is such that x is small compared to 1, the exponential is closely represented by the two leading terms of its Taylor expansion. Then

$$\begin{aligned} A &= \frac{2}{\Delta v} \int_0^{\infty} \frac{2x}{1+v'^2} dv' \\ &= \frac{4\alpha x}{\Delta v} \tan^{-1}(v') \Big|_{v'=0}^{v' \rightarrow \infty} \\ &= \frac{4\alpha x}{\Delta v} \left(\frac{\pi}{2} - 0 \right) \\ A &= \frac{S\mu_a}{\Delta v} \end{aligned}$$

(3.8)

This is the well known weak line limit. The mean absorption of a spectral line is linear with μ_a and independent of the half-width α . If there are N lines, with line strengths S_i , in the interval $\Delta\nu$ then under the same assumptions given above the mean absorption over the interval becomes

$$A = \frac{\mu_a}{\Delta\nu} \sum_{i=1}^N S_i \quad (3.9)$$

provided that any line overlap which occurs does not invalidate the two term Taylor expansion of the exponential. Similarly if there are several absorbing molecules, and S_{ij} is the line strength of the i^{th} line of the j^{th} molecule then

$$A = \frac{1}{\Delta\nu} \sum_j \sum_i \mu_{aj} S_{ij} \quad (3.10)$$

The independence of A from the line half-widths means that the result is independent of the pressure.

When x is large compared to 1, but much smaller than $1 + (\nu_0/\alpha)^2$, another sort of approximation can be made. In this case when $\nu' \approx 1$ the exponential is very close to zero. Only when $\nu'^2 \gg 1$ is the exponential factor large enough to make a difference. Physically this means that the line core is strongly saturated and only in the line wings is there less than 100% absorption. Under these conditions the 1 in the $1 + \nu'^2$ term may be neglected so that equation (3.6) becomes

$$A = \frac{2\alpha}{\Delta\nu} \int_0^{\infty} [1 - e^{-2x/v'^2}] dv' \quad (3.11)$$

provided the improper integral exists. Substituting

$$Z = \frac{\sqrt{2x}}{v'} \text{ gives}$$

$$A = \frac{2\alpha}{\Delta\nu} \sqrt{2x} \int_0^{\infty} (1 - e^{-Z^2}) \frac{dZ}{Z^2} \quad (3.12)$$

Now using integration by parts

$$\begin{aligned} \int_0^{\infty} (1 - e^{-Z^2}) \frac{dZ}{Z^2} &= -\frac{1}{Z} (1 - e^{-Z^2}) \Big|_{Z=0}^{Z \rightarrow \infty} + \\ &2 \int_0^{\infty} e^{-Z^2} dZ = 0 + 2[\frac{1}{2}\sqrt{\pi}] = \sqrt{\pi} \end{aligned} \quad (3.13)$$

so

$$A = \frac{2\alpha}{\Delta\nu} \sqrt{2\pi x} = \frac{2}{\Delta\nu} \sqrt{S\alpha\mu_a} \quad (3.14)$$

In this limit A increases as $\sqrt{\mu_a}$. This is the strong line limit. The slower growth of A with μ_a is due to the saturation of the line core; in the line core the absorption cannot increase further despite any increase in μ_a . Here A has an explicit pressure dependence through α . In this case $\Delta\nu$ must be larger than in the weak line case for a given value of ν .

The general equation for A when N lines, all due to one molecule, are present within the interval is (where the i^{th} line has a line strength S_i , a line half-width α_i and a center frequency ν_{oi})

$$A = \frac{1}{\Delta\nu} \int_{\Delta\nu} \left[1 - e^{-\sum_{i=1}^N \frac{S_i \alpha_i \mu_a}{\pi[(\nu - \nu_{oi})^2 + \alpha_i^2]} } \right] d\nu \quad (3.15)$$

for a homogeneous path. The equivalent for an inhomogeneous path is

$$A = \frac{1}{\Delta\nu} \int_{\Delta\nu} \left[1 - e^{-\sum_{i=1}^N \int_0^{\mu_a} \frac{S_i \alpha_i}{\pi[(\nu - \nu_{oi})^2 + \alpha_i^2]} d\mu'_a} \right] \quad (3.16)$$

The inhomogeneous medium requires an integration over the column density along the path. The line parameters will be functions of μ'_a because of changes in pressure and the temperature along the path. This form explicitly assumes the Lorentz profile to apply at every point. ν_{oi} has a very slight pressure dependence due to small perturbations of a molecule's energy levels by the presence of other molecules. This effect is small enough to be neglected. Under this assumption S_i is independent of the pressure, but has a temperature dependence. α_i is a function of both pressure and temperature.

In the earth's atmosphere the temperature variations are relatively small for the majority of the gas. Until high altitudes are reached, a temperature range from 200 K to 300 K is typical of a mean vertical profile at most locations. Above about 100 km from the earth's surface the temperature increases rapidly to values in the range 800 K to 1100 K, but only 1 part in roughly

10^7 of the total gas content of the atmosphere is in this layer. For these reasons the variation in S_i over the path is relatively small. In the extreme upper atmosphere the Lorentz profile does not apply anyway, so there the value of S_i does not matter. α_i is the main variable quantity in equation (3.15).

Sometimes it is said that the approximations which will be outlined here assume that the superposition of a series of Lorentz line profiles with different α values produces another Lorentz profile. Actually what is done is to seek for parameters such that the Lorentz line profile from a homogeneous path gives the same mean absorption as the superposition of Lorentz line profiles from the inhomogeneous path. A point by point match of the absorption function is not sought in the approximations which will be described here. This distinction must be kept in mind. For the numerical simulation of an observed object's magnitude to match the exact value, the interval $\Delta\nu$ over which the approximation applies must be such that the object spectrum does not change much over $\Delta\nu$. Otherwise errors will result in the numerical magnitude. Late-type stars have strong infrared spectral features due to the same molecules which predominate in causing atmospheric extinction, so if $\Delta\nu$ is chosen to satisfy the assumptions given above for one of these lines then the stellar spectrum will vary over $\Delta\nu$ due to the same spectral line. To some extent, then, these

approximations are less suitable for late-type stars than for early-type stars. Fortunately this effect is reduced when the filters are introduced into the simulation, as the strong absorption line regions tend to be excluded by the filter design.

If the weak line approximation applies, the inhomogeneous path equation becomes

$$A = \frac{1}{\Delta\nu} \int_{\Delta\nu} \sum_{i=1}^N \int_0^{\mu_a} \frac{S_i \alpha_i}{\pi[(\nu - \nu_{oi})^2 + \alpha_i^2]} d\mu'_a d\nu \quad (3.17)$$

Once again, assuming $\Delta\nu$ to be large enough that the lines in the summation have no significant absorption outside the interval, the range of integration over ν may be extended to all ν . Exchanging the order of integration and taking the sum outside the integrals gives

$$A = \frac{1}{\Delta\nu} \sum_{i=1}^N \int_0^{\mu_a} S_i \int_0^{\infty} \frac{\alpha_i d\nu}{\pi[(\nu - \nu_{oi})^2 + \alpha_i^2]} d\mu'_a \quad (3.18)$$

Proceeding in the same manner as before,

$$\begin{aligned} A &= \frac{1}{\Delta\nu} \sum_{i=1}^N \int_0^{\mu_a} S_i \int_{-\nu_{oi}}^{\infty} \frac{i}{\pi(x^2 + \alpha_i^2)} dx d\mu'_a \\ &= \frac{1}{\Delta\nu} \sum_{i=1}^N \int_0^{\mu_a} S_i \frac{2}{\pi} \int_0^{\infty} \frac{\alpha_i}{x^2 + \alpha_i^2} dx d\mu'_a \\ &= \frac{1}{\Delta\nu} \sum_{i=1}^N \int_0^{\mu_a} S_i \frac{2}{\pi} (\tan^{-1}[x] \Big|_{x=0}^{x \rightarrow \infty}) d\mu'_a \\ &= \frac{1}{\Delta\nu} \sum_{i=1}^N \int_0^{\mu_a} S_i \frac{2}{\pi} (\frac{\pi}{2} - 0) d\mu'_a \\ A &= \frac{1}{\Delta\nu} \sum_{i=1}^N \int_0^{\mu_a} S_i d\mu'_a \quad (3.19) \end{aligned}$$

Comparison with the homogeneous result (equation 3.8),

$$A_n = \frac{1}{\Delta\nu} \sum_{i=1}^N S_{ih} \mu_{ah} \quad (3.20)$$

where subscript h denotes quantities of the homogeneous layer, shows that for a general inhomogeneous layer assigning

$$\mu_{ah} = \frac{\sum_{i=1}^N \int_0^{\mu_a} S_i d\mu'_a}{\sum_{i=1}^N S_{ih}} \quad (3.21)$$

gives agreement between A and A_h . In the weak line limit A does not depend upon α_i , so that adjusting μ_{ah} to take care of the line strength S along the path is all that is needed. The S_{ih} values are found by assigning some temperature to the homogeneous path, usually chosen to be near the mean value of T along the inhomogeneous path although this is not required. A pressure value corresponding to the mean temperature is then chosen so that the α_i values can be found for calculational purposes, but the result is independent of this choice as long as the weak line limit applies.

The parameters for the equivalent homogeneous layer are also independent of ν and $\Delta\nu$ provided that the ratios $\frac{\nu_{oi}}{\alpha_i}$ and $\frac{\Delta\nu}{\alpha_i}$ are large enough that the integrations are accurate. The approximation can be done separately for each absorbing molecule as long as any line overlap which occurs does not invalidate the weak line assumption.

Considering now the strong line limit, and neglecting α_i^2 in the denominator of the exponential term of equation (3.15) gives

$$A = \frac{1}{\Delta\nu} \int_{\Delta\nu} \left[1 - e^{-\sum_{i=1}^N \int_0^{\mu_a} \frac{S_i \alpha_i}{\pi(\nu - \nu_{oi})^2} d\mu'_a} \right] d\nu \quad (3.22)$$

while the homogeneous form is

$$A_h = \frac{1}{\Delta\nu} \int_{\Delta\nu} \left[1 - e^{-\sum_{i=1}^N \frac{S_{ih} \alpha_{ih}}{\pi(\nu - \nu_{oi})^2} \mu_{ah}} \right] d\nu \quad (3.23)$$

In this limit no integrations can be performed without specific information about the spectral lines and the path under consideration. However, if things can be arranged so that

$$\sum_{i=1}^N \frac{S_{ih} \alpha_{ih}}{(\nu - \nu_{oi})^2} \mu_{ah} = \sum_{i=1}^N \int_0^{\mu} \frac{S_i \alpha_i}{\pi(\nu - \nu_{oi})^2} d\mu'_a \quad (3.24)$$

over the interval $\Delta\nu$ then A and A_h will be identical.

Putting in the pressure and temperature dependence of α_i gives

$$\sum_{i=1}^N \frac{S_{ih} \alpha_{oi} P_h T_o^{\frac{1}{2}}}{P_o T_h^{\frac{1}{2}} (\nu - \nu_{oi})^2} \mu_{ah} = \sum_{i=1}^N \frac{\alpha_{oi} T_o^{\frac{1}{2}}}{P_o \pi (\nu - \nu_{oi})^2} \int_0^{\mu_a} S_i P T^{-\frac{1}{2}} d\mu'_a$$

or

$$\sum_{i=1}^N \frac{\alpha_{oi} S_{ih} P_h}{T_h^{\frac{1}{2}} (\nu - \nu_{oi})^2} \mu_{ah} = \sum_{i=1}^N \frac{\alpha_{oi}}{(\nu - \nu_{oi})^2} \int_0^{\mu_a} S_i P T^{-\frac{1}{2}} d\mu'_a \quad (3.25)$$

This may be simplified further by assuming α_{oi} to be the same for all the lines. The α_o value is then a constant and may be eliminated from the equation. A constant value for α_o implies that the molecule has the same collision cross-section in any of the energy levels involved in producing the infrared lines. What is left is still rather complicated

$$\sum_{i=1}^N \frac{1}{(\nu - \nu_{oi})^2} S_{oi} P_h T_h^{-1/2} \mu_{ah} = \sum_{i=1}^N \frac{1}{(\nu - \nu_{oi})^2} \int_0^{\mu_a} S_i P T^{-1/2} d\mu'_a \quad (3.26)$$

The overt dependence upon ν is a problem, as the equation must hold for a range $\Delta\nu$ and yet have the homogeneous path parameters independent of ν over the interval in order to have achieved a simplification of the problem. Somehow the summation must be eliminated from equation (3.25) to get a useful result.

There are several cases under which the desired simplification occurs. If all of the lines have the same relative temperature dependence, so that $S_i = S_{oi} S(T)$ then the summation over i becomes common on both sides of equation (3.25). What is left is

$$P_h T_h^{-1/2} S(T_h) \mu_{ah} = \int_0^{\mu_a} S(T) T^{-1/2} P d\mu'_a \quad (3.27)$$

which may be satisfied by a variety of P_h , T_h and μ_{ah} values. Another useful situation occurs when the inhomogeneous path is isothermal, so with $T = T_h$ and $S_i = S_{ih}$ equation (3.25) becomes

$$P_h \mu_{ah} = \int_0^{\mu_a} P d\mu'_a \quad (3.28)$$

This has two parameters, thus again a whole range of values of P_h and μ_{ah} may be chosen to fit the condition. No unique result is found.

The strong line limit does not yield as general a result as the weak line limit, because the ν integration cannot be evaluated within the summation. When conditions are such that the ν dependence can be eliminated from the relation between the homogeneous and the inhomogeneous paths, the result holds for any set of lines within $\Delta\nu$ whether there is line overlap or not provided that the strong line approximation is valid.

The Curtis-Godson approximation is obtained by combining the approximation given for the weak line limit with that given for the strong line limit. The weak line limit requires T_h to be set, whereupon μ_{ah} is found, but P_h is arbitrary. In the strong line limit if T_h and μ_{ah} are set then P_h will be fixed by the constraint found to make A equal to A_h . Thus, the two can be combined in such a way that for a given inhomogeneous path the three parameters for an equivalent homogeneous path are fixed and as a result the mean absorption is matched in both the weak line limit and the strong line limit. The main limitation on the combined approximation is that the line strengths S_i must obey restrictions in order for a

useful strong line limit constraint to be obtained; for a group of lines with different line strengths and temperature dependences of these line strengths the inhomogeneous path must be nearly isothermal for any useful approximation to be made to a homogeneous path.

Where the Curtis-Godson approximation method can be applied, it is quite accurate for any arbitrary set of lines. Some errors occur due to lines of intermediate strength, but the errors are not too serious because the lines blend smoothly from the weak line limit through to the strong line limit. Any function which matches for strong and weak lines will match intermediate lines reasonably well too.

The isothermal case gives the most general and most useful form of the Curtis-Godson approximation. The weak line limit gives

$$\mu_{ah} = \frac{\sum_{i=1}^N \int_0^{\mu_a} S_i d\mu'_a}{\sum_{i=1}^N S_{ih}} = \frac{\sum_{i=1}^N S_{ih}}{\sum_{i=1}^N S_{ih}} \int_0^{\mu_a} d\mu'_a = \mu_a \quad (3.29)$$

provided T_h is chosen to be the same as T for the inhomogeneous layer. The strong line limit gives

$$P_h = \frac{\int_0^{\mu_a} P d\mu'_a}{\mu_a} \quad (3.30)$$

The equivalent homogeneous path has the same total column density and the same temperature as the inhomogeneous path, and a weighted mean pressure value. This assumes an isothermal path, a pressure-broadened Lorentz line shape and that the ratios μ_a and μ_{ah} are large for all the lines under consideration.

Often it is easier to use P as the variable of integration rather than μ_a . If the curvature of the atmosphere is neglected, then with ρ representing the total gas density and C the fractional abundances of the absorbing molecule

$$d\mu'_a = C\rho \sec\theta dZ \quad (3.31)$$

for a path at an angle θ to the vertical Z axis. The barometric law is

$$dP = -\rho g dZ \quad (3.32)$$

with g the acceleration of gravity. Combining these two equations gives

$$d\mu'_a = -\frac{C}{g} \sec\theta dP \quad (3.33)$$

Let the layer under consideration have a pressure range $P_1 \leq P \leq P_2$, and assume that θ is a constant along the path; then

$$\begin{aligned} \mu_{ah} = \mu_a &= \int_{P_2}^{P_1} \frac{C}{g} \sec\theta dP \\ &= \sec\theta \int_{P_2}^{P_1} \frac{C(P)}{g} dP \end{aligned} \quad (3.34)$$

$$\begin{aligned}
 P_h &= \frac{1}{\mu_{ah}} \int_{P_1}^{P_2} \frac{PC(P)}{g} dP \\
 &= \frac{\int_{P_1}^{P_2} \frac{PC(P)}{g} dP}{\int_{P_1}^{P_2} \frac{C(P)}{g} dP} \quad (3.35)
 \end{aligned}$$

g is usually taken to be constant over the layer, which is more reasonable than assuming the atmosphere to be isothermal. The parameter equations then become

$$\mu_a = \frac{\sec \theta}{g} \int_{P_1}^{P_2} C(P) dP \quad (3.36)$$

$$P_h = \frac{\int_{P_1}^{P_2} PC(P) dP}{\int_{P_1}^{P_2} C(P) dP} \quad (3.37)$$

For a molecule which is uniformly mixed $C(P)$ becomes a constant, so

$$\mu_a = \frac{C}{g} \sec \theta (P_2 - P_1) \quad (3.38)$$

$$P = \frac{1}{2} (P_2 + P_1)$$

The parameters may be evaluated for each molecule which contributes line absorption over the interval being simulated, to apply to every line of that molecule. Then the atmospheric absorption can be calculated using the simple formulae which hold for a

homogeneous path. The scaling relation between the absorption at any wavelength and the air mass is the same as for the monochromatic case, as is implicit in the μ_a formula. The $\sec\theta$ term is simply replaced by X once atmospheric curvature is taken into account.

The overall accuracy of the Curtis-Godson approximation is a difficult quantity to judge when it is applied to atmospheric models. The three crucial questions are

- 1) how well does the isothermal assumption apply;
- 2) how many lines are of intermediate strength; and
- 3) how well is $C(P)$ known?

Each of these will cause some uncertainty in the calculated absorption profile. The first two problems are inherent in the method, while the third problem is a problem of atmospheric physics. In any single layer model, in which the Curtis-Godson approximation is applied to the whole atmosphere, the assumption of an isothermal layer is the most troublesome aspect of the model. It would seem that some allowance should be made for this save that, when dealing with thousands of lines with differences in the temperature dependence, evaluating the strong line limit parameters or μ_{ah} from the weak line limit becomes a very difficult task. Under those circumstances the isothermal assumption is necessary to produce any results at all. Otherwise a full numerical integration over the path would have to be done point by point, which is simply impractical.

The uncertainty in $C(P)$ is serious for H_2O and O_3 , but not for the other atmospheric gases. In the case of such molecules as CO_2 , CO , O_2 , CH_4 and N_2O it is reasonable to assume $C(P)$ to be constant provided there are no local sources of these molecules at the site under consideration. H_2O and O_3 are so strongly variable over time and with position in the atmosphere that finding $C(P)$ is very difficult. There is really no alternative but to use some sort of mean profile for these molecules and hope that the results reflect a type of average condition for the site.

When broad regions of the infrared spectrum are to be simulated by the Curtis-Godson technique to calculate the atmospheric absorption, the assumptions about the $\frac{\nu_0}{\alpha}$ and $\frac{\Delta\nu}{\alpha}$ ratios are quite well satisfied. Typical α values for the seven molecules listed above are of the order of 0.07 cm^{-1} for $P \approx 1$ atmosphere and $T \approx 298 \text{ K}$. For O_3 the α values are typically 0.11 cm^{-1} under such conditions, but it exists higher in the atmosphere so the α values will still be near 0.07 cm^{-1} on the average. In the $1\mu\text{m}$ to $2.5\mu\text{m}$ wavelength range ν varies from 4000 cm^{-1} to $10\,000 \text{ cm}^{-1}$, so $\frac{\nu_0}{\alpha} \gtrsim 5 \times 10^4$. $\frac{\Delta\nu}{\alpha}$ is of the same order as $\frac{\nu}{\alpha}$. Clearly, there will be no problem with the weak line limit approximation.

Chapter Four

The Single Layer Model Results

In view of the results obtained by Manduca and Bell (1979) [once again denoted as MB], the normal extinction correction procedure must be considered as being suspect. This is supported by the general theory of atmospheric absorption, as was outlined in Chapter 1. Nevertheless, before this deeply ingrained procedure in infrared photometry is discredited, the calculations of MB must be verified. For this reason a set of calculations were undertaken using very similar methods to those used in MB. The results of these calculations are discussed in this chapter.

The calculations dealt with here are not, strictly speaking, directly comparable to those of MB because of several small differences in approach which stem from independently developing a set of programs to do the numerical simulation. Also, MB give no explicit details about the assumed photometer response or the stellar source functions which they use, although they state that an InSb detector (77K) response function was used for the calculations and give the parameters of the stellar models used, so in the new calculations these are somewhat different. The program used here to calculate the atmospheric transmittance, denoted as MC, differs somewhat from IRTRANS. The filter response profiles for the new (1979) Kitt Peak National

Observatory filter set are slightly different than the previous set for which MB perform their calculations. As a result, quantitative comparisons between these results and the MB results are difficult. The qualitative features turn out to be quite similar in the two cases, so the implications for the relevance of the linear extinction law are reinforced.

The program MC is an adapted version of a spectral simulation program developed by McClatchey, et. al., (1973) and coded for the University of Calgary computer by R.T. Boreiko. The original program was intended to simulate a transmittance spectrum including a convolution with a slit function, to allow comparison with spectroscopic data. This was modified to eliminate the convolution, just producing the transmittance as a function of wavelength. The resulting program calculates the transmittance for a layer of gas drawing upon the McClatchey line parameter compilation (McClatchey, et. al., 1973). The layer is assumed to be homogeneous. Pressure, temperature and column density values can be chosen separately for each of the seven absorbing molecules. The Lorentz profile was assumed throughout. The program produces data at points spaced by $\Delta\nu$ in wavenumber.

Transmittance calculations were carried out from $\nu = 3840 \text{ cm}^{-1}$ to $\nu = 10\,970 \text{ cm}^{-1}$, at 0.2 cm^{-1} resolution. In wavelength units this corresponds to $0.912 \mu\text{m}$ to

2.60 μm . That range includes the J, H and K filters, equivalent to the Kitt Peak JHK filters for which MB carried out their calculations. The L filters were not covered for two reasons: MB performed only preliminary calculations for this wavelength region, and computer runs showed that beyond 2.60 μm a large number of lines occur. This group of lines would have resulted in costly computation in order to extend the calculations out to 4.3 μm . The final transmittance data served as input to a second program which performed the numerical integration to produce magnitude values.

Once the molecular parameters are set, the additional input data required for the transmittance calculation is $\Delta\nu$, interval limits ν_1 and ν_2 over which the calculations are to be done, and a parameter ν' which is chosen so that for the spectral lines under consideration absorption beyond a distance ν' from line center is negligible. Each run of MC covered only a small part of the total range for which calculations were done, typically on interval of 300 cm^{-1} .

Given the correct input data, and the McClatchey data files, program MC proceeded in the following way. Starting at $\nu_1 - \nu'$ the data files were searched for lines. Using the column density data plus the line parameters as adjusted to the proper temperature and pressure values, the optical depth at line center was

then calculated for each line as it was reached. Any line with an optical depth below 0.001 at line center was then ignored. The process continued until either 3000 lines had been read in, in which case ν_2 was redefined so that the 3001st line was beyond $\nu_2 + \nu'$ and $\nu_2 - \nu_1$ was a multiple of $\Delta\nu$, or until $\nu_2 + \nu'$ was reached. MC was set up so that the interval $\nu_1 \leq \nu \leq \nu_2$ must be less than 3001 $\Delta\nu$, since the arrays in the program were defined to be this size. If the line density was such that more than 3000 lines fall between $\nu_1 - \nu'$ and $\nu_1 + \nu'$ an error message resulted and the program halted.

The sequence of grid points $\nu_1, \nu_1 + \Delta\nu, \dots, \nu_2 - \Delta\nu, \nu_2$ was then dealt with point by point. At a particular grid point ν_i all the lines which satisfied the minimum absorption condition in the range $\nu_i - \nu' \leq \nu \leq \nu_i + \nu'$ were used to produce k_λ by summation. For lines within $\pm 2\Delta\nu$ of ν_i instead of the Lorentz formula for k_λ an integrated average

$$k'_\lambda(\nu_i) = \frac{1}{\Delta\nu} \int_{\nu_i - \frac{1}{2}\Delta\nu}^{\nu_i + \frac{1}{2}\Delta\nu} k_\lambda(\nu) d\nu \quad (4.1)$$

is used. It can easily be shown that for a Lorentz line of half-width α_j and line strength S_j centered at ν_{oj}

$$k'_\lambda(\nu_i) = \frac{S_j}{\pi\Delta\nu} \left[\tan^{-1} \frac{\nu_i + \frac{1}{2}\Delta\nu - \nu_{oj}}{\alpha_j} - \tan^{-1} \frac{\nu_i - \frac{1}{2}\Delta\nu - \nu_{oj}}{\alpha_j} \right] \quad (4.2)$$

The same comments about the accuracy of this approximation apply here as they did in Chapter 2 when IRTRANS was outlined. This is good in the weak line case, but otherwise k'_λ will be systematically too large. The saving feature is that for saturated lines the k_λ value are so large that the exact value makes little difference. As long as $\frac{\Delta\nu}{\alpha}$ is not too large this type of integration is useful, but otherwise it will cause a systematic error.

In IRTRANS the Voigt profile was used for some lines. This was not done in MC, but this should make little difference when ground-based sites are being modelled. An adjustment which was attempted was to refine the k'_λ equation by extending the approximation to second order, but problems were encountered and no better approximation was obtained. When the total k_λ was found, exponentiation gave the fractional transmittance at ν_i . The aerosol and Rayleigh contributions were added later, in the numerical integration program.

If the difference between the Voigt profile and the Lorentz profile is ignored, then three main differences between the approach in IRTRANS and that in MC remain:

1) IRTRANS includes lines down to a minimum line center optical depth of 0.0005, while MC includes lines down to 0.001;

2) IRTRANS eliminates line wings when their optical depth falls below 0.0005, while MC cuts off line wings

at ν' , 30 cm^{-1} in actual value, from line center regardless of what the optical depth is at that point;

3) IRTRANS moves lines onto the grid points, while MC treats the lines in their actual positions. A minor difference is that the line core integration is done for lines within $\pm 2\Delta\nu$ of each grid point in MC, but only $\pm 1/2 \Delta\nu$ in IRTRANS.

The effect of these discrepancies is somewhat difficult to evaluate. If weak lines are present, (1) will cause an underestimate of the absorption by MC compared to IRTRANS, but this will be partially offset by (2) as with $\alpha \approx 1/2 \Delta\nu$ in IRTRANS lines which contribute between 0.001 and 0.0005 to k_λ at line center will be included only at the 'home' grid point. For slightly stronger lines (2) implies that IRTRANS would underestimate the absorption if the line wing beyond 30 cm^{-1} from line center is still of importance. This effect was looked for in the case of strong lines by examining the print-out of the atmospheric transmittance calculations. Looking near 30 cm^{-1} from line center, no discontinuity was seen. This search was not exhaustive and does not rule out a small effect of this type. Difference (3) would tend to make the MC results more accurate than those of IRTRANS.

The criterion for strong line absorption in the wings beyond ν' from line center may be quantified as follows. For any line, with the Lorentz profile,

$$k_{\lambda}(\nu) = k_{\lambda}(\nu_0) \left[\left(\frac{\nu - \nu_0}{\alpha} \right)^2 + 1 \right]^{-1} \quad (4.3)$$

When $|\nu - \nu_0| = \nu'$, differences occur if $k_{\lambda}(\nu)$ is greater than 0.0005. No problem occurs if

$$k_{\lambda}(\nu \pm \nu') = k_{\lambda}(\nu_0) \left[\left(\frac{\nu'}{\alpha} \right)^2 + 1 \right]^{-1} \leq 0.0005 \quad (4.4)$$

If $\alpha \approx 0.05 \text{ cm}^{-1}$ and $\nu' = 30 \text{ cm}^{-1}$ equation (4.4) requires that $k_{\lambda}(\nu_0) \leq 180$, while if $\alpha \approx 0.02$ the corresponding limitation is $k_{\lambda}(\nu_0) \leq 1125$. These limits seem high enough to be of no concern for the column density values of the atmosphere, except possibly for a few very strong H_2 and CO_2 lines. From the strong line data for these molecules given in McClatchey, et. al., (1973) and the column density values given in MB the $k_{\lambda}(\nu_0)$ values can be estimated for these lines. In a few isolated cases there is some cause for concern, but these lines should not produce a general effect in the resulting magnitude values.

In order to gain some idea of the accuracy of the transmittance calculations, which have $\Delta\nu = 0.20 \text{ cm}^{-1}$ to match MB, a set of calculations were carried out at a resolution of 0.0020 cm^{-1} . These calculations should be nearly exact because $\frac{\Delta\nu}{\alpha}$ is small. The resulting values were then degraded to 0.20 cm^{-1} resolution by simple averaging for comparison with the 0.20 cm^{-1} resolution values. A typical high resolution calculation would yield 30 comparison points. The error in the lower

resolution calculations was expressed in terms of a root mean square transmittance error, with the signs of the individual transmittance differences recorded to check for any systematic tendency in the differences.

The 0.2 cm^{-1} resolution calculations which were done without the line core integration had a root mean square deviation of about 6%, with the deviations being larger in regions where the transmittance changed by a large amount ($> 10\%$) over the 0.20 cm^{-1} interval. Including the line core integration reduced the error by a factor of 3, to just less than 2%. This error was deemed to be too large, as it would imply an error of about ± 0.02 magnitudes in the end results. MB's results should have had an error of this order or perhaps slightly more, because of the comparatively narrow range of near line integration and because the lines were centered on the grid points. The line wing problem is of little concern here unless there are a large number of strong lines which fail the criterion given above.

In order to reduce the error but still produce results at a 0.20 cm^{-1} resolution it was decided to decrease $\Delta\nu$ to 0.10 cm^{-1} for the calculations and average adjacent values to recover the 0.20 cm^{-1} resolution needed to match MB. Comparison with the high resolution calculations showed that this decreased the root mean square error to 0.80%, for a sample of 205

points drawn from seven different wavelength regions over the interval of interest. Three of the sample regions were in areas of strong absorption while the others were from the filter windows. In the latter group the root mean square errors were in the 0.5% to 0.6% range, while for the former group the errors ran to 1% on the average. No systematic trend was seen for the results to be positive or negative.

Considering that there will be some cancellation between positive and negative fluctuations and that the filters tend to exclude strong absorption regions, the overall accuracy of the average result for a filter bandpass is expected to be 0.5% to 0.6% leading to a magnitude error of 0.005 to 0.006 magnitudes. The input parameters must be considered as being exact for this type of modelling, so this will be the formal error of the results. There may be systematic errors, as noted above and in Chapter 3, in addition to this source of error.

The numerical integration program calculates the aerosol and Rayleigh extinction using the formulae of Hayes and Latham (1975). For the Kitt Peak altitude of 2.06 km the aerosol extinction contributes 0.02 to 0.01 magnitudes per air mass for the JHK filters, as was noted in Chapter 2, while the Rayleigh contribution is much smaller still.

The filter response profiles which were used here

are shown in Figures 5 through 7. The data is from filter response measurements obtained from Joyce (1982), sampled at least every 0.01 A. In the numerical integration program these discrete points were approximated by a continuous fit. For three points ν_1 , ν_2 and ν_3 with $\nu_1 < \nu_2 < \nu_3$ for which the filter response data is known, the program uses a quadratic fit to the three points to cover $1/2 (\nu_1 + \nu_2) < \nu < 1/2 (\nu_2 + \nu_3)$. At the end points a linear fit was used to avoid negative filter response values. Such a fitting procedure will introduce small errors except at the sampled points when compared to the real filter response, but the exact magnitude of this error depends upon the set of sample points and so is difficult to estimate in practice.

In the numerical integration program the stellar source functions were assumed to be blackbody source functions, because details of the models used by MB were not available and to reduce the cost of the calculations were not available. For Vega a 9100 K blackbody was used; this matches the colour temperature of Vega obtained from the infrared data of Gehrz, Hackwell and Jones (1974) beyond $2.3\mu\text{m}$. Indications from MB imply that the Δ values decrease with wavelength so the fit to longer wavelength measurements was presumed to be accurate. The standard T_{EFF} value of near 9650 K for Vega (Dreiling and Bell, 1980) is too

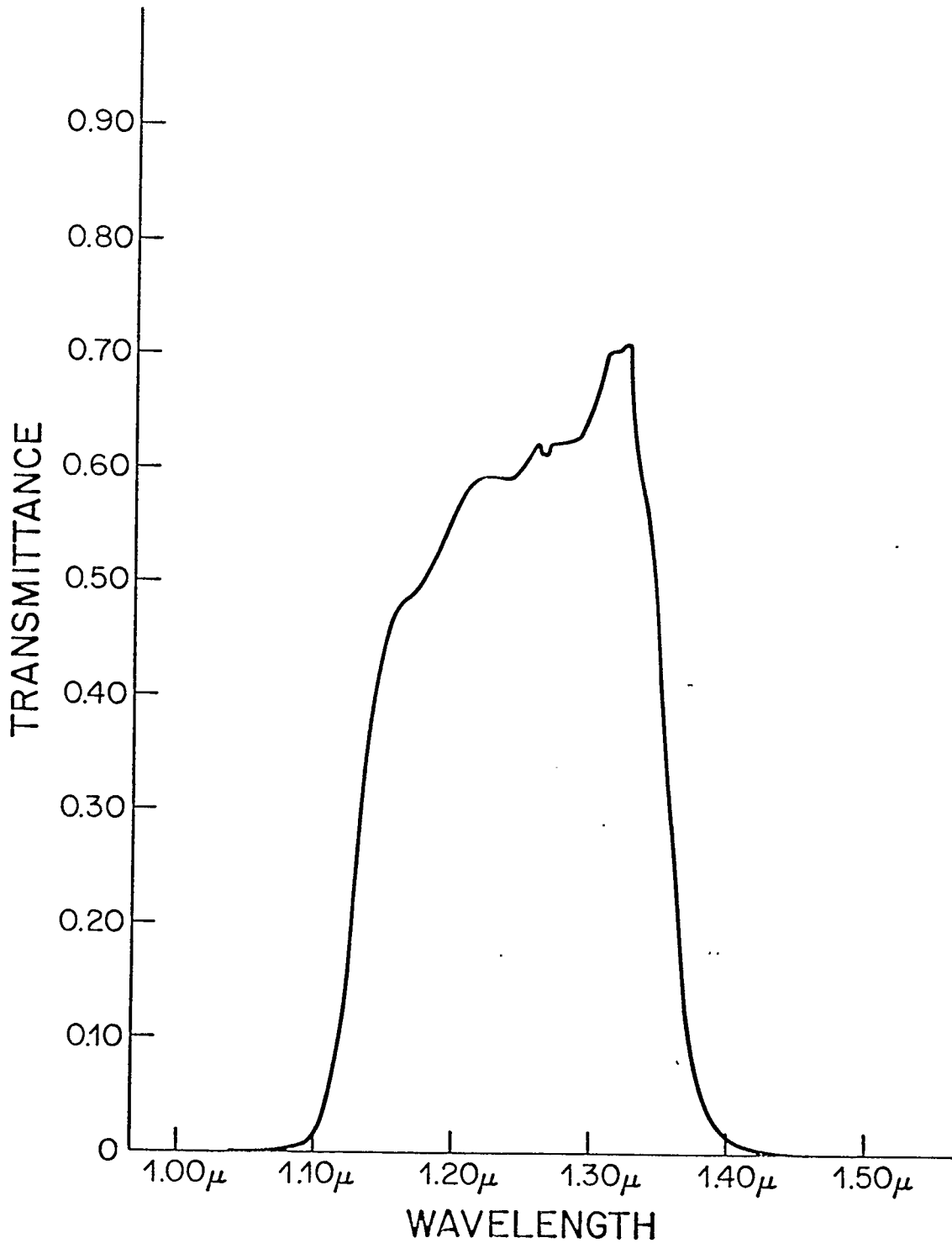


Figure 5- The filter response profile as a function of wavelength for the new (post-1979) Kitt Peak J filter (Joyce, 1982).

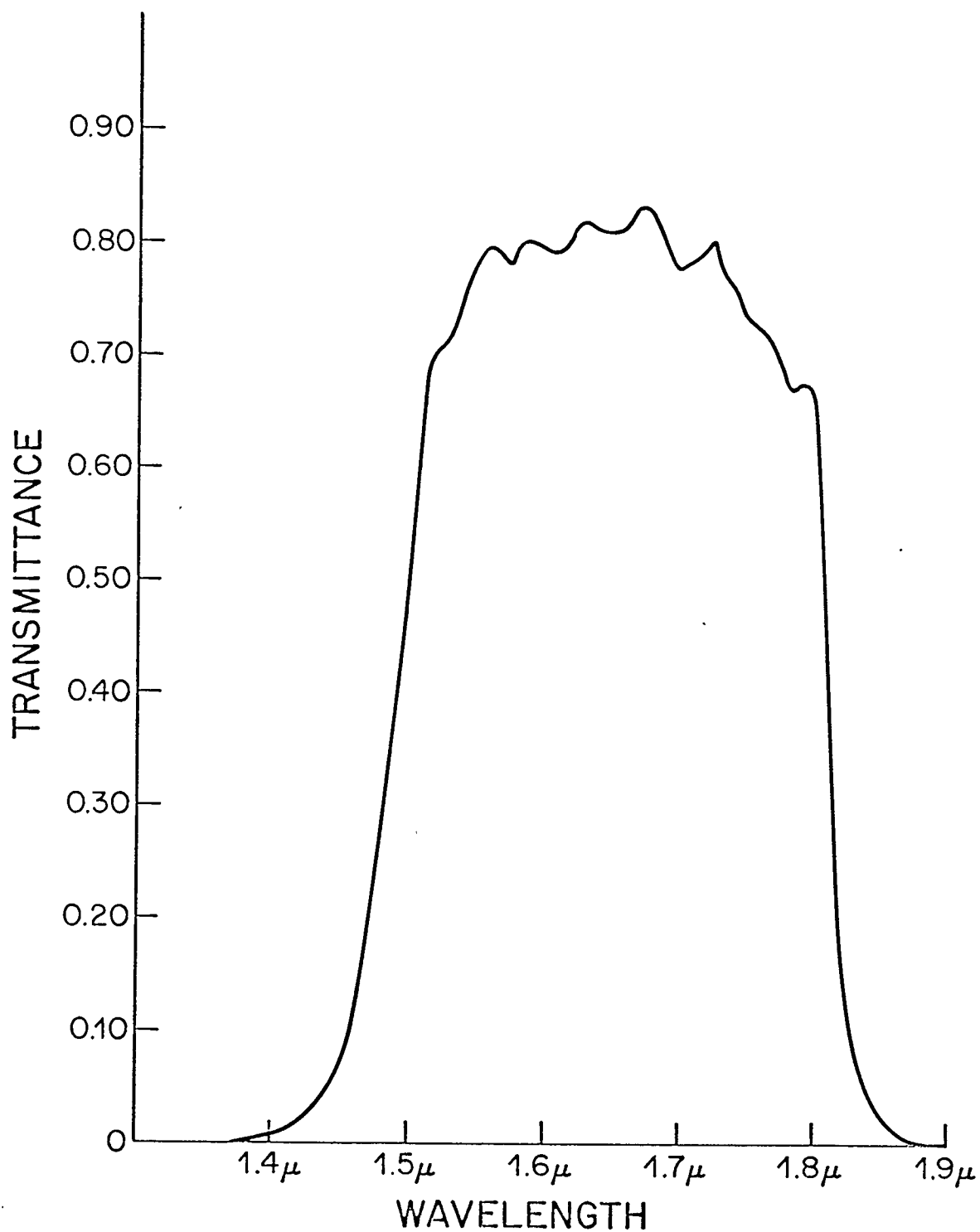


Figure 6- The filter response profile as a function of wavelength for the new (post-1979) Kitt Peak H filter (Joyce, 1982).

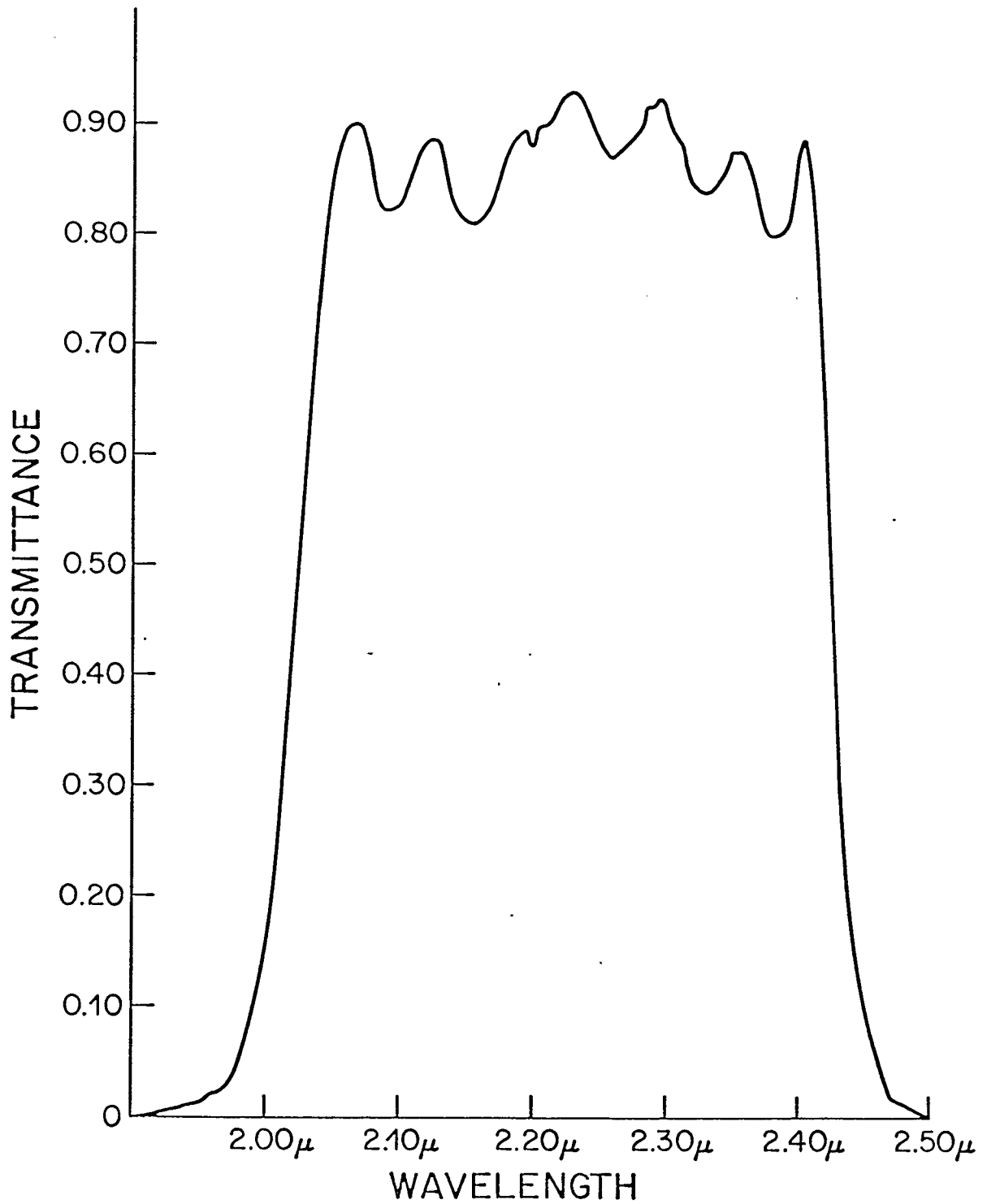


Figure 7- The filter response profile as a function of wavelength for the new (post-1979) Kitt Peak K filter (Joyce, 1982).

high to apply to the infrared, as is the case for the sun. If extinction errors have caused the colour temperature to be in error, the results should still apply reasonably well for some type of late B/early A type star. A 4000 K blackbody was also used for calculations, as in MB. If molecular line features are ignored this corresponds to a star of spectral type K5. Since the extinction should not depend upon overall intensity, there was no need to worry about setting the filter zero point flux values to match the observed magnitudes of Vega.

The photometer response was assumed to be constant over the entire wavelength range. Although this is somewhat unrealistic, this is the ultimate aim of good photometer design. The InSb detector response is nearly flat over the JHK filter range, so this is a very small concern. That is especially true because of the much larger difference in filter response functions.

All the calculations which were done with the single layer Curtis-Godson approximation used the set of parameters referred to as "Kitt Peak summer" by MB. The only quantity which was changed was the H₂O column density. A value equivalent to 5.05 Pmm was initially used, followed by calculations with values of 2.50, 7.54 and 10.10 Pmm of water.

The results obtained here are summarized in Table

3, and are presented in graphical form in Figures 8a through 8h. These results may be compared more or less directly with the results given in MB under "Kitt Peak summer". The qualitative features are the same as for the results of MB. For $X > 1.00$ there is some curvature in the extinction curves, which tend to flatten out as X increases. The main curvature occurs at very low air mass values, often below $X = 0.30$. This type of functional form is what is expected to result from the square-root law, although the aerosol extinction contributes a significant linear component to the curve.

One feature of these curves which does not appear in the MB results is the crossing over of the H and K extinction curves. This implies, contrary to MB, that a larger slope from $X = 1.00$ to $X = 2.00$ does not also imply a larger zero point correction. The cross-over point moves to higher X values as the H_2O column density increases. This particular feature implies that the extinction curves have distinct shapes, in which case it would not be possible to produce a 'standard extinction curve' which could be adopted to different sites and filters in a relatively simple manner.

Direct comparison with the MB results shows some systematic trends. In Figure 9 the two sets of results are given for the 4000 K source; the Vega results give a very similar diagram, and so are not plotted.

COLUMN DENSITY	MODEL	FILTER	E	Δ	Δ/E	δ
2.50 PPM	VEGA MODEL	J	0.069	0.067	0.970	0.0026
		H	0.044	0.031	0.705	0.0005
		K	0.051	0.031	0.597	-0.0009
	4000K MODEL	J	0.070	0.070	1.007	
		H	0.044	0.031	0.717	
		K	0.051	0.030	0.587	
5.05 PPM	VEGA MODEL	J	0.085	0.099	1.174	0.0036
		H	0.052	0.050	0.950	0.0007
		K	0.059	0.037	0.624	-0.0007
	4000K MODEL	J	0.084	0.103	1.221	
		H	0.052	0.050	0.965	
		K	0.058	0.036	0.624	
7.54 PPM	VEGA MODEL	J	0.093	0.119	1.284	0.0037
		H	0.055	0.059	1.074	0.0006
		K	0.062	0.039	0.640	-0.0007
	4000K MODEL	J	0.092	0.123	1.333	
		H	0.054	0.059	1.087	
		K	0.061	0.039	0.636	
10.10 PPM	VEGA MODEL	J	0.100	0.137	1.363	0.0037
		H	0.058	0.068	1.189	0.0007
		K	0.065	0.043	0.660	-0.0006
	4000K MODEL	J	0.099	0.140	1.412	
		H	0.057	0.069	1.202	
		K	0.065	0.043	0.657	

Table 3 - Results of the single layer Kitt Peak summer calculations. E, Δ and δ are defined in Manduca and Bell (1979) and on page 51. δ and Δ are in magnitudes, E is in magnitudes per air mass.

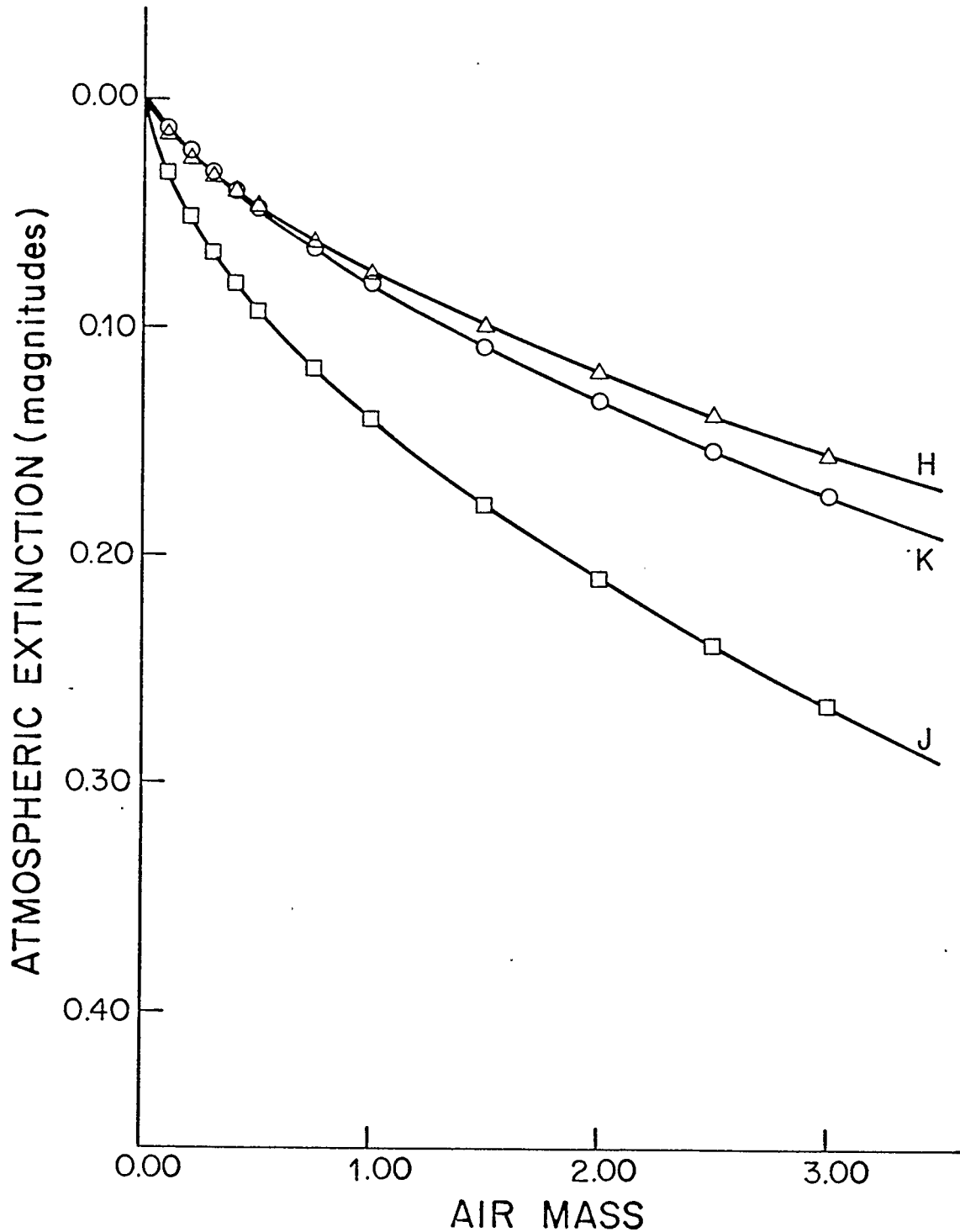


Figure 8a- Single layer results for Kitt Peak.

H₂O column density- 2.50 PMM; 4000 K model.
 Slopes (1.00 to 2.00 air mass) Zero point errors
 J- 0.0699 mag./a.m. J- 0.0702 mag.
 H- 0.0436 H- 0.0313
 K- 0.0508 K- 0.0298

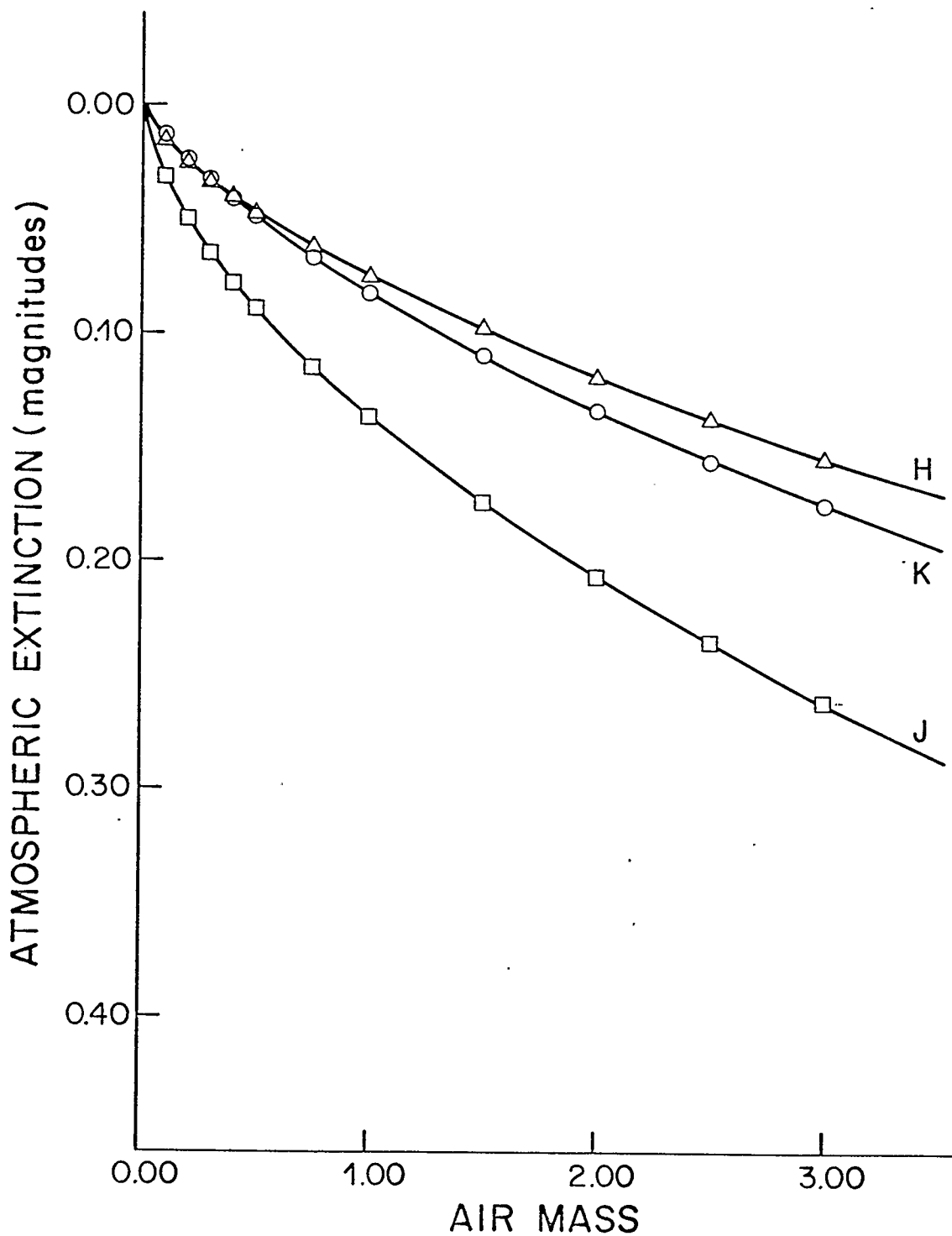


Figure 8b- Single layer results for Kitt Peak.

H₂O column density- 2.50 PMM; Vega/9100 K model.
 Slopes (1.00 to 2.00 air mass) Zero point errors
 J- 0.0695 mag./a.m. J- 0.0674 mag.
 H- 0.0437 H- 0.0308
 K- 0.0515 K- 0.0307

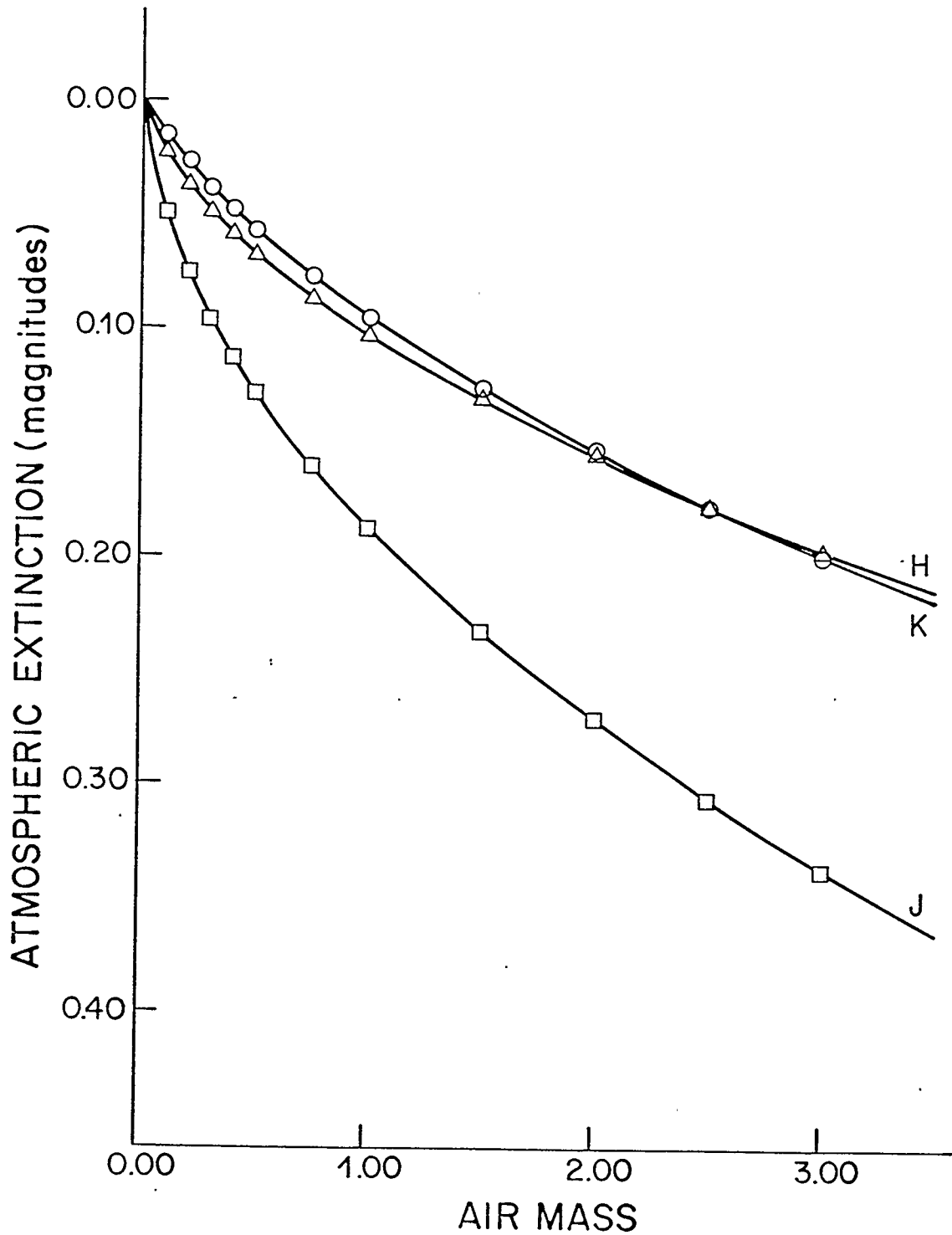


Figure 8c- Single layer results for Kitt Peak.

H₂O column density- 5.05 PMM; 4000 K model.
 Slopes (1.00 to 2.00 air mass) Zero point errors
 J- 0.0843 mag./a.m. J- 0.1029 mag.
 H- 0.0522 H- 0.0503
 K- 0.0582 K- 0.0370

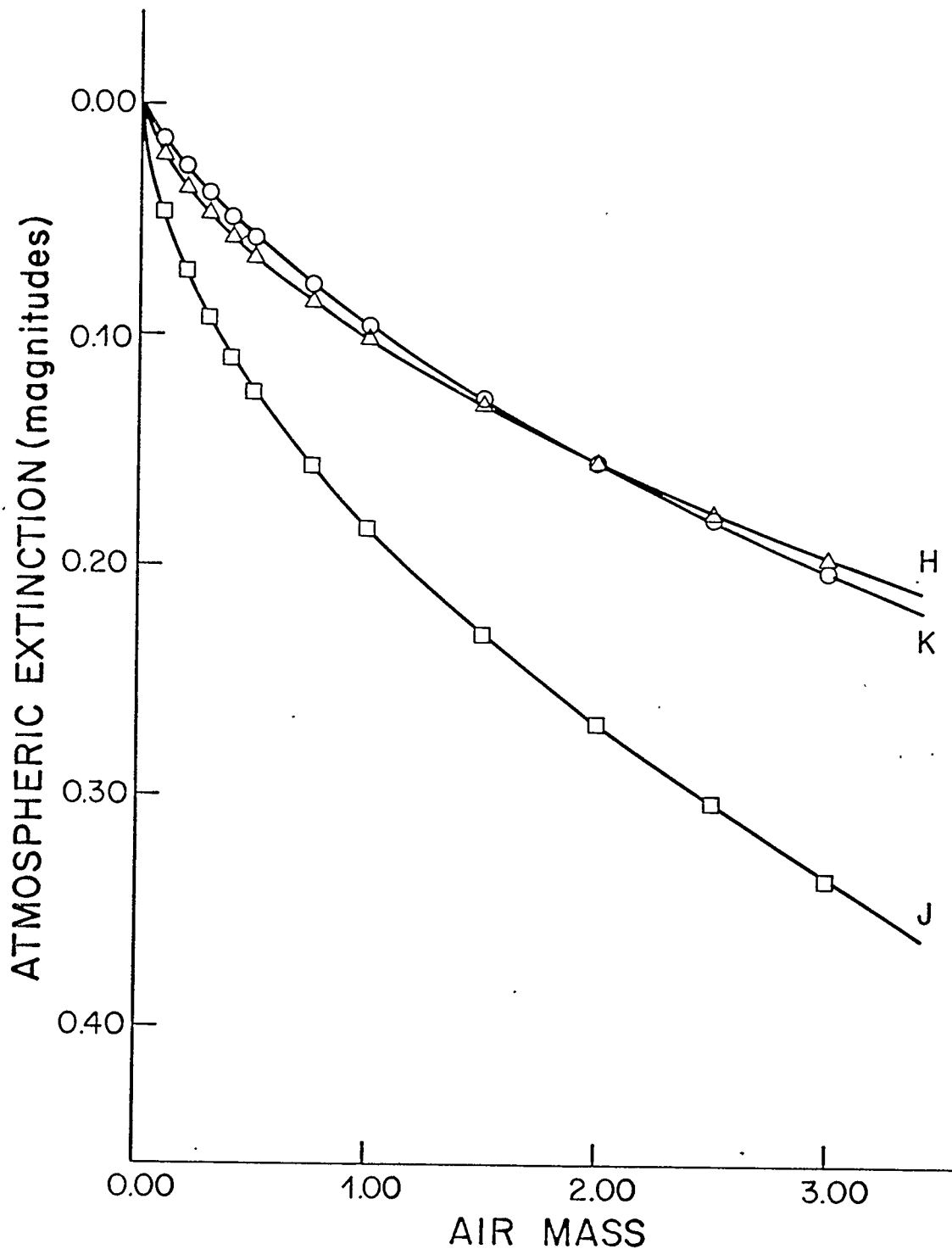


Figure 8d- Single layer results for Kitt Peak.

H₂O column density- 5.05 PMM; Vega/9100 K model.
 Slopes (1.00 to 2.00 air mass) Zero point errors
 J- 0.0846 mag./a.m. J- 0.0993 mag.
 H- 0.0522 H- 0.0496
 K- 0.0588 K- 0.0370

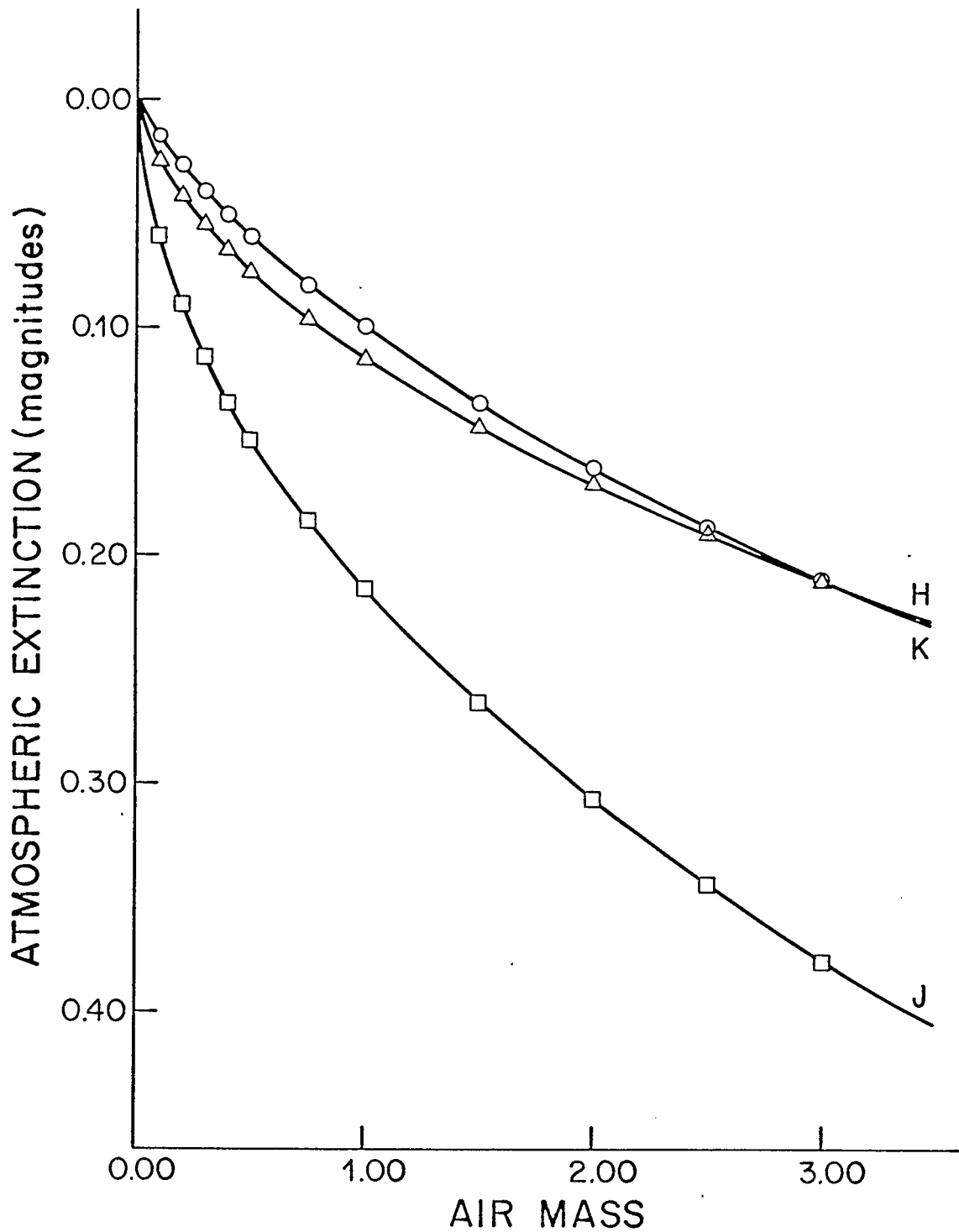


Figure 8e- Single layer results for Kitt Peak.

H ₂ O column density- 7.54 PMM;	4000 K model.
Slopes (1.00 to 2.00 air mass)	Zero point errors
J- 0.0920 mag./a.m.	J- 0.1226 mag.
H- 0.0544	H- 0.0591
K- 0.0609	K- 0.0387

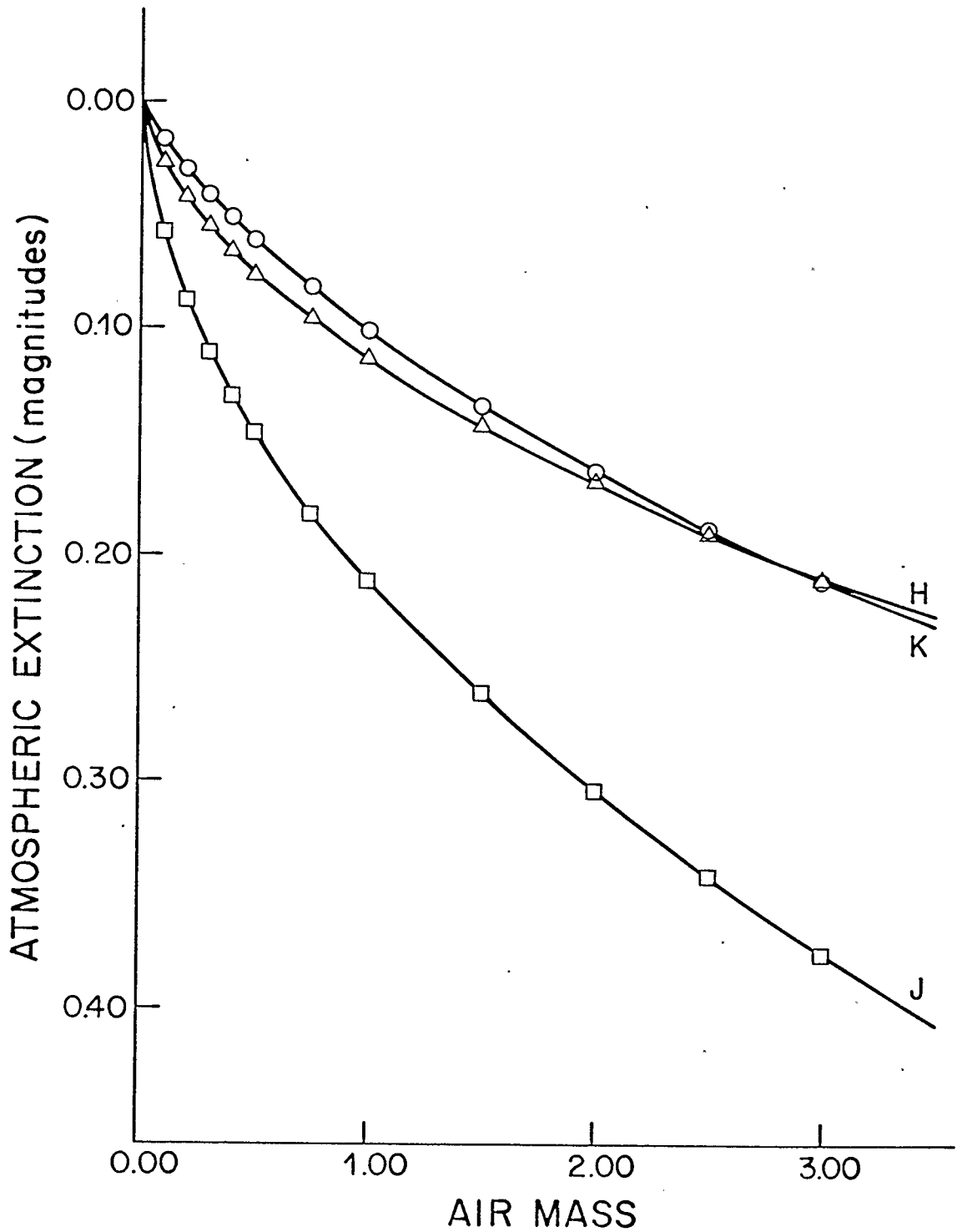


Figure 8f- Single layer results for Kitt Peak.

H₂O column density- 7.54 PMM; Vega/9100 K model.
 Slopes (1.00 to 2.00 air mass) Zero point errors
 J- 0.0926 mag./a.m. J- 0.1190 mag.
 H- 0.0545 H- 0.0585
 K- 0.0615 K- 0.0394

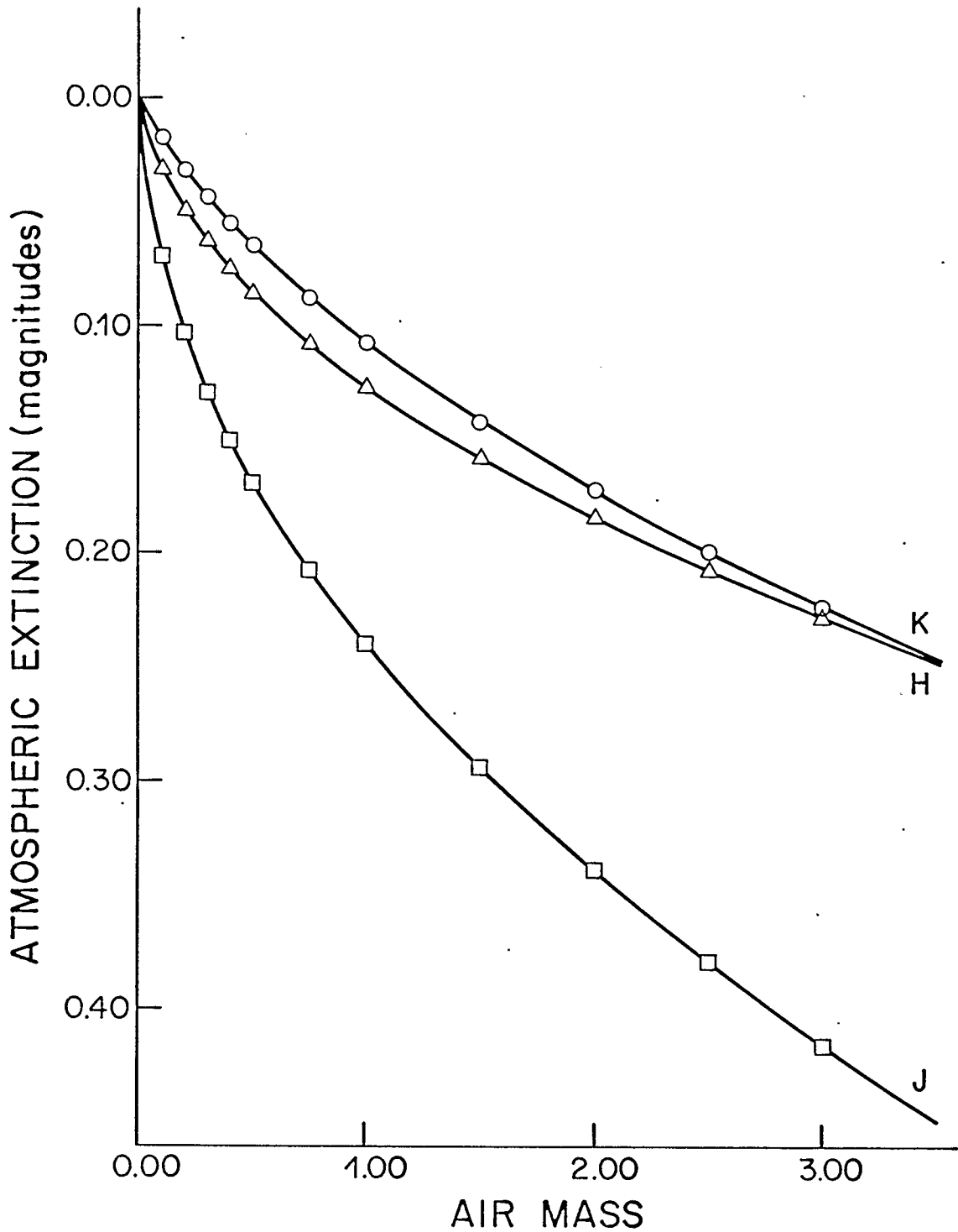


Figure 8g- Single layer results for Kitt Peak.

H ₂ O column density- .10.1 PMM;	4000 K model.
Slopes (1.00 to 2.00 air mass)	Zero point errors
J- 0.0995 mag./a.m.	J- 0.1405 mag.
H- 0.0575	H- 0.0691
K- 0.0647	K- 0.0425

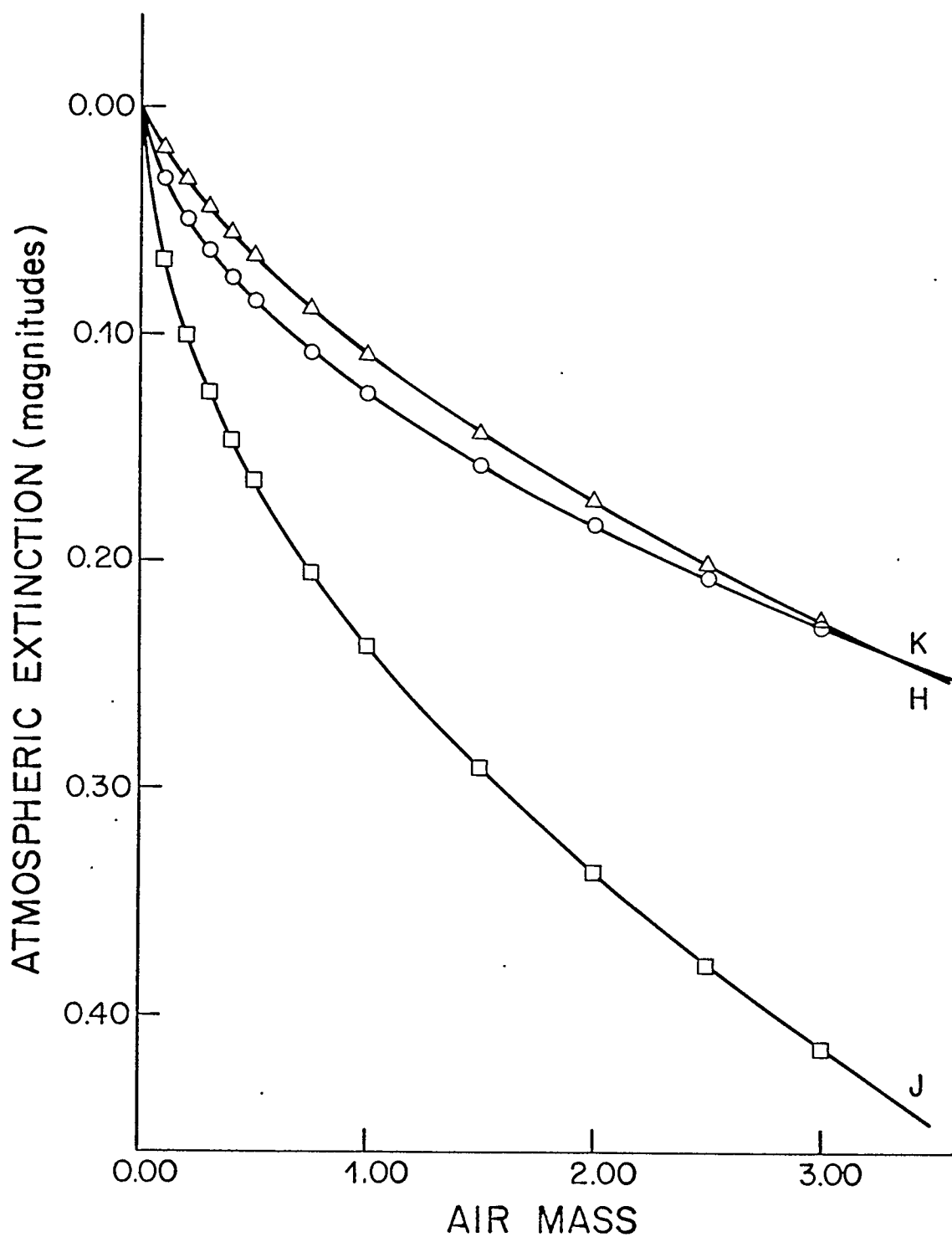


Figure 8h- Single layer results for Kitt Peak.

H₂O column density- .10.1 PMM; Vega/9100 K model.
 Slopes (1.00 to 2.00 air mass) Zero point errors
 J- 0.1004 mag./a.m. J- 0.1368 mag.
 H- 0.0576 H- 0.0684
 K- 0.0653 K- 0.0431

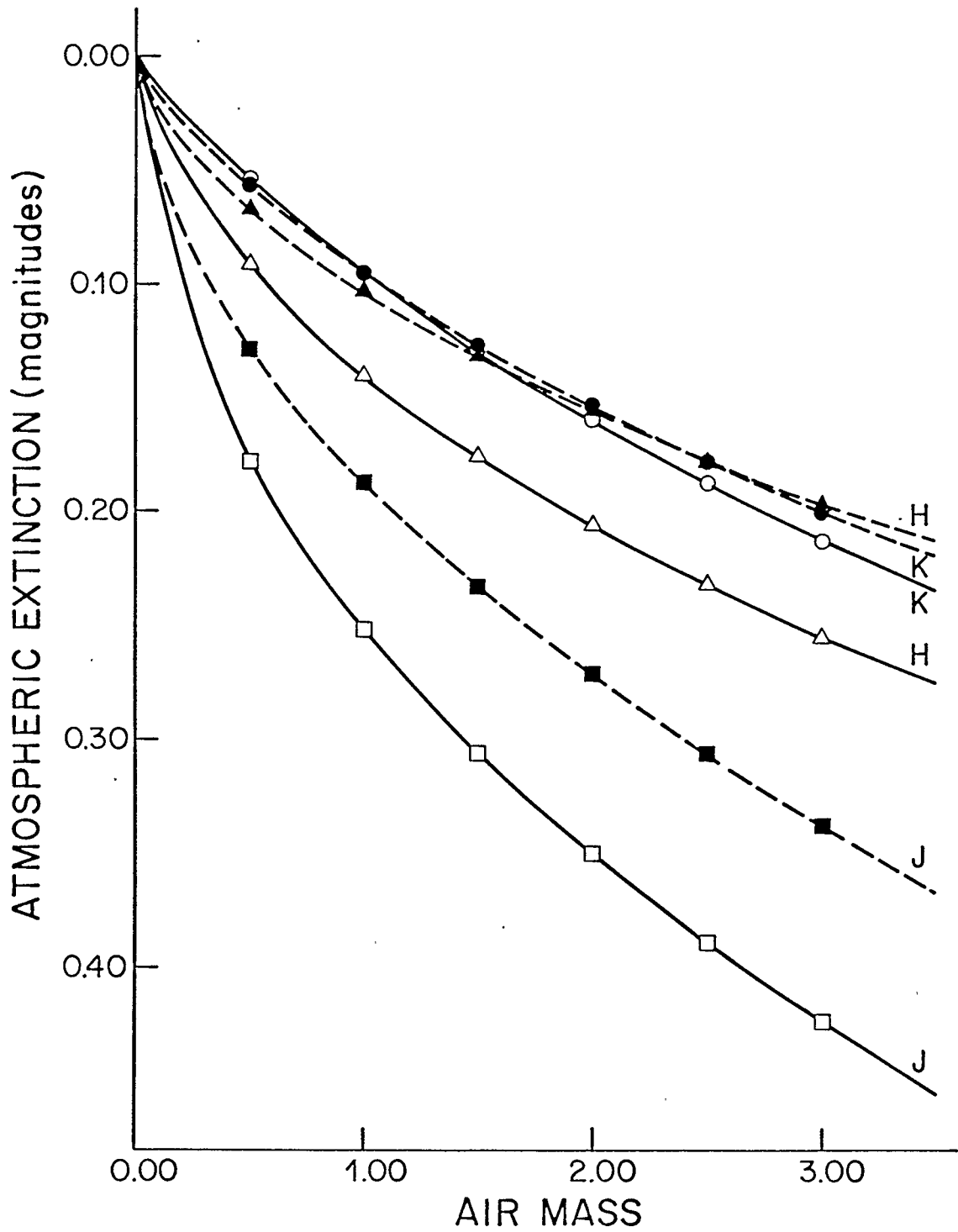


Figure 9- Comparison of the cool giant results of Manduca and Bell (1979) with the equivalent 4000 K results for "Kitt Peak summer" conditions. All the filters are Kitt Peak filters.

Open circles- Manduca and Bell (1979)

Filled circles- Single layer model calculations

Examination of Figure 9 shows that the K filter results are reasonably similar for both sets of calculations, while the MB J and H filter results show significantly greater extinction than their counterparts. The $\frac{\Delta}{E}$ ratios from MB are larger for the J and H filters than in the other calculations, while for the K filter the ratio is smaller. It is also of interest to note that the two K filter extinction curves almost coincide at $X = 1.00$, but deviate at all other points.

At least part of the difference is due to the filter characteristics used in the calculations. Comparisons between the profiles given in Figure 1 and Figures 5 through 7 show differences in each of the filters. The J filter from the 1979 filter set is narrower than its predecessor and has a spur at $1.35 \mu\text{m}$ which is not present in the earlier J filter. The H filter seems narrower in the 1979 version than that which was used earlier, although the overall profiles are quite similar. As for the K filter, the two profiles differ somewhat between $2.0 \mu\text{m}$ and $2.1 \mu\text{m}$ but otherwise they are very similar. It is not surprising therefore that the J filter results are different, but the H filter results are more difficult to explain.

The K filter results indicate that although the two calculations agree on the average there are still discrepancies in the transmission profiles which cause the deviations at air mass values other than 1.00

because of the scaling process. This also makes it seem unlikely that the deviations seen in the J and H filter results are due to some sort of systematic error unless some factor is present which does not apply to the K filter.

The three possible sources of systematic error which were noted previously are probably not the cause of the discrepancies. For the J filter the magnitude difference at $X = 1.00$ is 0.064 while for the H filter the figure is 0.036. Such large differences are unlikely to be due to either weak lines or the weak absorption in the far wings of very strong lines because of the number of lines which would be needed. In the case of weak lines, contributing between 0.01 and 0.0005 to k_λ at the nearest grid point, an increase of about 0.03 in k_λ on the average over the entire interval would require roughly 45 lines per grid point. This means that about 225 lines would be needed per 1 cm^{-1} over intervals of hundreds of cm^{-1} , a total which is far too large. As for strong lines, unless the line wings still contribute a lot more than 0.0005 to k_λ at 30 cm^{-1} from line center, certainly beyond 60 cm^{-1} from line center the k_λ value will fall below 0.0005. If this is assumed, roughly 45 such lines would be needed per grid point to produce a change of 0.03 in k_λ . Very roughly 1 to 2 such lines per cm^{-1} would be needed, amounting to very many of these lines over the entire filter ranges. It seems unlikely that no lines

of this type would be present over the K filter band if they are so common for the other filters, and equally unlikely that such strong lines would be missed in the McClatchey, et. al., (1973) strong line lists and not be mentioned in previous work. Finally, it seems unlikely that the line core integration or the movement of lines to grid points can be at fault because this would almost certainly affect all three filters rather than only two of the three.

The line centering in IRTRANS and the line wing cut-off in MC might together be responsible for a slightly stronger extinction in the MB results compared to the results given here, but judging from the K filters results, this effect is not all that strong.

The differences in the filter response functions for the two sets of calculations may be a major factor in the discrepancy for the J filter, but would not appear to be of importance for the H filter. The assumed photometer response might be a small factor as well, but as long as there is no large change in response over the filter band-pass this should be a negligible influence.

It is clear from the $\frac{\Delta}{E}$ ratios that the Johnson correction appears to be inaccurate and does not correct adequately for atmospheric extinction. The zero point errors would still be large, up to 0.1 magnitudes for the J filter under relatively humid conditions. The colour dependences are much smaller

and so are only of marginal concern. It is of interest to note that the δ values are much smaller than those in MB. This is surprising because the filter widths in the new filter set are only slightly less than those for the filters used by MB.

The single layer results are not the main feature of the project. As was noted in Chapter 2, the form of the Curtis-Godson approximation which was used assumes the atmosphere to be isothermal. For this reason a solution based upon several layers should be more accurate as each layer can more reasonably be assumed to be isothermal. Such a set of calculations has been carried out and the details, results and a comparison with the single layer results is given in the next chapter.

Chapter Five

The Multiple Layer Model Results

The results of MB, summarized in Chapter 2, and the equivalent results from Chapter 4 are based upon a single layer model atmosphere to which the Curtis-Godson approximation was applied. In doing so, it was necessary to make the assumption that the atmosphere is isothermal in order to calculate the molecular parameters without having to go to tremendous lengths. An obvious way to improve the atmospheric model is to use a series of layers rather than just a single layer. Each layer would still be assumed to be isothermal, but the overall model would be closer to the true state of the atmosphere because the range of temperature in each layer is reduced. The introduction of multiple layers also allows the comparison of sites at different altitudes under a consistent set of atmospheric conditions.

MB state that their results are relatively independent of the P_{EFF} and T_{EFF} values. If the results were completely independent of T_{EFF} then the multiple layer model would give exactly the same results as the single layer model for a given set of conditions. Even if this turns out to be the case it would be an important result, and the inter-comparison of sites remains important.

The layers in the multiple layer model for the atmosphere were initially chosen so that extinction curves could be calculated for three sites - Mauna Kea, Kitt Peak and Calgary. [When the opportunity arose to carry out an observing run at Mount Lemmon Observatory, Arizona, another layer was added to produce calculations for this site, since it was hoped that a direct comparison with experimental data would be possible. Unfortunately, no useful data was obtained on this run or on a subsequent observing session at Kitt Peak because of poor weather.] Mauna Kea is situated at $19^{\circ}50'N$ and an altitude of 4.20 km. Kitt Peak and Mount Lemmon are both near $32^{\circ}N$ latitude, at altitudes of 2.06 km and 2.79 km respectively. Calgary is at $50.8^{\circ}N$ latitude and an altitude of 1.27 km. This is a fairly wide range of latitude, which leads to somewhat different atmospheric conditions at the four sites. The physical conditions and weather patterns are similar for Arizona and southern Alberta, although Arizona is somewhat higher in altitude and dryer than southern Alberta. Calgary is near the area of transition from a semi-arid grassland to a coniferous forest, which is a reflection of the higher rainfall level in Alberta compared to areas to the south. Calgary and the Arizona sites are probably similar enough that an atmospheric model designed for Kitt Peak should give fairly representative results for Calgary.

Providing a single set of atmospheric conditions for Mauna Kea and any of the other sites is a problem, because Mauna Kea is subject to a considerably different climate than the continental sites. Another difference is that Mauna Kea is much higher above the ocean surface than the Arizona sites are above the surrounding plain.

It was decided to adopt the U.S. Standard Atmosphere (1976), hereafter denoted by USSA, as the atmospheric model and apply it to all the sites. This is acceptable in view of the absence of detailed information about the pressure, temperature and composition profiles for these sites under average conditions. Even were this information available, the different sites would not fit together into a single unified atmospheric model; the cost of the calculations would then be very high. The USSA is calculated to correspond to 45°N latitude, so it is most suitable for Calgary and least suitable for Mauna Kea. In general, the Mauna Kea results must be viewed with some caution for this reason.

The H₂O abundance profile is of key importance in shaping the results. Once again there is a lack of specific data, so the mean water vapour profile from the USSA was taken as standard except for an overall column density scaling factor. The mean mid-latitude water vapour profile from the USSA is presented in

Figure 10. The O_3 abundance profile was also assumed to follow the USSA mean values, presented in Figure 12.

The pressure values at Calgary, Kitt Peak, Mount Lemmon and Mauna Kea are 869.73 milli-bars (mb), 789.11 mb, 720.12 mb and 600.72 mb respectively from the USSA. Each of these values will be the upper pressure value of a layer. The lowest pressure value of the atmospheric model was taken to be the value at an altitude of 90 km, 1.853×10^{-3} mb; the atmosphere above this altitude was ignored. This was done to avoid the changes in composition which occur in the very high atmosphere, and represents the loss of about 1 part in 10^6 of the atmosphere as a whole, which is too small to alter the results significantly. Six layers were set up between 600.72 mb and 1.853×10^{-3} mb with layer boundaries at 500.00 mb, 400.00 mb, 300.00 mb, 200.00 mb and 100.00 mb. In each layer, the acceleration of gravity was assumed to be constant, and equal to the value at the mid-point of the layer. $g(Z)$ was calculated by the approximation

$$g(Z) = g_0[1 - 2Z/r_0] \quad (5.1)$$

with $g_0 = 9.80665 \text{ m/s}^2$ and $r_0 = 6367.65 \text{ km}$. With both g and T constant for each layer, and the composition changing only very slightly in each layer, the pressure scale height can be taken as a constant for each layer.

The layers are described in Table 4.

LAYER	PRESSURE RANGE	ALTITUDE RANGE	g
1	869.73mb \geq P \geq 789.11mb	1.27km \leq Z \leq 2.06km	9.8015m/s ²
2	789.11mb \geq P \geq 600.72mb	2.06km \leq Z \leq 4.20km	9.7970m/s ²
2a	720.12mb \geq P \geq 600.72mb	2.79km \leq Z \leq 4.20km	9.7959m/s ²
3	600.72mb \geq P \geq 500.00mb	4.20km \leq Z \leq 5.575km	9.7916m/s ²
4	500.00mb \geq P \geq 400.00mb	5.575km \leq Z \leq 7.20km	9.7870m/s ²
5	400.00mb \geq P \geq 300.00mb	7.20km \leq Z \leq 9.175km	9.7814m/s ²
6	300.00mb \geq P \geq 200.00mb	9.175km \leq Z \leq 11.80km	9.7743m/s ²
7	200.00mb \geq P \geq 100.00mb	11.80km \leq Z \leq 16.20km	9.7653m/s ²
8	100.00mb \geq P \geq 1.853x10 ⁻³ mb	16.20km \leq Z \leq 90.00km	9.6431m/s ²

Table 4 - Description of the atmospheric layers for the multiple layer model.

Layer 2a, from Mauna Kea to Mount Lemmon, is a separate terminating layer; the other layers from layer 1 to layer 8 are a continuous sequence. Layers 3 through 8 are all very similar in terms of column density because in each case the pressure range is nearly the same, 100 mb. Layers 2a and 2 are larger than the upper layers, while layer 1 has the smallest column density values because it has a pressure range of only 80.62 mb.

In each layer, P_h and μ_h must be calculated for each molecule via

$$P_h = \frac{\int_{P_1}^{P_2} PC(P)dP}{\int_{P_1}^{P_2} C(P)dP} \quad (5.2)$$

$$\mu_h = \frac{1}{g} \int_{P_1}^{P_2} C(P)dP \quad (5.3)$$

which for uniformly mixed molecules give

$$P_h = 1/2(P_2 + P_1) \quad (5.4)$$

$$\mu_h = C/g(P_2 - P_1)$$

One case which will be useful is where $C(Z)$ is linear with Z . This will be pertinent to the H_2O abundance profile and part of the O_3 abundance profile. With a constant scale height, H ,

$$P(Z) = P(Z_0) e^{-(Z-Z_0)/H} \quad (5.5)$$

and

$$C(Z) = A + BZ \quad (5.6)$$

where A and B are constants. These give

$$\begin{aligned} C(P) &= A + B(Z_0 - H \ln(P/P(Z_0))) \\ &= A + BZ_0 - BH \ln(P/P(Z_0)) \end{aligned} \quad (5.7)$$

Integration by parts readily gives

$$\int x \ln(x/a) dx = 1/2 x^2 \ln(x/a) - 1/4 x^2 + c \quad (5.8)$$

and

$$\int \ln(x/a) dx = x \ln(x/a) - x + c \quad (5.9)$$

Using these formulae with equation (5.7) and equations (5.2) and (5.3) produces the following equations

$$\begin{aligned} P_H &= \frac{\int_{P_1}^{P_2} P(A + BZ_0 - BH \ln(P/P(Z_0))) dP}{\int_{P_1}^{P_2} (A + BZ_0 - BH \ln(P/P(Z_0))) dP} \\ &= \frac{(A + BZ_0 - BH \ln(P/P(Z_0)) + \frac{1}{2} BH) \frac{1}{2} P^2 \Big|_{P_1}^{P_2}}{(A + BZ_0 - BH \ln(P/P(Z_0)) + BH) P \Big|_{P_1}^{P_2}} \\ &= \frac{\frac{1}{2} [(A + B[Z_0 + \frac{1}{2}H] + BH \ln(\frac{P(Z_0)}{P_2})) P_2^2 - (A + B(Z_0 + \frac{1}{2}H) + BH \ln(\frac{P(Z_0)}{P_1})) P_1^2]}{(A + B(Z_0 + H) + BH \ln(\frac{P(Z_0)}{P_2})) P_2 - (A + B(Z_0 + H) + BH \ln(\frac{P(Z_0)}{P_1})) P_1} \end{aligned} \quad (5.10)$$

$$\mu_h = \frac{1}{g} [(A + B(Z_0 + H) + BH \ln(\frac{P(Z_0)}{P_2})) P_2 - (A + B(Z_0 + H) + BH \ln(\frac{P(Z_0)}{P_1})) P_1] \quad (5.11)$$

If B is set to zero, these equations reduce to equations (5.4).

This can easily be extended to a series of linear segments. Let a layer be subdivided into a set of intervals $Z_1 \leq Z \leq Z_2$, $Z_2 \leq Z \leq Z_3$, ... up to $Z_j \leq Z \leq Z_{j+1}$, with corresponding pressure intervals $P_{j+1} \geq P \geq P_j$, $P_j \geq P \geq P_{j-1}$, ... up to $P_2 \geq P \geq P_1$. There are j intervals and at some Z_k value, $1 \leq k \leq j$, the pressure is P_{j+2-k} . In the k^{th} interval

$$P(Z) = P(Z_{0k}) e^{-(Z-Z_{0k})/H_k} \quad (5.12)$$

and

$$C(Z) = A_k + B_k Z \quad (5.13)$$

Clearly it is true that

$$\int_{P_1}^{P_{j+1}} f(P) dP = \sum_{i=1}^j \int_{P_j}^{P_{j+1}} f(P) dP \quad (5.14)$$

provided $f(P)$ remains well defined over the layer. This leads to a direct generalization of equations (5.10) and (5.11)

$$\rho_h = \frac{\frac{1}{a} \sum_{i=1}^j \left[P_{j+2-i}^2 (A_i + B_i (Z_{0i} + \frac{1}{2} H_i) + B_i H_i \ln \left(\frac{P(Z_{0i})}{P_{j+2-i}} \right)) - P_{j+1-i}^2 (A_i + B_i (Z_{0i} + H_i) + B_i H_i \ln \left(\frac{P(Z_{0i})}{P_{j+2-i}} \right)) - P_{j+1-i}^2 (A_i + B_i (Z_{0i} + \frac{1}{2} H_i) + B_i H_i \ln \left(\frac{P(Z_{0i})}{P_{j+1-i}} \right)) \right]}{\sum_{i=1}^j \left[P_{j+2-i} (A_i + B_i (Z_{0i} + H_i) + B_i H_i \ln \left(\frac{P(Z_{0i})}{P_{j+2-i}} \right)) - P_{j+1-i} (A_i + B_i (Z_{0i} + H_i) + B_i H_i \ln \left(\frac{P(Z_{0i})}{P_{j+2-i}} \right)) \right]} \quad (5.15)$$

$$\mu_h = \frac{1}{g} \left[P_{j+2-i} (A_i + B_i (Z_{0i} + H_i) + B_i H_i \ln \left(\frac{P(Z_{0i})}{P_{j+2-i}} \right)) - P_{j+1-i} (A_i + B_i (Z_{0i} + H_i) + B_i H_i \ln \left(\frac{P(Z_{0i})}{P_{j+2-i}} \right)) \right] \quad (5.16)$$

These equations are simplified somewhat if Z_{0i} is set to Z_i so $P(Z_{0i})$ becomes P_{j+2-i} . In that case, half

of the logarithmic terms are eliminated. The final forms are

$$P_h = \frac{\frac{1}{2} \sum_{i=1}^{\lambda} \left[P_{\lambda+2-i}^2 (A_i + B_i [Z_{0i} + \frac{1}{2} H_i]) - P_{\lambda+1-i}^2 (A_i + B_i (Z_{0i} + \frac{1}{2} H_i) + B_i H_i \ln(\frac{P_{\lambda+2-i}}{P_{\lambda+1-i}})) \right]}{\sum_{i=1}^{\lambda} \left[P_{\lambda+2-i} (A_i + B_i [Z_{0i} + H_i]) - P_{\lambda+1-i} (A_i + B_i (Z_{0i} + H_i) + B_i H_i \ln(\frac{P_{\lambda+2-i}}{P_{\lambda+1-i}})) \right]} \quad (5.17)$$

$$\mu_h = \frac{1}{q} \sum_{i=1}^{\lambda} \left[P_{\lambda+2-i} (A_i + B_i [Z_{0i} + H_i]) - P_{\lambda+1-i} (A_i + B_i [Z_{0i} + H_i] + B_i H_i \ln(\frac{P_{\lambda+2-i}}{P_{\lambda+1-i}})) \right] \quad (5.18)$$

These formulae are simple enough to be evaluated using a programmable hand calculator.

Figure 10 presents the mean midlatitude H₂O profile from the USSA, with a series of linear segments forming a nearly smooth curve through these points. Table 5 gives the parameters for the fit, and extends

RANGE (km)	A	B
0.00 to 1.00	4.686x10 ⁻³	-9.860x10 ⁻⁴ km ⁻¹
1.00 to 3.00	4.557x10 ⁻³	-8.570x10 ⁻⁴ km ⁻¹
3.00 to 4.00	4.140x10 ⁻³	-7.180x10 ⁻⁴ km ⁻¹
4.00 to 5.00	2.980x10 ⁻³	-4.280x10 ⁻⁴ km ⁻¹
5.00 to 6.00	2.270x10 ⁻³	-2.860x10 ⁻⁴ km ⁻¹
6.00 to 7.00	1.718x10 ⁻³	-1.940x10 ⁻⁴ km ⁻¹
7.00 to 8.00	1.368x10 ⁻³	-1.440x10 ⁻⁴ km ⁻¹
8.00 to 9.00	9.040x10 ⁻⁴	-8.60x10 ⁻⁵ km ⁻¹
9.00 to 10.00	9.112x10 ⁻⁴	-8.68x10 ⁻⁵ km ⁻¹
10.00 to 12.00	2.027x10 ⁻⁴	-1.60x10 ⁻⁵ km ⁻¹
12.00 to 14.00	5.93x10 ⁻⁵	-4.00x10 ⁻⁶ km ⁻¹
14.00 to 20.00	3.3x10 ⁻⁶	-
20.00 to 26.00	-4.24x10 ⁻⁵	+2.29x10 ⁻⁶ km ⁻¹
26.00 to 35.00	1.70x10 ⁻⁵	-
35.00 to 45.00	1.11x10 ⁻⁵	-
45.00 to 60.00	5.0x10 ⁻⁶	-
60.00 to 80.00	1.0x10 ⁻⁶	-

TABLE 5 - Linear segment fit for the USSA H₂O mass mixing ratio.

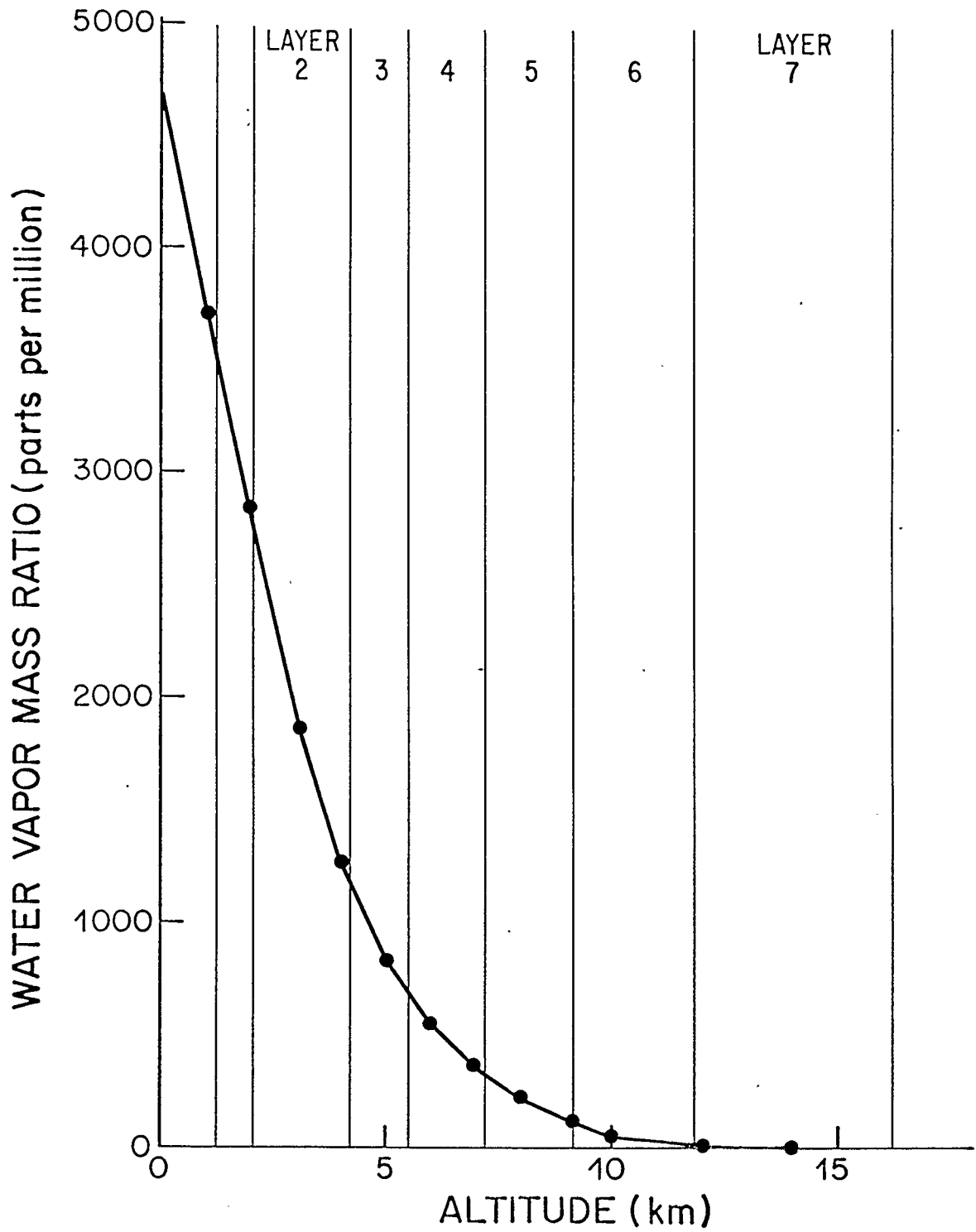


Figure 10- The mean mid-latitude water vapour mass mixing ratio as a function of altitude from the U.S. Standard Atmosphere (1976).

it up to an altitude of 80 km. Beyond 80 km, it is assumed that no water vapour is present. The values upon which this fit is based are the Table 20 and Table 21b values from the USSA (1976), which in turn draw upon frost point measurements for high clouds above an altitude of 10 km. Above 26 km the C(P) values are approximated by a series of intervals with constant water vapour concentration, because C(P) is so low that the difference can be ignored and this step simplifies calculations.

It must be remembered that the μ_h values are no longer the same as μ , which is true in the case of uniformly mixed molecules. In order to match H₂O column densities at Kitt Peak, the actual μ values must be found for each layer. This was done by evaluating the area under sections of a plot of C(P) against P, shown in Figure 11. The area values were found by direct counting of 0.01 cm² squares, each of which represented 10⁻⁴ mb with the scale that was used for layers 0 to 5 and 10⁻⁶ mb with the larger scale. Each area value should be accurate to at least ± 0.05 cm², an error small enough to be ignored. Each area value was converted to a μ value using the appropriate g value. Table 6 gives the layer-by-layer values. The total amount of water vapour above Kitt Peak is 5.363 Kg/m², very close to the 5.05 Kg/m² value initially used by MB. This is rather odd, for Arizona is a dry

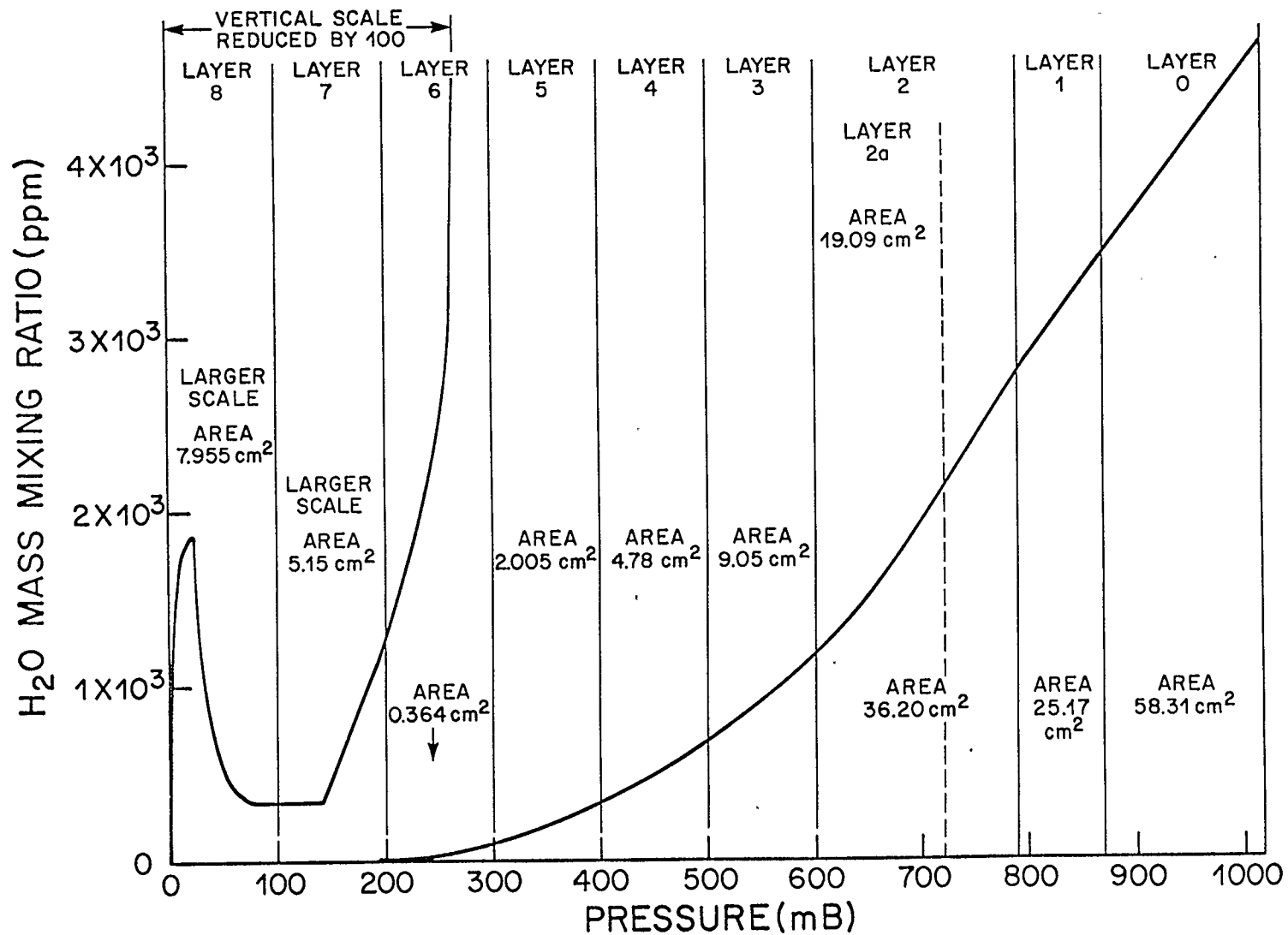


Figure 11- The water vapour mass mixing ratio as a function of pressure, from Figure 10 and the standard P(Z) profile. The area under the curve for each layer in the multiple layer model is also given.

area yet the water vapour column density falls near the USSA midlatitude mean value.

LAYER	AMOUNT OF WATER VAPOR	PERCENT OF TOTAL	PERCENT EXCLUDING LAYER 0	COLUMN DENSITY ABOVE LAYER
0	5.953 Kg/m ²	42.87	-	7.933 Kg/m ²
1	2.570 Kg/m ²	18.51	32.39	5.363 Kg/m ²
2	3.696 Kg/m ²	26.62	46.59	1.667 Kg/m ²
2a	1.949 Kg/m ²	-	-	1.667 Kg/m ²
3	0.924 Kg/m ²	6.65	11.65	0.743 Kg/m ²
4	0.488 Kg/m ²	3.51	6.15	0.255 Kg/m ²
5	0.205 Kg/m ²	1.47	2.58	0.050 Kg/m ²
6	0.037 Kg/m ²	0.268	0.468	0.013 Kg/m ²
7	0.0053 Kg/m ²	0.038	0.066	0.008 Kg/m ²
8	0.0081 Kg/m ²	0.0585	0.102	-
TOTAL	13.886 Kg/m ²			

TABLE 6 - Layer by layer H₂O column density values.

In order to convert μ in Kg/m² to the more usual units of molecules per cm² the equation

$$\text{column density (cm}^{-2}\text{)} = 6.022 \times 10^{22} \mu/M \quad (5.19)$$

is used, where M is the molecular mass in atomic mass units. The scale height is given by

$$H = \frac{kT}{\bar{m}g} = \frac{RT}{\bar{M}g} \quad (5.20)$$

where \bar{m} and \bar{M} are the mean molecular mass, in kilograms and atomic mass units respectively, R is the ideal gas constant 8.314 J/mole K and k is Boltzmann's constant. Taking M to be 28.964, which is the value for dry air,

$$H = 0.2871 T/g \text{ km} \quad (5.21)$$

This will be used to give H for each interval in Table 5, using T from the USSA and equation (5.1).

The details of the water vapour calculations may

now be presented for each layer:

Layer 1 1.27km $\leq Z \leq$ 2.06km 869.73mb $\geq P \geq$ 789.11mb

j=1

i	P_{j+2-i}	Z_i	A_i	B_i	H_i
1	869.73mb	1.27km	4.686×10^{-3}	$-9.860 \times 10^{-4} \text{ km}^{-1}$	8.123km
2	789.11mb	2.06km			

$$P_h = \frac{204.405 \text{ mb}^2}{0.24593 \text{ mb}} = 831.15 \text{ mb}$$

$$\mu_h = \frac{0.24593 \text{ mb}}{9.8015 \text{ m/s}^2} = \frac{24.593 \text{ n/m}^2}{9.8015 \text{ m/s}^2} = 2.509 \text{ Kg/m}^2$$

$$\text{column density} = 8.3946 \times 10^{21} \text{ cm}^{-2}$$

$$T = 277.49\text{K}$$

Layer 2 2.06km $\leq Z \leq$ 4.20km 789.11mb $\geq P \geq$ 600.72mb

j=3

i	P_{j+2-i}	Z_i	A_i	B_i	H_i
1	789.11mb	2.06km	4.686×10^{-3}	$-9.860 \times 10^{-4} \text{ km}^{-1}$	7.963km
2	701.21mb	3.00km	4.140×10^{-3}	$-7.180 \times 10^{-4} \text{ km}^{-1}$	7.778km
3	616.60mb	4.00km	2.980×10^{-3}	$-4.280 \times 10^{-4} \text{ km}^{-1}$	7.668km
4	600.72mb	4.20km			

$$P_h = \frac{(144.718 + 91.558 + 11.847) \text{ mb}^2}{(0.19341 + 0.13831 + 0.01946) \text{ mb}} = \frac{248.123}{0.35118} \text{ mb}$$

$$= 706.54 \text{ mb}$$

$$\mu_h = \frac{0.35118 \text{ mb}}{9.7970 \text{ m/s}^2} = \frac{35.118 \text{ n/m}^2}{9.7970 \text{ m/s}^2}$$

$$= 3.585 \text{ Kg/m}^2$$

$$\text{column density} = 1.1899 \times 10^{22} \text{ cm}^{-2}$$

$$T = 269.05\text{K}$$

Layer 2a 2.79km $\leq Z \leq$ 4.20km 720.12mb $\geq P \geq$ 600.72mb

j=3

i	P_{j+2-i}	Z_i	A_i	B_i	H_i
1	720.12mb	2.79km	4.686×10^{-3}	$-9.860 \times 10^{-4} \text{ km}^{-1}$	7.893km
2	701.21mb	3.00km	4.140×10^{-3}	$-7.180 \times 10^{-4} \text{ km}^{-1}$	7.778km
3	616.60mb	4.00km	2.980×10^{-3}	$-4.280 \times 10^{-4} \text{ km}^{-1}$	7.668km
4	600.72mb	4.20km			

$$P_h = \frac{(24.626+91.558+11.847) \text{ mb}^2}{(0.63467+0.13831+0.01946) \text{ mb}} = \frac{128.031}{0.19241} \text{ mb} = 665.41 \text{ mb}$$

$$\mu_h = \frac{0.19241 \text{ mb}}{9.7959 \text{ m/s}^2}$$

$$\text{column density} = 6.5653 \times 10^{21} \text{ cm}^{-2}$$

$$T = 265.72 \text{ K}$$

Layer 3 4.20km ≤ Z ≤ 5.575km 600.72mb ≥ P ≥ 500.00mb

j=2

i	P_{j+2-i}	Z_i	A_i	B_i	H_i
1	600.72mb	4.20km	2.980×10^{-3}	$-4.280 \times 10^{-4} \text{ km}^{-1}$	7.572km
2	540.48mb	5.00km	2.270×10^{-3}	$-2.860 \times 10^{-4} \text{ km}^{-1}$	7.446km
3	500.00mb	5.575km			

$$P_h = \frac{(69.337+15.989) \text{ mb}^2}{(0.12133+0.03069) \text{ mb}} = \frac{85.326}{0.15202} \text{ mb} = 561.28 \text{ mb}$$

$$\mu_h = \frac{0.15202 \text{ mb}}{9.7916 \text{ m/s}^2} = \frac{15.202 \text{ n/m}^2}{9.7916 \text{ m/s}^2} = 1.553 \text{ Kg/m}^2$$

$$\text{column density} = 5.1899 \times 10^{21} \text{ cm}^{-2}$$

$$T = 257.52 \text{ K}$$

Layer 4 5.575km ≤ Z ≤ 7.20km 500.00mb ≥ P ≥ 400.00mb

j=3

i	P_{j+2-i}	Z_i	A_i	B_i	H_i
1	500.00mb	5.575km	2.270×10^{-3}	$-2.860 \times 10^{-4} \text{ km}^{-1}$	7.349km
2	472.17mb	6.00km	1.718×10^{-3}	$-1.940 \times 10^{-4} \text{ km}^{-1}$	7.219km
3	411.05mb	7.00km	1.368×10^{-3}	$-1.440 \times 10^{-4} \text{ km}^{-1}$	7.102km
4	400.00mb	7.20km			

$$P_h = \frac{(8.3401+12.4541+1.5513) \text{ mb}^2}{(0.017142+0.028065+0.003825) \text{ mb}}$$

$$= \frac{22.3455}{0.049032} \text{ mb}$$

$$= 455.73 \text{ mb}$$

$$\mu_h = \frac{0.049032 \text{ mb}}{9.7870 \text{ m/s}^2} = \frac{4.9032 \text{ n/m}^2}{9.7870 \text{ m/s}^2} = 0.5010 \text{ Kg/m}^2$$

$$\text{column density} = 1.675 \times 10^{21} \text{ cm}^{-2}$$

$$T = 247.29 \text{ K}$$

Layer 5 7.20km ≤ Z ≤ 9.175km 400.00km ≥ P ≥ 300.00mb

j=3

i	P_{j+2-i}	Z_i	A_i	B_i	H_i
1	400.00mb	7.20km	1.368×10^{-3}	$-1.440 \times 10^{-4} \text{ km}^{-1}$	7.008km
2	356.51mb	8.00km	9.040×10^{-4}	$-8.60 \times 10^{-5} \text{ km}^{-1}$	6.839km
3	308.00mb	9.00km	9.112×10^{-4}	$-8.68 \times 10^{-5} \text{ km}^{-1}$	6.733km
4	300.00mb	9.175km			

$$P_h = \frac{(4.5296 + 2.8220 + 0.2976) \text{ mb}}{(0.011927 + 0.008443 + 0.000979) \text{ mb}} = \frac{7.6492}{0.021349} \text{ mb}$$

$$= 358.29 \text{ mb}$$

$$\mu_h = \frac{0.021349 \text{ mb}}{9.7814 \text{ m/s}^2} = \frac{2.1349 \text{ n/m}^2}{9.7814 \text{ m/s}^2} = 0.2183 \text{ Kg/m}^2$$

$$\text{column density} = 7.296 \times 10^{20} \text{ cm}^{-2}$$

$$T = 236.44 \text{ K}$$

Layer 6 9.175km ≤ Z ≤ 11.80km 300.00mb ≥ P ≥ 200.00mb

j=2

i	P_{j+2-i}	Z_i	A_i	B_i	H_i
1	300.00mb	9.175km	9.112×10^{-4}	$-8.68 \times 10^{-5} \text{ km}^{-1}$	6.634km
2	264.88mb	10.00km	2.027×10^{-4}	$-1.60 \times 10^{-5} \text{ km}^{-1}$	6.388km
3	200.00mb	11.80km			

$$P_h = \frac{(0.79673 + 0.44822) \text{ mb}^2}{(2.795 \times 10^{-3} + 1.884 \times 10^{-3}) \text{ mb}} = \frac{1.24495}{4.679 \times 10^{-3}} \text{ mb} = 266.07 \text{ mb}$$

$$\mu_h = \frac{4.679 \times 10^{-3} \text{ mb}}{9.7743 \text{ m/s}^2} = \frac{0.4679 \text{ n/m}^2}{9.7743 \text{ m/s}^2} = 0.0479 \text{ Kg/m}^2$$

$$\text{column density} = 1.601 \times 10^{20} \text{ cm}^{-2}$$

$$T = 223.14 \text{ K}$$

Layer 7 $11.80\text{km} \leq Z \leq 16.20\text{km}$ $200.00\text{mb} \geq P \geq 100.00\text{mb}$

$j=3$

i	P_{j+2-i}	Z_i	A_i	B_i	H_i
1	200.00mb	11.80km	2.027×10^{-4}	$-1.60 \times 10^{-5} \text{km}^{-1}$	6.367km
2	193.99mb	12.00km	5.93×10^{-5}	$-4.00 \times 10^{-6} \text{km}^{-1}$	6.368km
3	141.70mb	14.00km	3.30×10^{-6}	-	6.373km
4	100.00mb	16.20km			

$$P_h = \frac{(1.4636 \times 10^{-2} + 6.7717 \times 10^{-2} + 1.6630 \times 10^{-2}) \text{ mb}^2}{(7.42 \times 10^{-5} + 3.926 \times 10^{-4} + 1.376 \times 10^{-4}) \text{ mb}}$$

$$= \frac{9.8983 \times 10^{-2}}{6.044 \times 10^{-4}} \text{ mb} = 163.77 \text{ mb}$$

$$\mu_h = \frac{6.044 \times 10^{-4} \text{ mb}}{9.7635 \text{ m/s}^2} = \frac{6.044 \times 10^{-2} \text{ n/m}^2}{9.7635 \text{ m/s}^2} = 0.00619 \text{ Kg/m}^2$$

$$\text{column density} = 2.07 \times 10^{19} \text{ cm}^{-2}$$

$$T = 216.65 \text{ K}$$

Layer 8 $16.20\text{km} \leq Z \leq 90\text{km}$ $100.00 \geq P \geq 1.853 \times 10^{-3}$

$j=6$

i	P_{j+2-i}	Z_i	A_i	B_i	H_i
1	100.00mb	16.20km	3.30×10^{-6}	-	6.379km
2	55.293mb	20.00km	-4.24×10^{-5}	$+2.28 \times 10^{-6} \text{km}^{-1}$	6.376km
3	21.883mb	26.00km	1.70×10^{-5}	-	6.475km
4	5.7459mb	35.00km	1.11×10^{-5}	-	6.739km
5	1.4910mb	45.00km	5.0×10^{-6}	-	7.422km
6	0.21958mb	60.00km	1.0×10^{-6}	-	7.967km
7	0.01052mb	80.00km			

$$P_h = \frac{(1.1455 \times 10^{-2} + 1.0309 \times 10^{-2} + 3.790 \times 10^{-3} + 1.71 \times 10^{-4} + 5 \times 10^{-6} + 2 \times 10^{-7}) \text{ mb}^2}{(1.475 \times 10^{-4} + 2.957 \times 10^{-4} + 2.743 \times 10^{-4} + 4.72 \times 10^{-5} + 6.4 \times 10^{-6} + 2 \times 10^{-7}) \text{ mb}}$$

$$= \frac{2.5730 \times 10^{-2}}{7.743 \times 10^{-4}} \text{ mb} = 33.230 \text{ mb}$$

$$\mu_h = \frac{7.743 \times 10^{-4} \text{ mb}}{9.6432 \text{ m/s}^2} = \frac{7.743 \times 10^{-2} \text{ n/m}^2}{9.6431 \text{ m/s}^2} = 0.00803 \text{ Kg/m}^2$$

$$\text{column density} = 2.68 \times 10^{19} \text{ cm}^2$$

$$T = 219.84 \text{ K}$$

The pressure and temperature values given above will be used no matter how the column density values are scaled. They depend only upon the relative H₂O abundance profile. In order to match the single layer Kitt Peak calculation for 5.05 pmm H₂O, all the column density values must be multiplied by $\frac{5.05}{5.363}$, or 0.94164. The final values of the parameters are given in Table 7.

LAYER	P _h	T _h	column density	μ _h
1	831.15mb	277.49K	7.9047x10 ²¹ cm ⁻²	2.363Kg/m ²
2	706.54mb	269.05K	1.1205x10 ²² cm ⁻²	3.376Kg/m ²
2a	665.41mb	265.72K	6.1821x10 ²¹ cm ⁻²	1.849Kg/m ²
3	561.28mb	257.52K	4.8870x10 ²¹ cm ⁻²	1.462Kg/m ²
4	455.73mb	247.29K	1.577x10 ²¹ cm ⁻²	0.4718Kg/m ²
5	358.29mb	236.44K	6.870x10 ²⁰ cm ⁻²	0.2056Kg/m ²
6	266.07mb	223.14K	1.508x10 ²⁰ cm ⁻²	0.0451Kg/m ²
7	163.77mb	216.65K	1.95x10 ¹⁹ cm ⁻²	0.0058Kg/m ²
8	33.230mb	219.84K	2.52x10 ¹⁹ cm ⁻²	0.0076Kg/m ²

TABLE 7 - Final H₂O parameters for the atmospheric layers in the multiple layer model.

O₃ must be treated in a similar manner. The USSA mean O₃ profile is presented in Figure 12. The vast majority of the ozone profile is in layer 8, so a linear segment fit for this layer would be rather complex. For layers 1 through 7 the linear segment fit is easily done. It was decided that the linear segment approach would be done for layers 1 to 7, but that layer 8 would be done by drawing graphs of C(P) and PC(P) versus P and directly evaluating the areas under these curves to obtain P_h and μ_h.

The plot of C(P) and PC(P) against P is given in

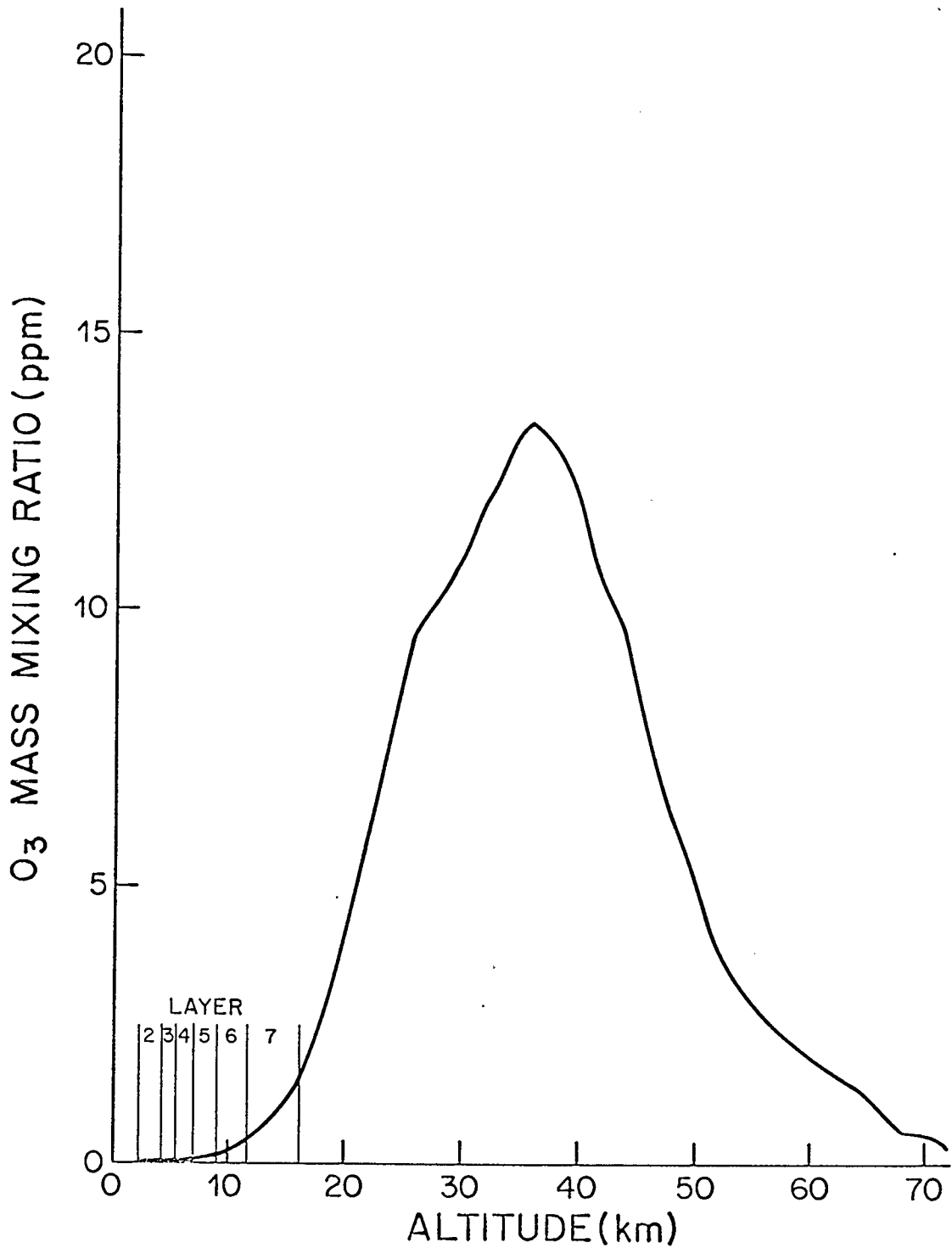


Figure 12- The mean mid-latitude ozone mass mixing ratio as a function of altitude from the U.S. Standard Atmosphere (1976).

Figure 13. The direct counting of 0.01cm^2 squares in the graph gives an area of 286.60 cm^2 for $\text{PC}(\text{P})$ and 141.21 cm^2 for $\text{C}(\text{P})$. Allowing for the scales gives

$$\int_0^{100\text{ mb}} \text{C}(\text{P})d\text{P} = 5.643 \times 10^{-3}\text{ mb}$$

$$\int_0^{100\text{ mb}} \text{PC}(\text{P})d\text{P} = 1.9107 \times 10^{-1}\text{ mb}^2$$

so

$$P_h = \frac{1.9107 \times 10^{-1}\text{ mb}}{5.648 \times 10^{-3}\text{ mb}} = 33.83\text{ mb}$$

$$\mu_h = \frac{5.648 \times 10^{-3}\text{ mb}}{9.6431\text{ m/s}^2} = \frac{0.5648\text{ n/m}^2}{9.6431\text{ m/s}^2} = 0.058575\text{ Kg/m}^2$$

This corresponds to a column density of $7.3492 \times 10^{19}\text{ cm}^{-2}$.

$T = 219.72\text{ K}$.

The linear segment fit parameters for O_3 are given in Table 8. The fit was found by simply joining the tabulated values from the USSA, which are given every 2 km. Following Table 8 are the details of the calculations in a similar form to that used for the H_2O calculations.

RANGE(KM)	A	B
0.00 to 2.00	5.4×10^{-8}	-
2.00 to 4.00	5.2×10^{-8}	$1 \times 10^{-9}\text{ km}^{-1}$
4.00 to 6.00	2.8×10^{-8}	$7 \times 10^{-9}\text{ km}^{-1}$
6.00 to 8.00	-2.5×10^{-8}	$1.55 \times 10^{-8}\text{ km}^{-1}$
8.00 to 10.00	-3.77×10^{-7}	$5.95 \times 10^{-8}\text{ km}^{-1}$
10.00 to 12.00	-1.27×10^{-6}	$1.49 \times 10^{-7}\text{ km}^{-1}$
12.00 to 14.00	-1.314×10^{-6}	$1.525 \times 10^{-7}\text{ km}^{-1}$
14.00 to 16.20	-3.302×10^{-6}	$2.945 \times 10^{-7}\text{ km}^{-1}$

TABLE 8 - Linear segment fit to the USSA mean O_3 abundance profile.

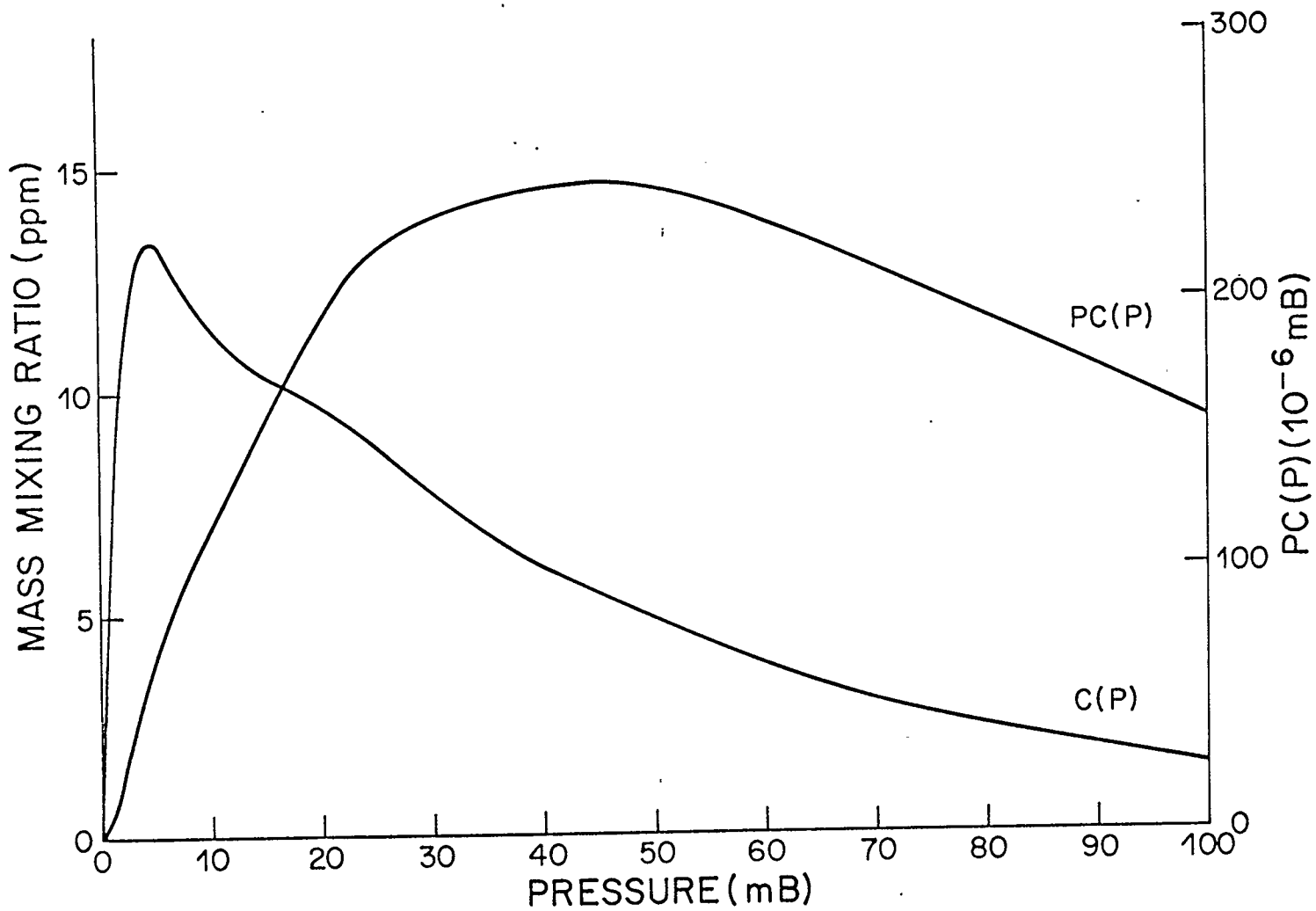


Figure 13- C(P) and PC(P) as a function of pressure for ozone in layer 8. The area under the C(P) curve was 141.25 cm^2 and the area under the PC(P) curve was 286.60 cm^2 at the original scale sizes.

Layer 1 j = 2

i	P_{j+2-i}	Z_i	A_i	B_i	H_i
1	869.73mb	1.27km	5.4×10^{-8}	$1 \times 10^{-9} \text{ km}^{-1}$	7.129km
2	795.01mb	2.00km	5.2×10^{-8}		8.055km
3	789.11mb	2.06km			

$$P_h = \frac{(3.3585 \times 10^{-3} + 2.525 \times 10^{-4}) \text{ mb}^2}{(4.0349 \times 10^{-6} + 3.188 \times 10^{-7}) \text{ mb}} = \frac{3.6110 \times 10^{-3}}{4.3537 \times 10^{-6}} \text{ mb}$$

$$= 829.41 \text{ mb}$$

$$\mu_h = \frac{4.3537 \times 10^{-6} \text{ mb}}{9.8015 \text{ m/s}^2} = \frac{4.3537 \times 10^{-4} \text{ n/m}^2}{9.8015 \text{ m/s}^2} = 4.4419 \times 10^{-5} \text{ Kg/m}^2$$

$$\text{column density} = 5.5731 \times 10^{17} \text{ cm}^{-2}$$

$$T = 277.38 \text{ km}$$

Layer 2 j = 2

i	P_{j+2-i}	Z_i	A_i	B_i	H_i
1	789.11mb	2.06km	5.2×10^{-8}	$1 \times 10^{-8} \text{ km}^{-1}$	7.867km
2	616.60mb	4.00km	2.8×10^{-8}	$7 \times 10^{-8} \text{ km}^{-1}$	7.666km
3	600.72mb	4.20km			

$$P_h = \frac{(6.6628 \times 10^{-3} + 5.480 \times 10^{-4}) \text{ mb}^2}{(9.4864 \times 10^{-6} + 9.004 \times 10^{-7}) \text{ mb}} = \frac{7.2108 \times 10^{-3}}{1.0387 \times 10^{-5}} \text{ mb}$$

$$= 694.23 \text{ mb}$$

$$\mu_h = \frac{1.0387 \times 10^{-5} \text{ mb}}{9.7970 \text{ m/s}^2} = \frac{1.0387 \times 10^{-3} \text{ n/m}^2}{9.7970 \text{ m/s}^2} = 1.0602 \times 10^{-4} \text{ Kg/m}^2$$

$$\text{column density} = 1.3302 \times 10^{17} \text{ cm}^{-2}$$

$$T = 268.15 \text{ K}$$

Layer 2a j = 2

i	P_{j+2-i}	Z_i	A_i	B_i	H_i
1	720.12mb	2.79km	5.2×10^{-8}	$1 \times 10^{-9} \text{ km}^{-1}$	7.978km
2	616.60mb	4.00km	2.8×10^{-8}	$7 \times 10^{-9} \text{ km}^{-1}$	7.666km
3	600.72mb	4.20km			

$$P_h = \frac{(3.8305 \times 10^3 + 5.480 \times 10^4) \text{ mb}}{(5.7329 \times 10^6 + 9.004 \times 10^7) \text{ mb}} = \frac{4.3785 \times 10^3}{6.6333 \times 10^6} \text{ mb}$$

$$= 660.08 \text{ mb}$$

$$\mu_h = \frac{6.6333 \times 10^{-6} \text{ mb}}{9.7959 \text{ m/s}^2} = \frac{6.6333 \times 10^{-4} \text{ n/m}^2}{9.7959 \text{ m/s}^2} = 6.7715 \times 10^{-5} \text{ Kg/m}^2$$

$$\text{column density} = 8.4960 \times 10^{16} \text{ cm}^{-2}$$

$$T = 265.62 \text{ K}$$

Layer 3 j = 1

i	Z _i	P _{j+2-i}	A _i ⁻⁸	B _i ⁹ km ⁻¹	H _i
1	4.20 km	600.72 mb	2.8 × 10 ⁻⁸	7 × 10 ⁹ km ⁻¹	7.518 km
2	5.575 km	500.00 mb			

$$P_h = \frac{3.4332 \times 10^{-3} \text{ mb}^2}{6.2528 \times 10^{-6} \text{ mb}} = 549.06 \text{ mb}$$

$$\mu_h = \frac{6.2528 \times 10^{-6} \text{ mb}}{9.7916 \text{ m/s}^2} = \frac{6.2528 \times 10^{-4} \text{ n/m}^2}{9.7916 \text{ m/s}^2} = 6.3859 \times 10^{-5} \text{ Kg/m}^2$$

$$\text{column density} = 8.0122 \times 10^{16} \text{ cm}^{-2}$$

$$T = 256.44 \text{ K}$$

Layer 4 j = 2

i	P _{j+2-i}	Z _i	A _i ⁻⁸	B _i ⁹ km ⁻¹	H _i
1	500.00 mb	5.575 km	2.8 × 10 ⁻⁸	7 × 10 ⁹ km ⁻¹	7.353 km
2	472.17 mb	6.00 km	-2.5 × 10 ⁻⁸	1.55 × 10 ⁻⁸ km ⁻¹	7.196 km
3	400.00 mb	7.20 km			

$$P_h = \frac{(9.263 \times 10^{-4} + 2.4152 \times 10^{-3}) \text{ mb}^2}{(1.9059 \times 10^{-6} + 5.5567 \times 10^{-6}) \text{ mb}} = \frac{3.3415 \times 10^{-3}}{7.4626 \times 10^{-6}} \text{ mb}$$

$$= 447.76 \text{ mb}$$

$$\mu_h = \frac{7.4626 \times 10^{-6} \text{ mb}}{9.7870 \text{ m/s}^2} = \frac{7.4626 \times 10^{-4} \text{ n/m}^2}{9.7870 \text{ m/s}^2} = 7.6250 \times 10^{-5} \text{ Kg/m}^2$$

$$\text{column density} = 9.5669 \times 10^{16} \text{ cm}^{-2}$$

$$T = 246.68 \text{ K}$$

Layer 5 $j = 2$

i	P_{j+2-i}	Z_i	A_i	B_i	H_i
1	400.00mb	7.20km	-2.5×10^{-8}	$1.55 \times 10^{-8} \text{ km}^{-1}$	7.008km
2	356.51mb	8.00km	-1.77×10^{-7}	$5.95 \times 10^{-8} \text{ km}^{-1}$	6.822km
3	300.00mb	9.175km			

$$P_h = \frac{(1.5235 \times 10^{-3} + 2.4489 \times 10^{-3}) \text{ mb}^2}{(4.0329 \times 10^{-6} + 7.5170 \times 10^{-6}) \text{ mb}} = \frac{3.9724 \times 10^{-3}}{1.1550 \times 10^{-5}} \text{ mb}$$

$$= 343.93 \text{ mb}$$

$$\mu_h = \frac{1.1550 \times 10^{-5} \text{ mb}}{9.7814 \text{ m/s}^2} = \frac{1.1550 \times 10^{-3} \text{ n/m}^2}{9.7814 \text{ m/s}^2} = 1.1808 \times 10^{-4} \text{ Kg/m}^2$$

$$\text{column density} = 1.4815 \times 10^{17} \text{ cm}^{-2}$$

$$T = 234.60 \text{ K}$$

Layer 6 $j = 2$

i	P_{j+2-i}	Z_i	A_i	B_i	H_i
1	300.00mb	9.175km	-3.77×10^{-7}	$5.95 \times 10^{-8} \text{ km}^{-1}$	6.625km
2	264.99mb	10.00km	-1.272×10^{-6}	$1.49 \times 10^{-7} \text{ km}^{-1}$	6.387km
3	200.00mb	11.80km			

$$P_h = \frac{(1.9025 \times 10^{-3} + 5.1282 \times 10^{-3}) \text{ mb}^2}{(6.725 \times 10^{-6} + 2.2462 \times 10^{-5}) \text{ mb}} = \frac{7.0307 \times 10^{-3}}{2.9214 \times 10^{-5}} \text{ mb}$$

$$= 240.66 \text{ mb}$$

$$\mu_h = \frac{2.9214 \times 10^{-5} \text{ mb}}{9.7743 \text{ m/s}^2} = \frac{2.9214 \times 10^{-3} \text{ n/m}^2}{9.7743 \text{ m/s}^2} = 2.9889 \times 10^{-4} \text{ Kg/m}^2$$

$$\text{column density} = 3.7500 \times 10^{17} \text{ cm}^{-2}$$

$$T = 219.20 \text{ K}$$

Layer 7 $j = 3$

i	P_{j+2-i}	Z_i	A_i	B_i	H_i
1	200.00mb	11.80km	-1.272×10^{-6}	$1.49 \times 10^{-7} \text{ km}^{-1}$	6.367km
2	193.99mb	12.00km	-1.314×10^{-6}	$1.525 \times 10^{-7} \text{ km}^{-1}$	6.368km
3	141.70mb	14.00km	-3.302×10^{-6}	$2.945 \times 10^{-7} \text{ km}^{-1}$	6.372km
4	100.00mb	16.20km			

$$P_h = \frac{(5.926 \times 10^{-4} + 5.728 \times 10^{-3} + 9.6191 \times 10^{-3}) \text{ mb}^2}{(.3009 \times 10^{-6} + 3.4540 \times 10^{-5} + 7.2101 \times 10^{-5}) \text{ mb}}$$

$$= \frac{1.4940 \times 10^{-2}}{1.0965 \times 10^{-4}} \text{ mb} = 136.25 \text{ mb}$$

$$\mu_h = \frac{1.0965 \times 10^{-4} \text{ mb}}{9.7635 \text{ m/s}^2} = \frac{1.0965 \times 10^{-2} \text{ n/m}^2}{9.7635 \text{ m/s}^2} = 1.1231 \times 10^{-3} \text{ Kg/m}^2$$

$$\text{column density} = 1.4091 \times 10^{18} \text{ cm}^{-2}$$

$$T = 216.65 \text{ K}$$

The O₃ parameters are summarized in Table 9.

Although μ_h is not the same as μ , for a trace gas the difference is negligible.

LAYER	P_h	T	μ_h	column density
1	829.41mb	277.38K	$4.4419 \times 10^{-5} \text{ Kg/m}^2$	$5.5731 \times 10^{16} \text{ cm}^{-2}$
2	694.23mb	268.15K	$1.0602 \times 10^{-4} \text{ Kg/m}^2$	$1.3302 \times 10^{17} \text{ cm}^{-2}$
2a	660.08mb	265.72K	$6.7715 \times 10^{-5} \text{ Kg/m}^2$	$8.4960 \times 10^{16} \text{ cm}^{-2}$
3	549.06mb	256.44K	$6.3859 \times 10^{-5} \text{ Kg/m}^2$	$8.0122 \times 10^{16} \text{ cm}^{-2}$
4	447.76mb	246.68K	$7.6250 \times 10^{-5} \text{ Kg/m}^2$	$9.5669 \times 10^{16} \text{ cm}^{-2}$
5	343.93mb	234.60K	$1.1808 \times 10^{-4} \text{ Kg/m}^2$	$1.4815 \times 10^{17} \text{ cm}^{-2}$
6	240.66mb	219.20K	$2.9889 \times 10^{-4} \text{ Kg/m}^2$	$3.7500 \times 10^{17} \text{ cm}^{-2}$
7	136.25mb	216.65K	$1.1231 \times 10^{-3} \text{ Kg/m}^2$	$1.4091 \times 10^{18} \text{ cm}^{-2}$
8	33.83mb	219.72K	$5.8575 \times 10^{-3} \text{ Kg/m}^2$	$7.3492 \times 10^{18} \text{ cm}^{-2}$

TABLE 9 - O₃ parameters for the atmospheric layers in the multiple layer model.

For the uniformly mixed molecules equation (5.4) may be used provided that the atmospheric composition is known. The standard sea-level dry air composition is given in Table 10. These values can only be used if the H₂O contribution to μ is removed. That is easily done as

$$\mu_{\text{TOTAL}} = 1/g (P_2 - P_1) \quad (5.22)$$

for each layer. The O₃ contribution will also be

removed using the μ_h values from Table 9. Once these variable constituents have been removed, the μ values are ready for conversion to column density via equation (5.18). The resulting values are given in Table 11. The P_h and T values are the same for all the uniformly mixed molecules. These are given in Table 12.

MOLECULE	MASS (AMU)	% BY VOLUME	% BY MASS
N ₂	28.0134	78.084	75.521
O ₂	31.9988	20.9476	23.1425
Ar	39.948	0.934	1.288
CO ₂	44.0095	0.0314	0.0477
CH ₄	16.04303	0.0002	0.00011
N ₂ O	44.0128	5×10^{-5}	7.6×10^{-5}
CO	28.01055	7×10^{-6}	7×10^{-6}
OTHER	-	0.0027	0.0006

MEAN MOLECULAR MASS - 28.964 AMU

TABLE 10 - Normal (sea-level) dry air composition from the USSA (1976).

MOLECULE	LAYER			
	1	2	2a	3
O ₂	3.5712×10^{23}	8.3591×10^{23}	5.3002×10^{23}	4.4761×10^{23}
CO ₂	5.3532×10^{20}	1.2530×10^{21}	7.9449×10^{20}	6.7096×10^{20}
CO	1.1934×10^{17}	2.7933×10^{17}	1.7712×10^{17}	1.4958×10^{17}
CH ₄	3.4097×10^{18}	7.9809×10^{18}	5.0605×10^{18}	4.2736×10^{18}
N ₂	8.5242×10^{17}	1.9952×10^{18}	1.2651×10^{18}	1.0684×10^{18}

MOLECULE	LAYER		
	4	5	6
O ₂	4.4481×10^{23}	4.4527×10^{23}	4.4560×10^{23}
CO ₂	6.6676×10^{20}	6.6746×10^{20}	6.6794×10^{20}
CO	1.4864×10^{17}	1.4880×10^{17}	1.4890×10^{17}
CH ₄	4.2469×10^{18}	4.2513×10^{18}	4.2544×10^{18}
N ₂	1.0628×10^{18}	1.0628×10^{18}	1.0636×10^{18}

MOLECULE	LAYER	
	7	8
O ₂	4.4609×10^{23}	4.5165×10^{23}
CO ₂	6.6868×10^{20}	6.7702×10^{20}
CO	1.4907×10^{17}	1.5093×10^{17}
CH ₄	4.2591×10^{18}	4.3122×10^{18}
N ₂	1.0636×10^{18}	1.0781×10^{18}

TABLE 11 - Column density values, in cm^{-2} , for the uniformly mixed molecules.

LAYER	P	T
1	829.42mb	277.38K
2	694.92mb	268.20K
2a	660.42mb	265.61K
3	550.36mb	256.56K
4	450.00mb	246.92K
5	350.00mb	235.39K
6	250.00mb	220.85K
7	150.00mb	216.65K
8	50.001mb	217.23K

TABLE 12 - Pressure and temperature parameters for the uniformly mixed molecules.

Using this data, the atmospheric transmittance function was calculated for each layer. The same program, MC, that was used to carry out the single layer calculation was also used for this, with one small change. In the single layer calculation any molecular line which contributed less than 0.001 to k_λ at line center was ignored. Here, because the layer column densities are smaller, this value was reduced by a factor of ten to 0.0001. The smallest layer, layer 1, has roughly 10% of the total column density of all 8 layers, so the condition will closely match the single layer criterion when expressed in terms of molecular line strengths. The individual layer transmittances were combined by point by point multiplication to produce atmospheric transmittance values for Calgary, Kitt Peak, Mount Lemmon and Mauna Kea. Once this had been done, the scaling to other air mass values and the numerical integrations were carried out in the same way as before. The quantitative values which resulted are

given in Table 13, while the individual extinction curves are given in Figures 14a through 14h. The Vega and cool giant models are the same as before.

The column density, pressure and temperature values for Kitt Peak in the multiple layer model are somewhat different than the MB 'Kitt Peak summer' values, although the comparison must be done cautiously. The total O_3 column density above Kitt Peak is $9.50 \times 10^{18} \text{ cm}^{-2}$ for the multiple layer model as compared to $8.56 \times 10^{18} \text{ cm}^{-2}$ in MB. Similarly, O_2 shows a 1% discrepancy, CO_2 a 5% discrepancy and CO a 7% discrepancy, with the multiple layer values being smaller in these cases. N_2O shows a considerable disagreement, roughly a factor of two, but this is not serious because N_2O is a very minor constituent of the atmosphere. The change in CO_2 column density may have a small effect upon the results, which must be kept in mind. The pressure and temperature values for O_3 and H_2O can be roughly compared with the single layer values by doing a μ_h weighted average over the layers. The resulting values are 687 mb and 267K for H_2O and 84mb and 221K for O_3 . The only significant difference between these values and the MB values is that the O_3 pressure value is larger by a factor of 1.5. The difference would be of concern for the R and I filters, shortward of $1 \mu\text{m}$, where O_3 is a key source of absorption. For the JHK filters this factor should not

SITE	SOURCE	FILTER	E	Δ	Δ/E	δ
MAUNA KEA (1.57 PMM)	VEGA MODEL	J	0.047	0.052	1.122	0.0023
		H	0.027	0.023	0.867	0.0004
		K	0.033	0.025	0.744	-0.0008
	4000K MODEL	J	0.047	0.055	1.160	
		H	0.027	0.024	0.882	
		K	0.0325	0.024	0.730	
MOUNT LEMMON (3.62 PMM)	VEGA MODEL	J	0.067	0.083	1.223	0.0032
		H	0.040	0.039	1.034	0.0006
		K	0.046	0.033	0.713	-0.0008
	4000K MODEL	J	0.067	0.085	1.270	
		H	0.040	0.040	0.983	
		K	0.046	0.032	0.704	
KITTE PEAK	VEGA MODEL	J	0.083	0.100	1.210	0.0036
		H	0.050	0.049	0.974	0.0007
		K	0.056	0.038	0.683	-0.0008
	4000K MODEL	J	0.083	0.104	1.258	
		H	0.050	0.050	0.988	
		K	0.056	0.038	0.676	
CALGARY (7.47 PMM)	VEGA MODEL	J	0.107	0.125	1.170	0.0038
		H	0.066	0.064	0.965	0.0008
		K	0.072	0.047	0.651	-0.0007
	4000K MODEL	J	0.106	0.129	1.214	
		H	0.066	0.064	0.979	
		K	0.071	0.046	0.646	

TABLE 13 - MULTIPLE LAYER MODEL RESULTS FOR THE FOUR SITES.
E, Δ AND δ ARE DEFINED IN MANDUCA AND BELL (1979)
AND ON PAGE 51. E IS IN MAGNITUDES PER AIR MASS,
 Δ AND δ ARE IN MAGNITUDES.

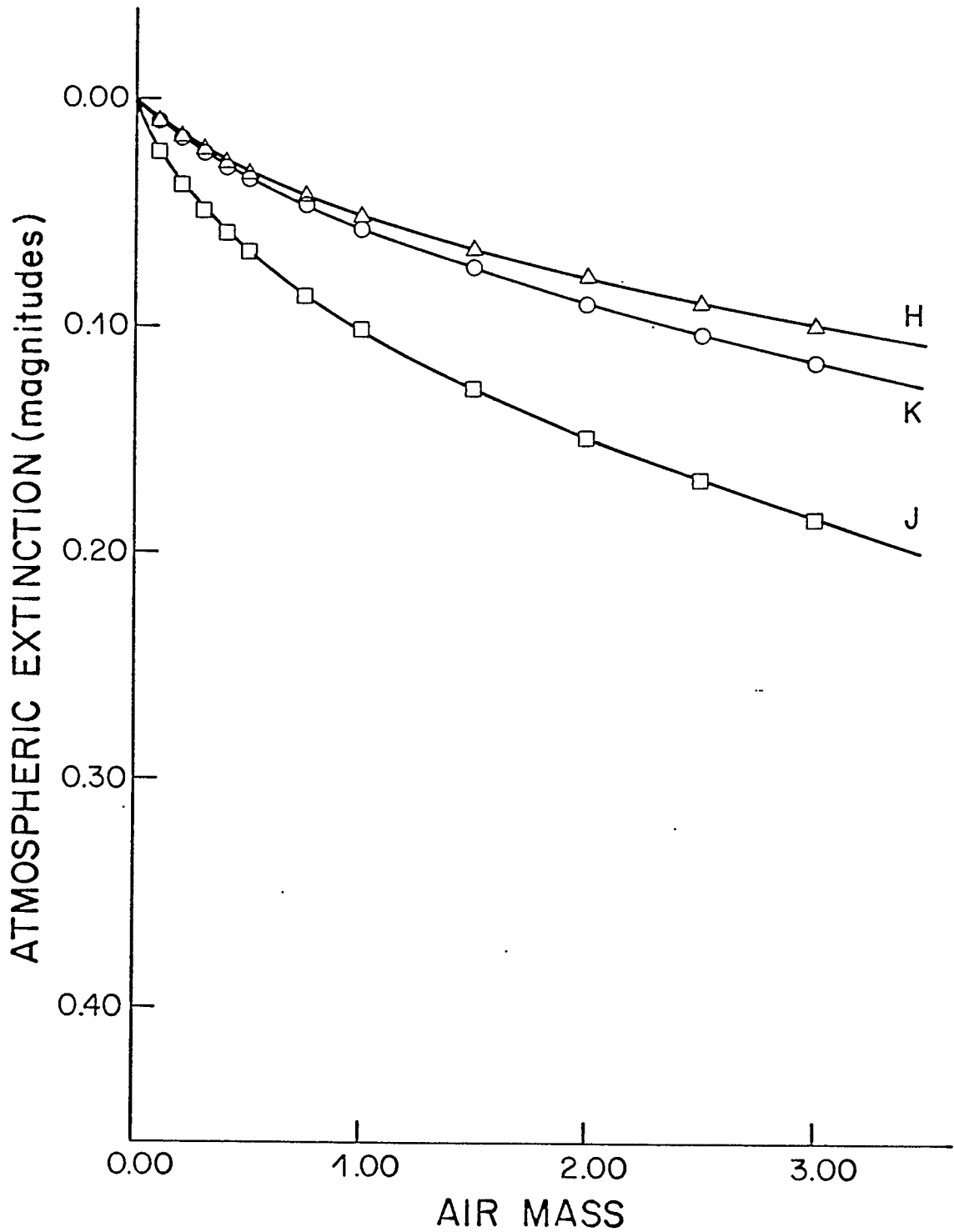


Figure 14a- Multiple layer results for Mauna Kea.

H₂O column density- 1.57 PMM; 4000 K model.
 Slopes (1.00 to 2.00 air mass) Zero point errors
 J- 0.0470 mag./a.m. J- 0.0546 mag.
 H- 0.0268 H- 0.0236
 K- 0.0325 K- 0.0237

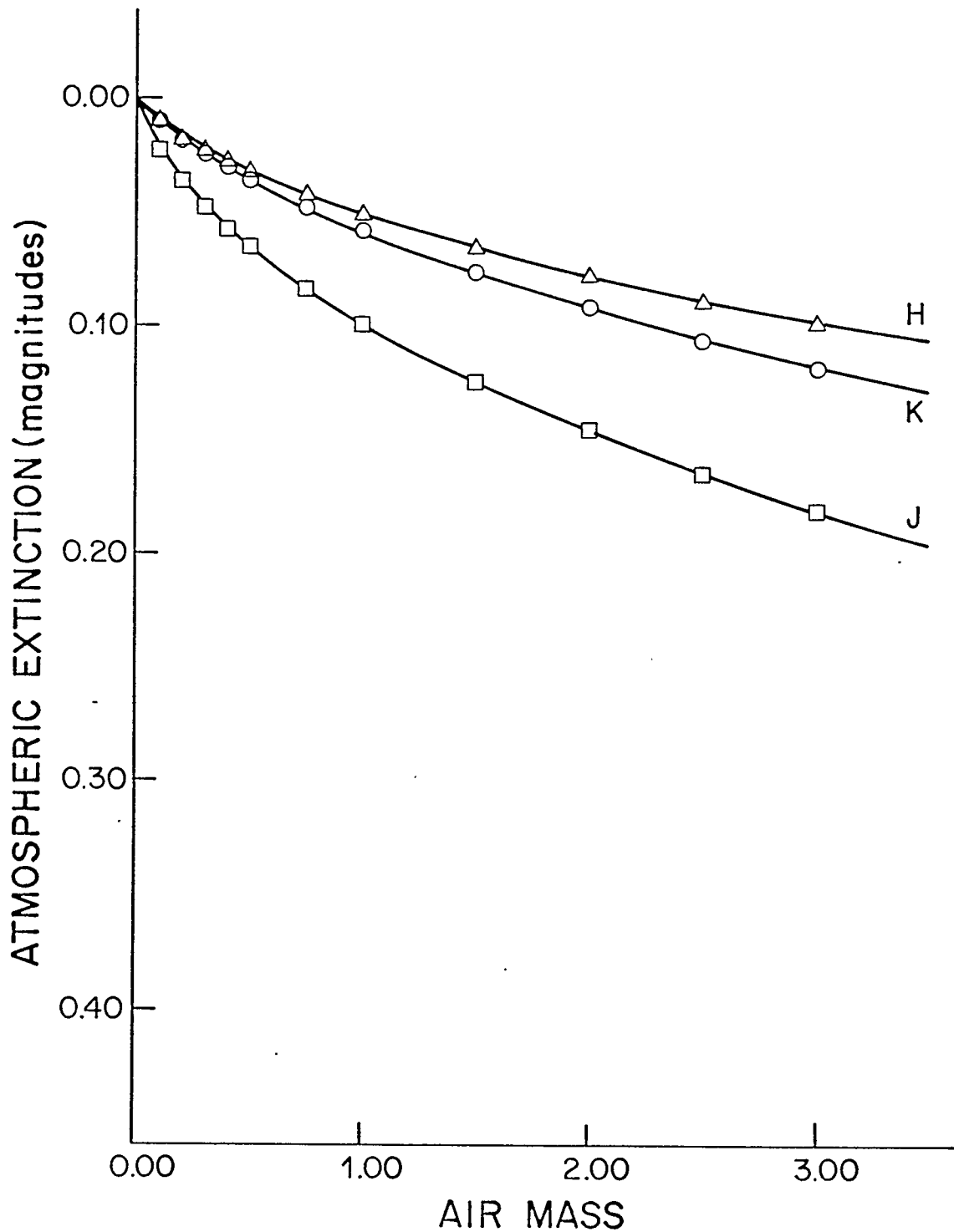


Figure 14b- Multiple layer results for Mauna Kea.

H₂O column density- 1.57 PMM; Vega/9100 K model.

Slopes (1.00 to 2.00 air mass)

J- 0.0466 mag./a.m.

H- 0.0268

K- 0.0330

Zero point errors

J- 0.0523 mag.

H- 0.0232

K- 0.0245

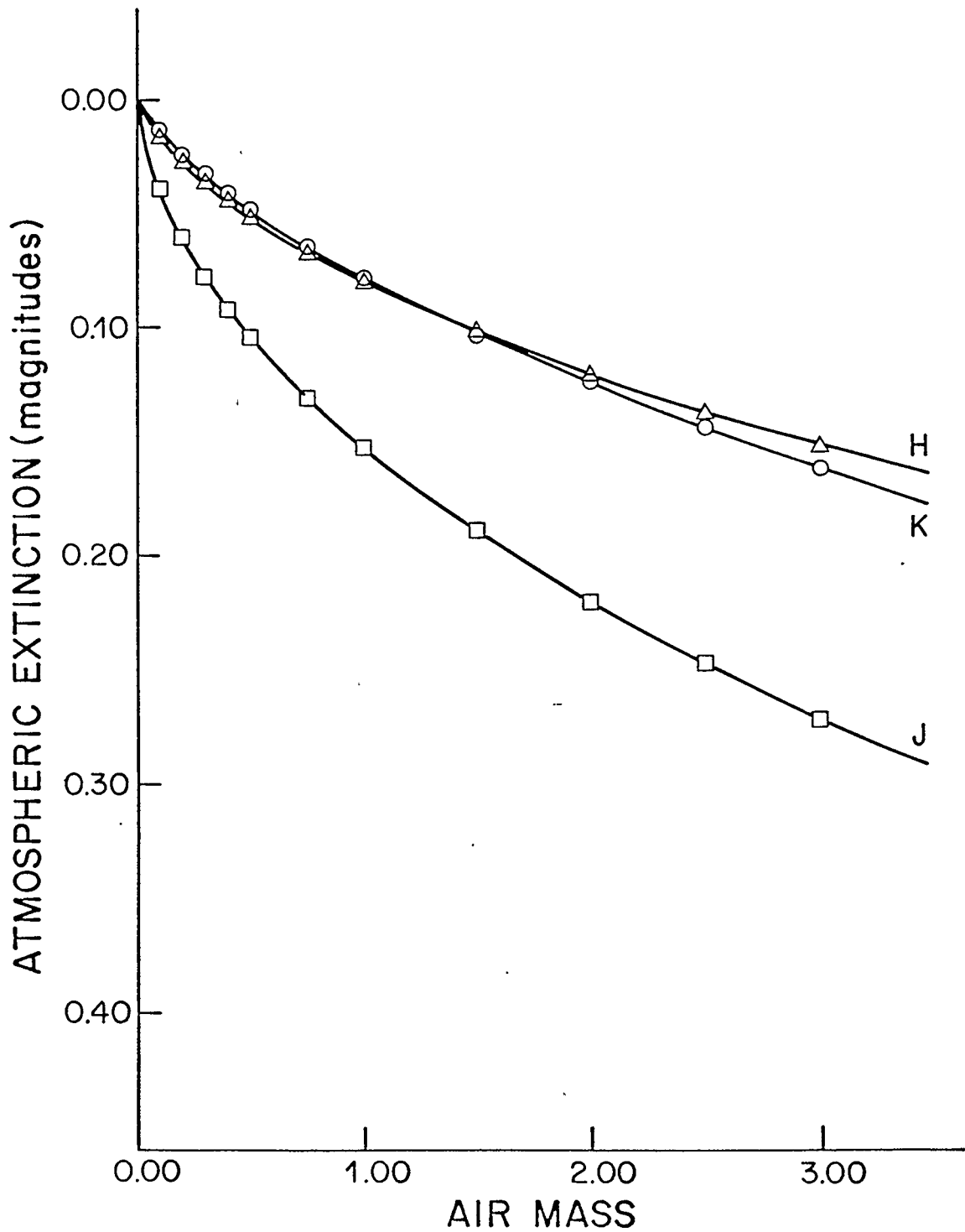


Figure 14c- Multiple layer results for Mt. Lemmon.

H₂O column density- 3.62 PMM; 4000 K model.
 Slopes (1.00 to 2.00 air mass) Zero point errors
 J- 0.0673 mag./a.m. J- 0.0855 mag.
 H- 0.0402 H- 0.0395
 K- 0.0458 K- 0.0322

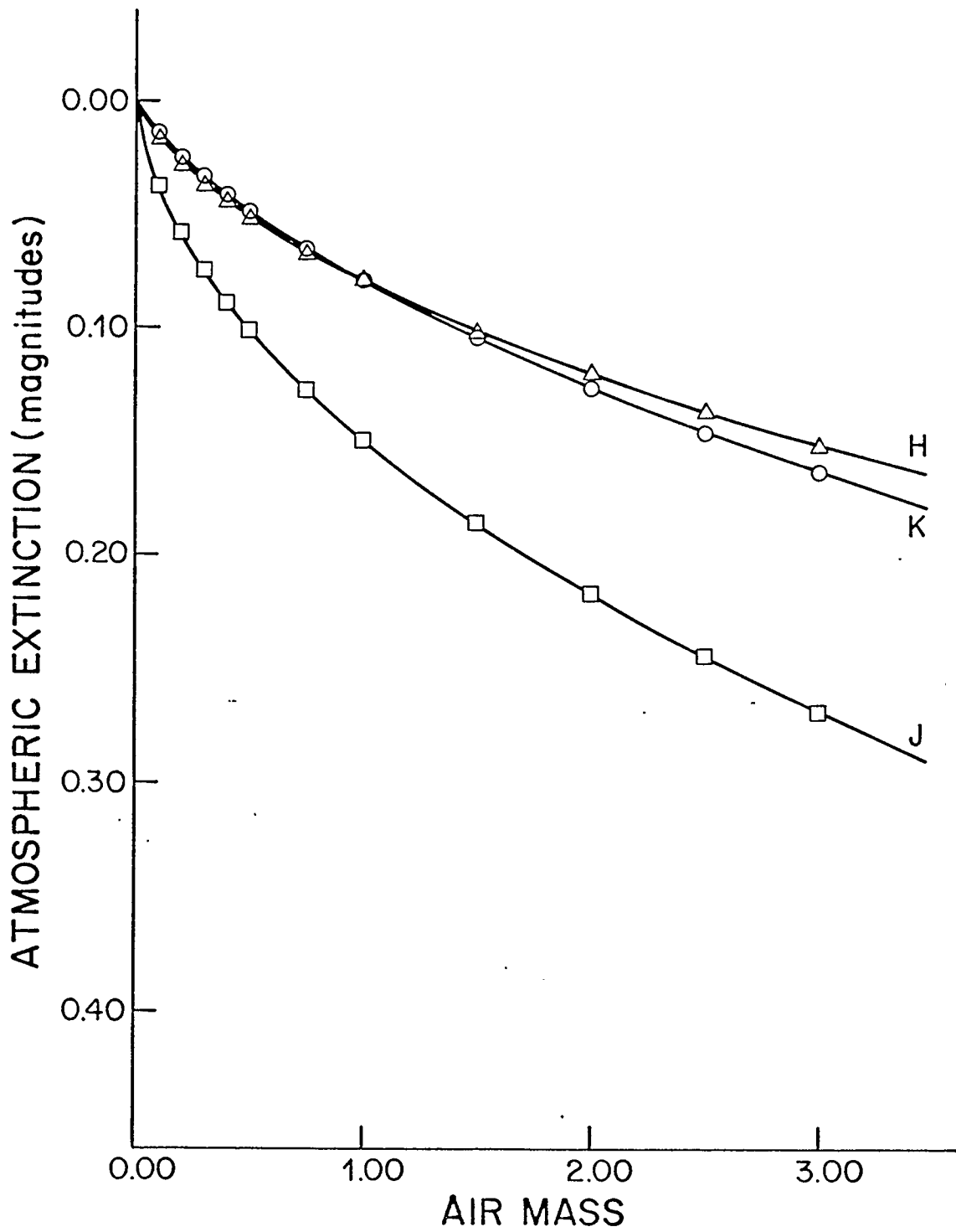


Figure 14d- Multiple layer results for Mt. Lemmon.

H₂O column density- 3.62 PMM; Vega/9100 K model.
 Slopes (1.00 to 2.00 air mass) Zero point errors
 J- 0.0673 mag./a.m. J- 0.0823 mag.
 H- 0.0403 H- 0.0339
 K- 0.0463 K- 0.0330

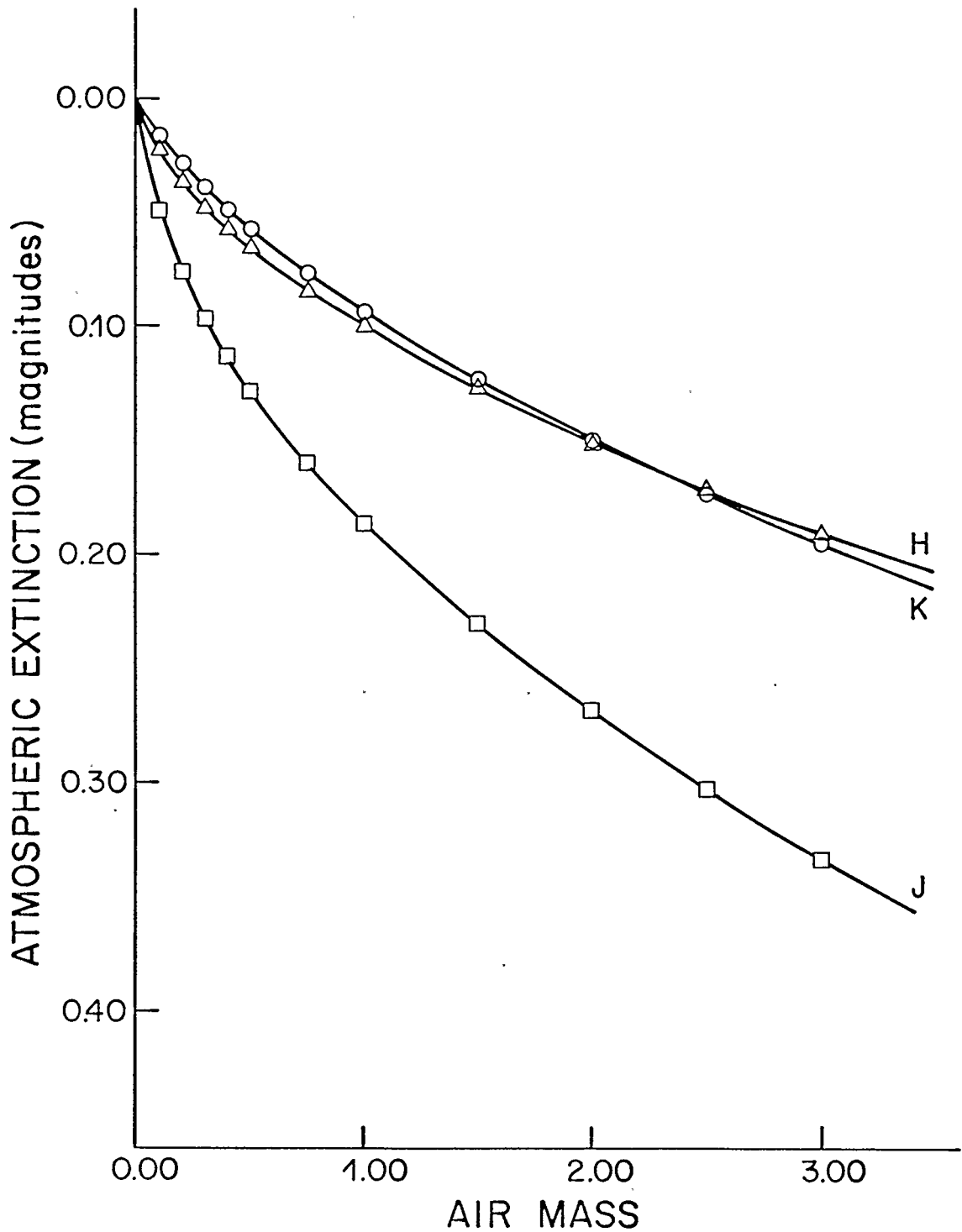


Figure 14e- Multiple layer results for Kitt Peak.

H₂O column density- 5.05 PMM; 4000 K model.
 Slopes (1.00 to 2.00 air mass) Zero point errors
 J- 0.0826 mag./a.m. J- 0.1039 mag.
 H- 0.0503 H- 0.0497
 K- 0.0563 K- 0.0377

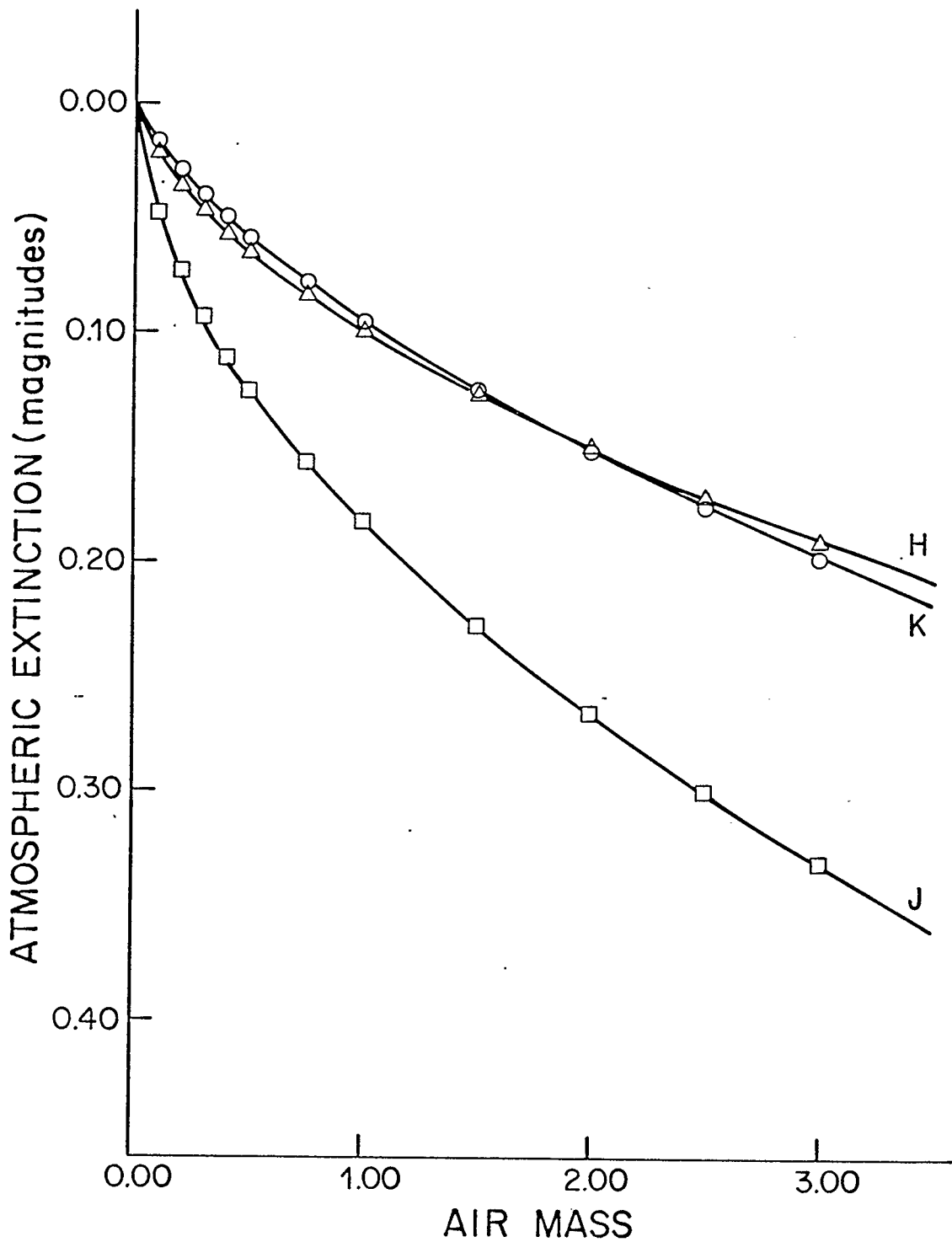


Figure 14f- Multiple layer results for Kitt Peak.

H₂O column density- 5.05 PMM; Vega/9100 K model.
 Slopes (1.00 to 2.00 air mass) Zero point errors
 J- 0.0829 mag./a.m. J- 0.1003 mag.
 H- 0.0504 H- 0.0490
 K- 0.0563 K- 0.0384

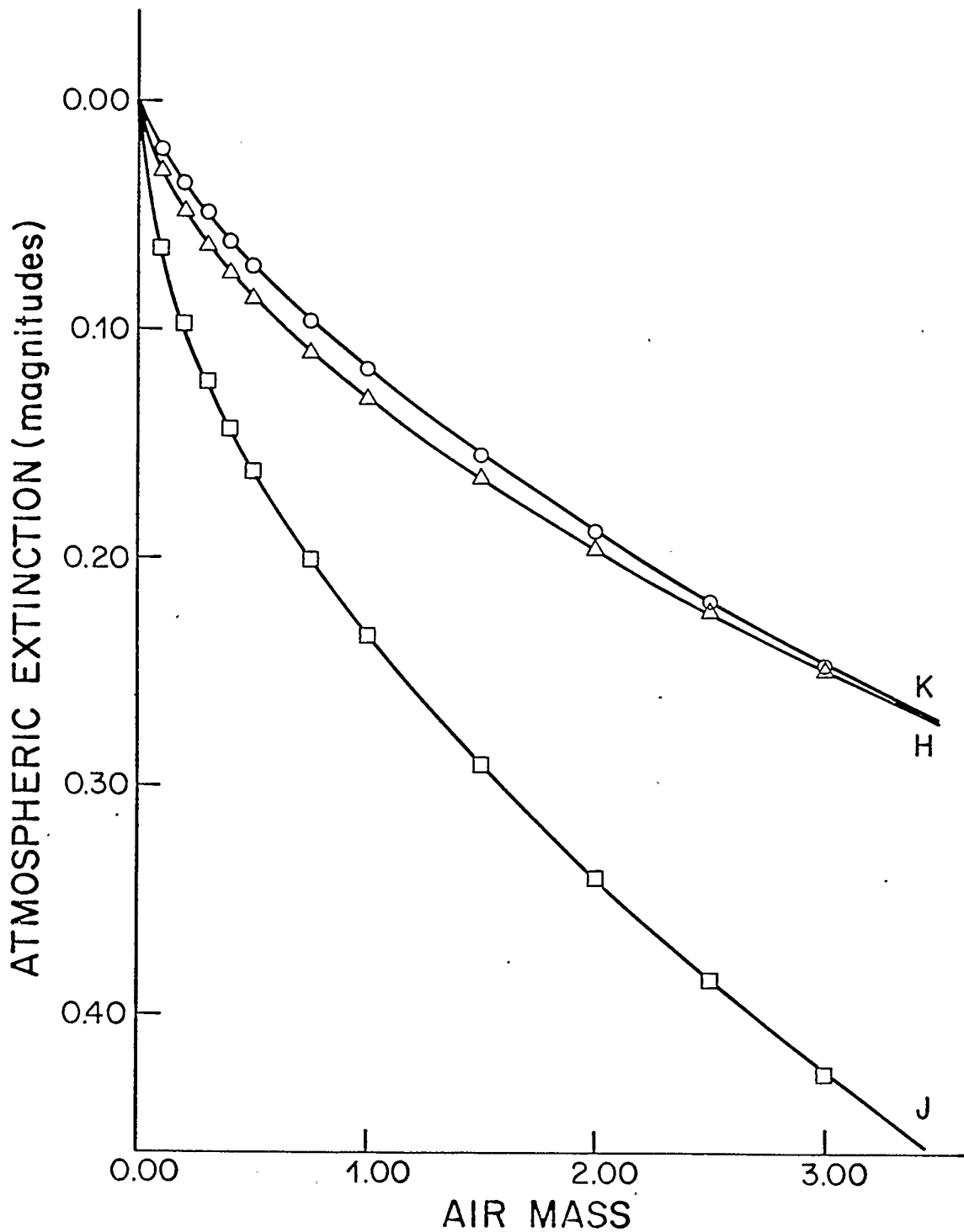


Figure 14g- Multiple layer results for Calgary.

H₂O column density- 7.47 PMM; 4000 K model.
 Slopes (1.00 to 2.00 air mass) Zero point errors
 J- 0.1060 mag./a.m. J- 0.1249 mag.
 H- 0.0659 H- 0.0644
 K- 0.0710 K- 0.0466

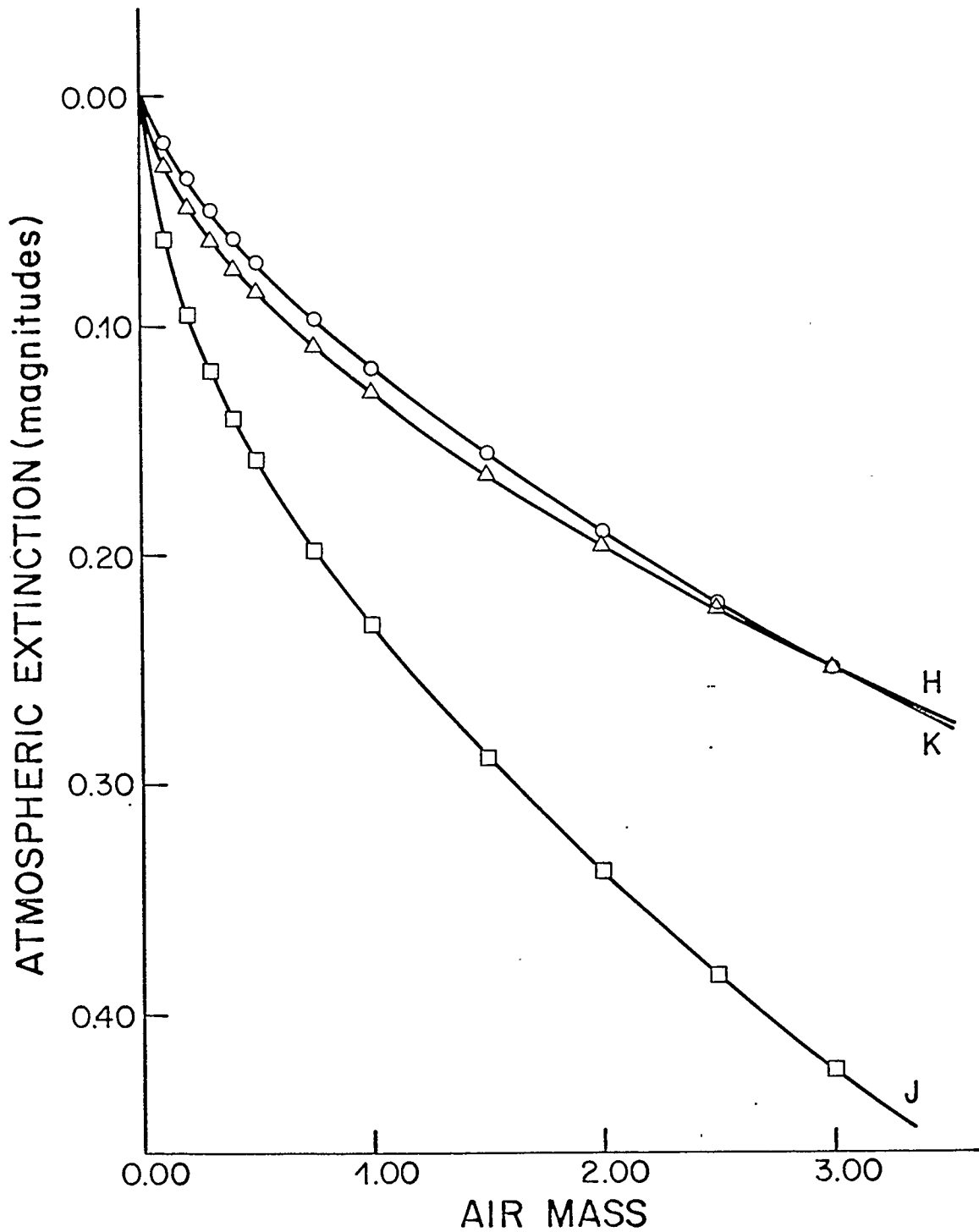


Figure 14h- Multiple layer results for Calgary.

H ₂ O column density- 7.47 PMM; Vega/9100 K model.	
Slopes (1.00 to 2.00 air mass)	Zero point errors
J- 0.1067 mag./a.m.	J- 0.1249 mag.
H- 0.0660	H- 0.0637
K- 0.0715	K- 0.0466

cause serious problems.

Direct comparison of the multiple layer Kitt Peak results with the single layer Kitt Peak results shows that the two sets of results are very similar. Figure 15 presents a plot of $m(\text{multiple layer model}) - m(\text{single layer model})$ as a function of air mass for the three filters, from the Vega model results. The cool giant results yield a similar set of values, so these are not plotted. The $X = 1.00$ points are a reflection of the mean difference in transmittance between the two calculations, weighted by the object spectrum and the filter response function. The percentage values for this difference are 0.22% for the H filter, 0.11% for the K filter and 0.065% for the J filter; the single layer model gives a slightly larger mean absorption than the multiple layer model in each case.

The variation in the magnitude difference as a function of air mass reflects differences in the relative shape of the transmittance functions. If the mean differences which are listed above were due to a constant factor at all wavelengths, the magnitude difference would be a linear function of air mass. Any deviations from linearity indicate something about the distribution of the transmittance differences. The curves in Figure 15 all show the same qualitative features: at low X values the multiple layer model calculations give a larger amount of absorption than

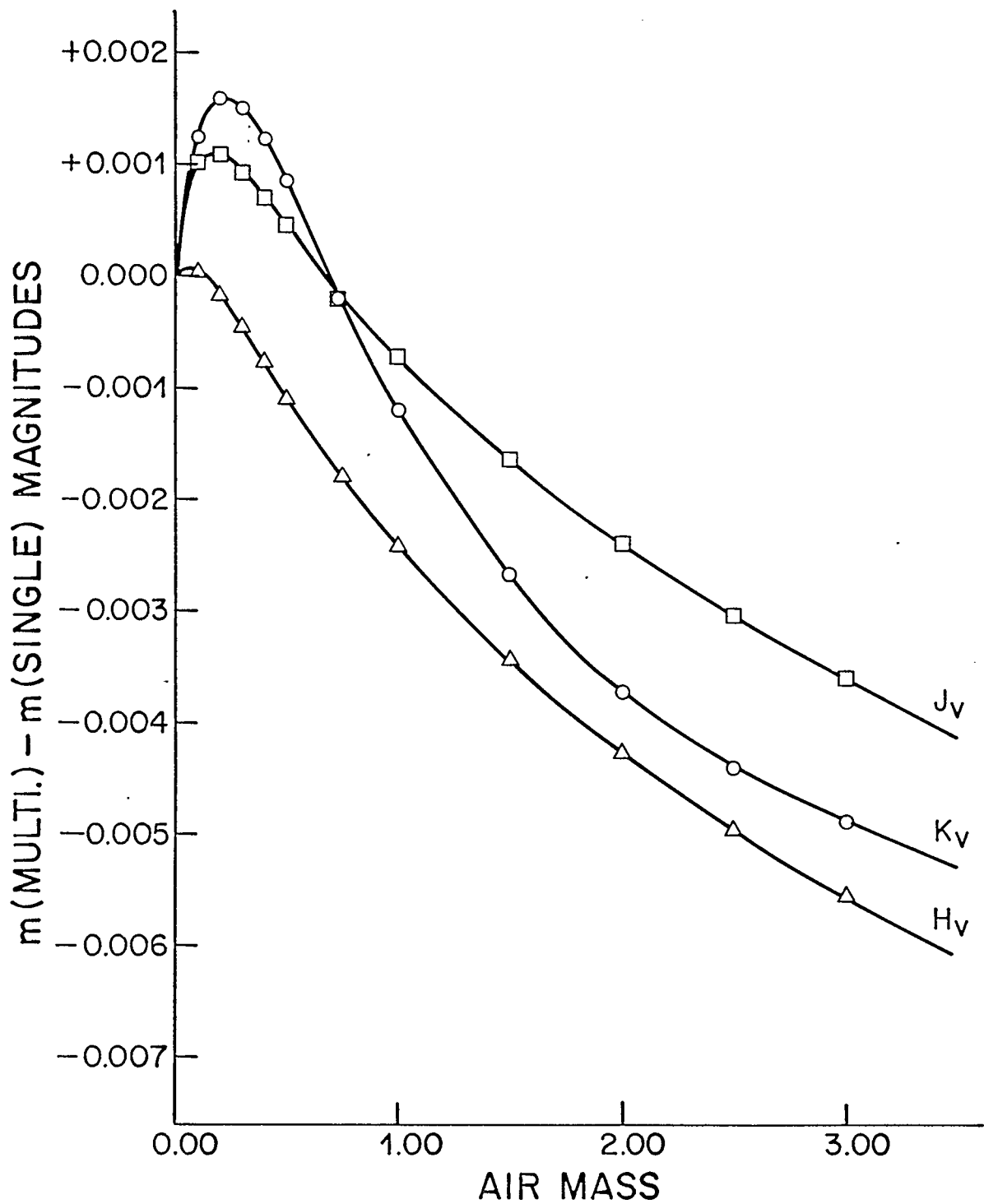


Figure 15- The magnitude difference as a function of air mass for the Vega model under 'Kitt Peak summer' conditions. ΔM is defined as $M(\text{multiple layer model}) - M(\text{single layer model})$.

the single layer model calculations, while as X increases this trend reverses strongly to give a larger transmittance for the multiple layer model over most of the range of X . Whatever causes this tendency is much weaker for the H filter than for the other filters. In all cases the curve of Δm versus X flattens out at large X values. It may be that the low air mass effect and the high air mass effect stem from the same cause, because when one is larger so is the other.

At very small X values, the line cores are dominant in determining the absorption because the line wings essentially give no absorption when $X = 0.10$ or 0.20 . At large X values, changes in the transmittance are mainly due to the line wings because the cores are generally saturated and cannot give more absorption. The tendency for Δm to be positive at low X values suggests that the line cores are stronger in the multiple layer model than in the single layer model. The tendency for Δm to be negative at high X values implies that the line wings are stronger in the single layer model than in the multiple layer model. This sort of pattern is to be expected because in the multiple layer model a large fraction of the column density is in the higher layers where P and T are low and hence α is small, so these layers enhance the line core at the expense of the line wing. The effect is smaller for the H filter than for the others, which

presumably is due to being in a better atmospheric window. The change in the mean absorption at $X = 1.00$ may be due to this factor or may be due to the small parameter changes noted above. It appears that the low percentage deviation at $X = 1.00$ for the J filter does not reflect a better point by point match. Instead, the line wing to line core absorption redistribution nearly cancels out for the J filter.

The change in the minimum line absorption criterion allows some inferences to be drawn about the importance of weak lines in the transmittance results. In the single layer model for Kitt Peak the range in pressure is 796mb, while in the multiple layer model for Kitt Peak the smallest range in pressure is 100mb. Ignoring the slight changes in composition, the column density values for the individual layers in the multiple layer model are smaller by a factor of 8; the line center absorption minimum decreased by a factor of 10 so in effect any line with a contribution of more than 0.0008 to k_λ at line center for Kitt Peak will be included in the multiple layer calculations as compared to the single layer value of 0.001. The inclusion of weak lines between these values has only a very small influence upon the extinction curve, even if all the change is due to this factor. This provides further confirmation that the difference in the minimum line intensity between IRTRANS and MC is not the cause of

the discrepancy between the single layer results here and those of MB.

The extinction curves for the Kitt Peak single layer model and the Kitt Peak multiple layer model are surprisingly similar. The use of the USSA instead of one of the supplemental atmospheric models had little, if any, effect upon the results. It seems that the single layer model calculations will give the accuracy needed for comparison with real data, provided that the systematic errors in the calculation process itself are dealt with correctly.

The intercomparison of sites shows some interesting features. Looking at the $\frac{\Delta}{E}$ ratios, this value stays reasonably constant for the three continental sites. In fact, the mean values for these three sites are 1.224 ± 0.036 for the J filter, 0.987 ± 0.024 for the H filter and 0.679 ± 0.027 for the K filter ($\pm 1\sigma$ - error values) under these conditions. This implies that a crude extinction correction for continental sites may be done by applying the Kitt Peak $\frac{\Delta}{E}$ ratio to other sites. Such a correction procedure would require that the H_2O column density at the site under consideration be converted to an equivalent Kitt Peak value, and then the proper $\frac{\Delta}{E}$ value found from Kitt Peak calculations. The $\frac{\Delta}{E}$ values show a tendency to decrease as the site altitude increases, but this is not a regular trend.

Assuming that the calculations accurately portray the real conditions, the results for the 4 sites show clearly that Mauna Kea is a much better site than the others. None the less, despite the small curvature shown by the extinction curves for $X > 1.00$ the non-linearity is present quite strongly. The $\frac{\Delta}{E}$ values have not changed drastically from the values for the other sites. Comparison of Mount Lemmon to Kitt Peak shows that a relatively small change in site altitude can cause a significant change in atmospheric extinction. Calgary is beginning to show a serious amount of atmospheric extinction, especially for the J filter. Comparison of the δ values at the 4 sites shows that from Calgary to Mount Lemmon there is only a 20% change in δ , compared to a 40% change in E or Δ , but from Mount Lemmon to Mauna Kea δ changes by about the same percentage as E or Δ .

Looking at the individual Δ and E values, these values increase as the altitude decreases in all cases. These changes are somewhat erratic, either viewed as a function of altitude or viewed as a function of pressure, so a plot of E against $\Delta + E$ is more useful. This is given in Figures 16 and 17, for the Vega model, with both the single layer and multiple layer results included. The results for the cool giant model are quite similar. One thing which is apparent

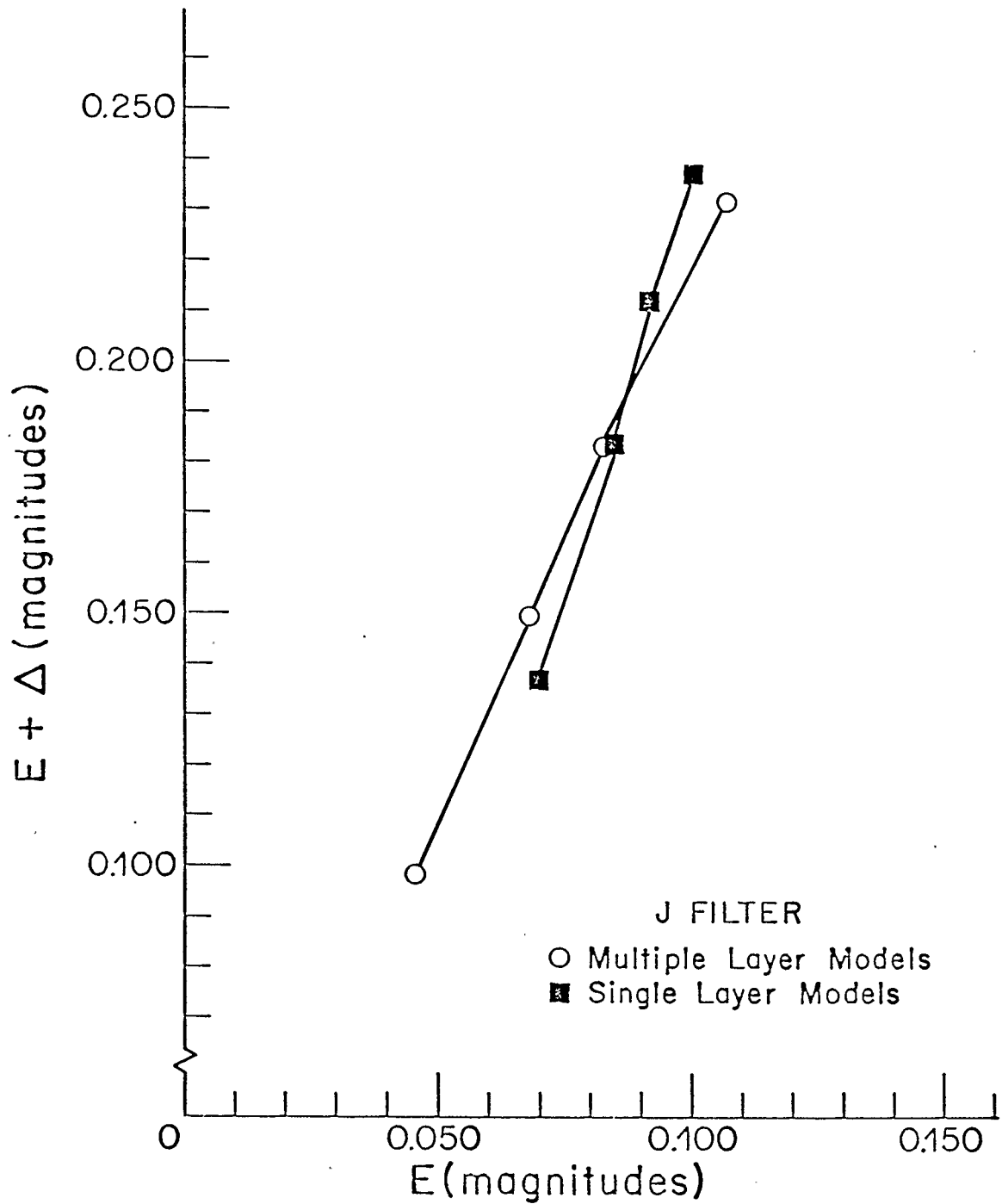


Figure 16- The extinction between $X=1.00$ and $X=2.00$ plotted against the extinction between $X=0.00$ and $X=1.00$ for the J filter results for Vega in both the multiple layer model and the single layer model.

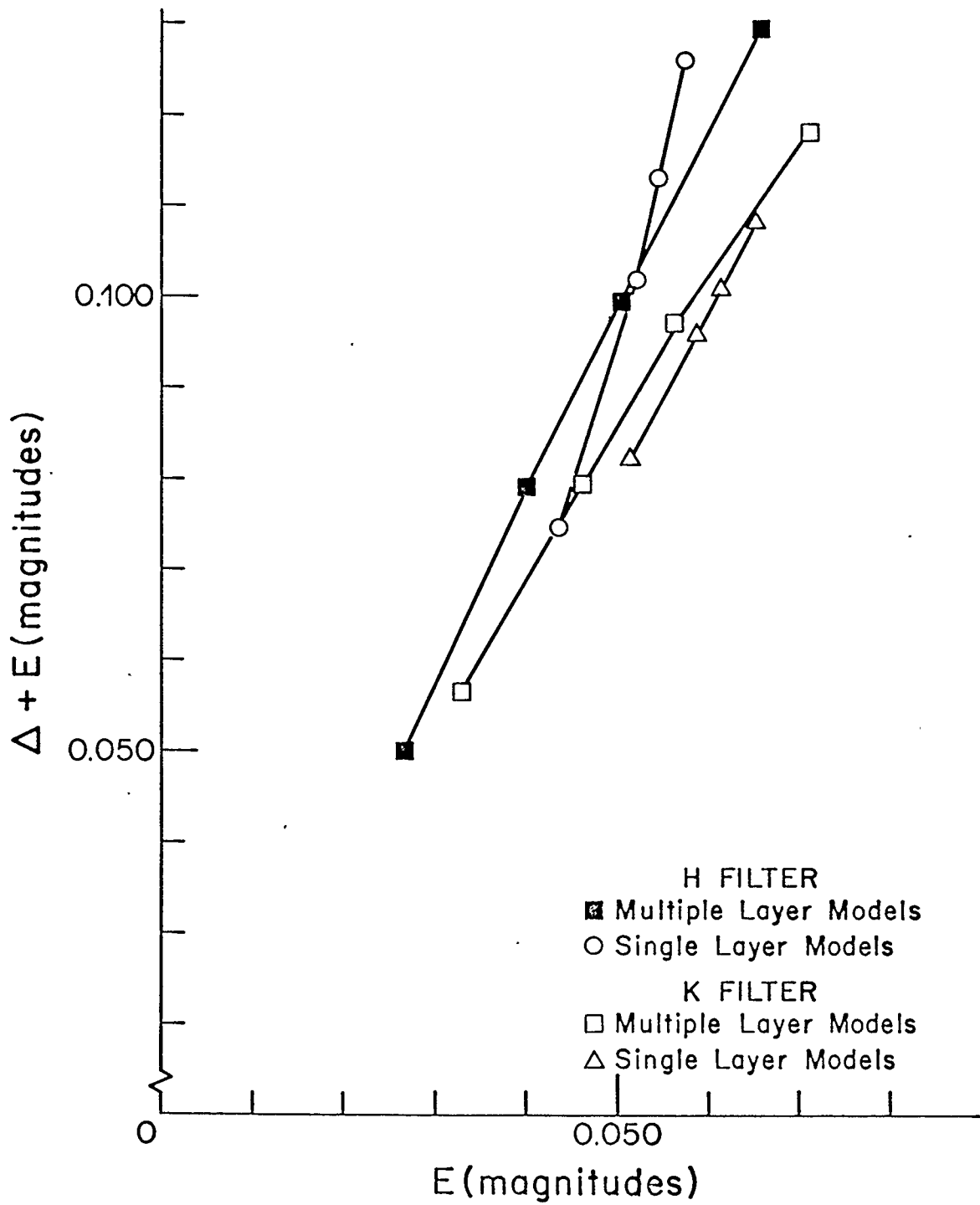


Figure 17- The extinction between $X=1.00$ and $X=2.00$ plotted against the extinction between $X=0.00$ and $X=1.00$ for the H and K filter results for Vega in both the multiple layer model and the single layer model.

from the figures is that the slope of the E versus $E + \Delta$ curve from the single layer models for Kitt Peak is steeper than the slope from the multiple layer models for the various sites. The curves are not subject to a large amount of curvature, indeed they are very close to straight lines, where the MB equivalents which are given in Figures 4 and 5 show much more curvature, considering the difference in scales.

The comments from Chapter 4 comparing the single layer results found here to those of MB also apply, with little change, to a comparison of the multiple layer results to the MB results. Further discussion of this problem and of the search for a suitable correction method will be deferred until the next chapter.

Chapter SixConclusions

In the previous chapters the results of numerical simulations of atmospheric extinction from MB and from both single layer and multiple layer calculations performed here at Calgary have been presented. These calculations imply that Johnson (1965a) drew the wrong conclusion about the suitability of the linear extinction law for use in infrared photometry. Presumably the models upon which his conclusions were based were too simple to reflect atmospheric conditions correctly. The problem now is to find a better method of dealing with the extinction, to allow for the curvature evident in the simulated extinction curves. This could either be an extension of the linear extinction law or some other approach. The difference between the MB extinction curves and those derived here must be explained; further, the effect of this work upon the initial establishment of the standard stars which define the magnitude system must be considered. These matters will be considered, if not resolved, in this chapter.

The extinction curves presented in MB and in Chapters 4 and 5 show very little curvature above an air mass of 1.00. It is not surprising, therefore, that the initial measurements of atmospheric extinction

in the infrared led to the adoption of a linear extinction law. Observation of the curvature in the $m(X)$ function, assuming it to follow the results of the numerical simulation, would be difficult. Either very stable sky conditions over a period of several hours under conditions where the H_2O column density is reasonably large or an accuracy of 0.001 magnitudes under good sky conditions would be needed to observe this curvature. It appears that knowledge of the shape of the extinction curve for $X > 1.00$ would not allow the determination of the true zero point magnitude because there is a change in the curvature below $X = 1.00$. This region is fictitious, as was noted in Chapter 2, and because no meaning can be assigned to $X < 1.00$ there is no way to observe this section of the extinction curve. In order to retain the linear extinction law a correction factor would have to be tabulated as a function of the observing conditions for each site and each filter. Such an approach is somewhat less than ideal, and could be unworkable. Yet there may be no alternative unless a method is found to observe routinely the curvature of the extinction function and relate it to a zero point correction.

The only alternative to the linear extinction law that has been proposed for carrying out extinction corrections, as far as the author is aware, is the square-root law which Johnson (1965a) discredited.

This extinction law is based upon the result for strong spectral lines, derived in Chapter 3 [equation (3.14)], that the mean line absorption increases in proportion to the square-root of the column density. Assuming that the air mass is a measure of the relative column density along the path for all molecules present, which is the same as assuming the atmosphere to be horizontally stratified, and assuming that the lines do not overlap an equation similar to (1.30) results for all the lines which are in the strong line limit. The square-root law does not apply to all the sources of extinction, but it is useful for cases in which the strong lines are the dominant source of extinction. When applying the square-root law to the JHK filters the aerosol component of the extinction, which is a linear function of air mass, must be removed from the data because it is a significant component of the total extinction.

The square-root law applies, strictly speaking, to the case of a homogeneous absorbing medium for which the Lorentz profile correctly describes the spectral line profiles. The latter may not be true, while the former is definitely not true for the atmosphere and its representation by the multiple layer model. Comparison of how well the square-root law fits the single layer models and the multiple layer models should give some indication of the effect of the inhomogeneity upon the results.

The aerosol extinction is a relatively weak function of ν in the infrared. In moving from a value ν_0 to another value $\nu_0 + \Delta\nu$, the relative change in aerosol extinction is $(1 + \frac{\Delta\nu}{\nu_0})^{0.80} - 1$, nearly equal to $0.80 \frac{\Delta\nu}{\nu_0}$ if the ratio is small. If ν_0 is chosen to be the central wavelength of a medium-band filter then over the range of the filter $|\frac{\Delta\nu}{\nu_0}| < 0.10$ and so the aerosol extinction varies by $\pm 8\%$ or so over the filter. This corresponds to $\pm 2\%$ to $\pm 3\%$ variation in the total extinction curve slope, which is small enough to ignore for the moment. Taking ν_0 values of $0.8000 \mu\text{m}^{-1}$ for the J filter, $0.6061 \mu\text{m}^{-1}$ for the H filter and $0.4494 \mu\text{m}^{-1}$ for the K filter, aerosol extinction values at the 4 sites for the JHK filters are presented in Table 14.

	J	H	K
CALGARY	0.0301	0.0241	0.0190
KITT PEAK	0.0178	0.0143	0.0112
MT. LEMMON	0.0109	0.0088	0.0069
MAUNA KEA	0.0043	0.0064	0.0027

TABLE 14 - Aerosol extinction values (magnitudes/air mass for subtraction from the extinction curves.

Removing the aerosol extinction contribution using the values in Table 14, the $X = 1.00$ and $X = 2.00$ extinction values were used with the square-root law to produce zero air mass values. In Tables 15a through 15c the zero point errors which resulted - equivalent to Δ from the linear law case - are given for the

a) SOURCE VEGA 4000 K	FILTER	CALGARY	KITT PEAK	MT. LEMMON	MAUNA KEA	
	J	0.03621	0.02263	0.01354	-0.00126	
	H	0.01070	0.00261	-0.00204	-0.00781	
	K	-0.01813	-0.01812	-0.01722	-0.01500	
	J	0.04071	0.02654	0.01673	0.00055	
	H	0.01159	0.00366	-0.00141	-0.00743	
	K	-0.01826	-0.01827	-0.01741	-0.01522	
	b) SOURCE VEGA 4000 K	FILTER	2.50 PMM	5.05 PMM	7.54 PMM	10.1 PMM
		J	0.00358	0.02000	0.03190	0.04205
H		-0.00770	0.00101	0.00733	0.01379	
K		-0.02049	-0.02232	-0.02294	-0.02328	
J		0.00617	0.02388	0.03616	0.04712	
H		-0.00722	0.00181	0.00806	0.01456	
K		-0.02057	-0.02236	-0.02294	-0.02322	
c) SOURCE VEGA COOL GIANT		FILTER	KITT PEAK		MAUNA KEA	
			SUMMER	WINTER		
	j		0.03981	0.00438		-0.00661
	h		0.00813	-0.01247		-0.01827
	k		-0.03808	-0.03404		-0.03131
	J		0.07770	0.01960		0.00073
	K	0.03430	-0.01496	-0.03263		
		j	0.06197	0.01326	-0.00098	
		h	0.00913	-0.01147	-0.01727	
		k	-0.03704	-0.03191	-0.02913	
		J	0.11901	0.03683	0.01118	
		K	0.03705	-0.01114	-0.03163	

Table 15 - Square-root law zero point errors, using the aerosol correction. All values in magnitudes. (a) multiple layer model calculations. (b) single layer model calculations. (c) Manduca and Bell (1979).

multiple layer models, the single layer models and those MB calculations for which detailed data is available. The above ν_0 values were used for all forms of each filter, which could introduce a small error into the Johnson J and K filter results. As before, the zero point error is $m(0)$ from the extinction law minus the true $m(0)$ value. Both negative and positive values are present, unlike the linear law zero point errors.

The square-root law gives zero point errors which are at least a factor of 2 or 3 smaller in absolute value than the equivalent linear extinction law values. In a few cases the zero point error is of the order of 0.001 magnitudes. Values of about 0.02 to 0.01 magnitudes are typical. Such values, although much later than the equivalent Δ values, are still large enough to be worrisome.

In general the K filter seems to act differently than the other filters when conditions are changed. The K filter zero point error changes very little from site to site, and is little changed by a factor of 4 range in H_2O column density. The zero point error is affected only slightly by substitution of the 4000 K source for the 9100 K source. This feature is not shared by the earlier K filter results of MB, although the Kitt Peak K filter results show much less variation of zero point error than any other filter in the MB

results. The application of the square-root law to the K filters nearly always results in overestimating the zero air mass intensity.

The J and H filters show a range of zero point values. An obvious pattern is that these zero point errors increase as the H₂O column density increases, either from moving to lower altitudes or from an increase in the water vapor content above a given site. Under the conditions of the USSA (1976), the zero point errors for the H filter at altitudes of 2 km to 3 km are quite small. For the J filter the zero point errors become very small around an altitude of 4 km. These filters show a larger colour dependence than does the K filter. Once again, the earlier filter sets treated by MB show larger zero point errors than does the 1979 filter set. As with the linear extinction law, the J filters show the largest colour dependence and the largest zero point errors.

The colour dependence of the zero point errors from the square-root law is similar to that from the linear extinction law. For the K filter the colour dependence is reduced by a factor of 4 in going to the square-root law. The J and H filter colour dependences are not changed so much; the H filter values are almost unchanged, while the J filter values are reduced by about 30%. The J filter is the only one which has a colour dependence which is large enough to be observed,

at least in principle.

The zero point errors for the single layer models are slightly smaller than the corresponding multiple layer model values. The differences are of the order of 0.002 magnitudes, which is a small change. This change is due, at least in part, to the overall inhomogeneity of the multiple layer model atmosphere. It appears that this factor is not of serious concern, so the square-root law can be applied to the atmosphere in spite of its inhomogeneity.

The errors in the square-root law fit are due in part to deviations of the spectral lines from the square-root law. Lines of intermediate strength will not obey either of the proposed extinction laws. They impose a limit upon how accurately a combination of the square-root law and the linear extinction law can match the extinction curve.

Some trials were made to attempt to obtain a better fit. First, calculations were done to assess how changes in the ν_0 values would alter the results. For each filter, with a response function $\phi(\lambda)$, a weighted mean ν_0 value was calculated via

$$\nu_0^{0.80} = \frac{\int_0^{\infty} \nu^{0.80} \phi(\nu) d\nu}{\int_0^{\infty} \phi(\nu) d\nu} \quad (6.1)$$

and these values were used in place of the values given

above. This produced shifts of only 0.0001 in the zero point errors, which is even smaller than had been expected. The next trial was to try different values of the slope of the linear portion of the extinction. If weak lines are contributing an additional linear component, then the choice of a different slope for the linear part will improve the results. To test this possibility, the linear contribution was adjusted until the square-root law zero point error was 0.00. In some cases, a negative value for the slope was needed. Often these values were lower than the aerosol contribution values given in Table 14. Thus, the idea of reducing the square-root law zero point errors by putting in an additional source of linear extinction turns out to be futile. Increasing the linear extinction component makes the square-root law zero point error increase, so only in those cases where the zero point error is negative will an increase of the linear component reduce this error. Even in these cases, some of the required linear component slopes were too large to make any sense.

The zero point errors from the square-root law were also evaluated for different maximum X values - 1.50, 2.50 and 3.00 - instead of $X = 2.00$ as was used to obtain the Table 15 values. As the maximum X value increases from 1.50 to 3.00, the zero point error changes by a small positive value. Typically changing

the maximum X value from 2.00 to 3.00 caused a change of 0.0025 in the zero point error. This seems strange, because it would seem that the square root law would be more nearly followed at large X, so the error would decrease when values at large X are used. Apparently this is an oversimplification of what actually occurs.

The square-root law assumes that non-overlapping lines caused the absorption. Actually, as the air mass becomes large this assumption breaks down. Also, the term in the square-root law (equation 1.30) is actually a function of air mass. If it were not, eventually I would become negative. Actually γ will be affected by both the line overlap and intermediate strength lines becoming saturated as the column density values increase. Thus, it is not surprising that the square-root law does not fit the theoretical extinction curves exactly.

These results imply that in relative photometry, where only the magnitude difference between an object and a nearby comparison star is of concern, there is little difference between the square-root law and the linear extinction law. The required corrections are of the same order as the colour dependence of the zero point error. Over a small range in X, the extinction curves may be treated as linear without causing a significant error. There might be a problem with a very cool source or an unusual type of object which has

a spectrum very different than that of a blackbody source with a temperature in the 4000 K to 9100 K range, but not for stars on the main sequence or on the giant branch.

Any attempt to apply this square-root law algorithm to real situations would require an accurate measurement of the aerosol extinction so that this could be removed from the data. Most likely this would be done with observations using a set of narrow band filters, chosen to look at spectral regions which are nearly free of absorption from spectral lines. If it is still assumed that an AOV star has zero colour indices as measured above the atmosphere, observations of such a star at 3 or 4 wavelengths would give the aerosol extinction function. Like other extinction quantities, how often this measurement would have to be made depends upon how stable the atmospheric conditions are. Provided that an accurate set of standard star data was available, this measurement could be incorporated into a quick Hardie-style method for measuring the extinction. The necessity of doing this measurement would then be only a slight drawback for astronomers.

If no provision is made for the aerosol extinction and the square-root law is still applied to the data as an extinction correction, the zero point errors change significantly. Table 16 gives the zero point errors

which result from this approach for the multiple layer models. All the zero point errors have changed by a negative value from the Table 15 figures, increasing the zero point errors in some cases and reducing them in other cases. The K filter results are adversely affected, increased to values which are only slightly better than the Δ values from the linear law. The H filter zero point errors are increased, but also are less variable from site to site. The J filter zero point errors are smaller, by a factor of 2 to 4, than the equivalent values in Table 15a. It is remarkable that the square-root law applied directly to J filter data appears to give zero point values accurate to ± 0.015 magnitudes.

SOURCE	FILTER	CALGARY	KITT PEAK	MT. LEMMON	MAUNA KEA
VEGA	J	0.01040	0.00579	0.00247	-0.00601
	H	-0.01390	-0.01335	-0.01225	-0.01204
	K	-0.03734	-0.03020	-0.02497	-0.01821
4000 K	J	0.01479	0.00967	0.00566	-0.00419
	H	-0.01394	-0.01261	-0.00163	-0.01166
	K	-0.03753	-0.03038	-0.02517	-0.01844

TABLE 16 - Square-root law zero point errors, in magnitudes, for the multiple layer models when the aerosol correction is ignored.

The results from Tables 15 and 16 show that in order to apply the square-root law to real data some kind of correction factor must be applied to bring the accuracy to less than 0.01 magnitudes, unless part of the discrepancy is due to a systematic error in the calculation process. The correction factor would be

specific to a given site, and a function of the H₂O column density. Perhaps a plot of zero point error as a function of the slope of the extinction curve from $X = 1.00$ to $X = 2.00$ would be sufficient to give accurate extinction corrections. The advantage would be that these corrections are smaller than the equivalent linear law corrections. The question is whether the advantage of using the square-root law is worth the effort of modifying the procedure. This matter requires more attention before this question can be resolved.

The theoretical models clearly indicate that a change must be made in the data reduction process, but unless some direct observational support is found these model calculations are not sufficient to motivate a change. No doubt there exists a large body of extinction data for the major observatories, but such data is not, as far as the author is aware, available in the general literature. An attempt was made to obtain raw extinction data from Mauna Kea Observatory, which is considered by many to be the best infrared observing site in the world, but unfortunately no data was forthcoming during the present period of work.

In the last 2 years, three attempts were made (by University of Calgary observers) to measure an extinction curve for Vega using telescope facilities in Arizona. The first attempt involved the use of the 1.3

m infrared telescope at Kitt Peak National Observatory by a group headed by Dr. E.F. Milone during July 10-15, 1981. For most of the 5 day period there were thunderstorms in the vicinity, as is usual for Kitt Peak during July through September, so only one night was suitable for the type of observations needed here.

Subsequently, two attempts were made to do extinction observations for Vega. During the period January 28 to February 10, 1983 a group headed by Dr. T.A. Clark was granted time on the 1.3 m infrared telescope at Mount Lemmon Observatory. Over this period observations were only possible on 4 nights of marginal sky conditions. In general snow, fog and low cloud made observations impossible. The data so obtained was not good enough to use to test the calculations. An individual data point might have a small error value, but the point to point scatter was generally large. The magnitude/air mass plots generally showed slopes of about 0.7 magnitudes/air mass, a very large value which was attributed to the formation of a cap cloud above the peak.

The final attempt was made during July 25-30, 1983 using the Kitt Peak telescope once again. As in the run 2 years before, there were thunderstorms each evening. This time, no useful data was obtained because of these storms. The data turned out to be similar to the Mount Lemmon data, with a very steep slope in all the filters. Thus, out of the three

observing runs only one night of reasonable data was obtained. No water vapour column density value was measured for that night.

In Figures 18, 19 and 20 the extinction curve observed for Vega in the J, H and K filters are presented along with the theoretical extinction curves which fit the data best - the 10.1 Pmm calculation. The experimental data shows considerable scatter below 1.50 air masses, while around 2.00 air masses there seems to be more consistent data. For this reason, the theoretical extinction curves were normalized to the data at 2.00 air masses. A line was also drawn to fit the points between 1.50 and 2.00 air masses in each case. For the J and H filters these lines fit all the data fairly well, but for the K filter there is a problem with the data at both low and high air mass values. If the data near 2.00 air masses is deemed suspect and emphasis is given to the high air mass values, a much steeper fit is obtained. The linear fits are extrapolated to zero air mass to illustrate the zero point disagreement between this and the theoretical fit.

The theoretical extinction values have error bars which show the uncertainty of about ± 0.006 magnitudes which was deduced from the comparison with the high resolution calculations. The data values are not given error bars because the point to point scatter is more indicative of the uncertainty in the points than is the

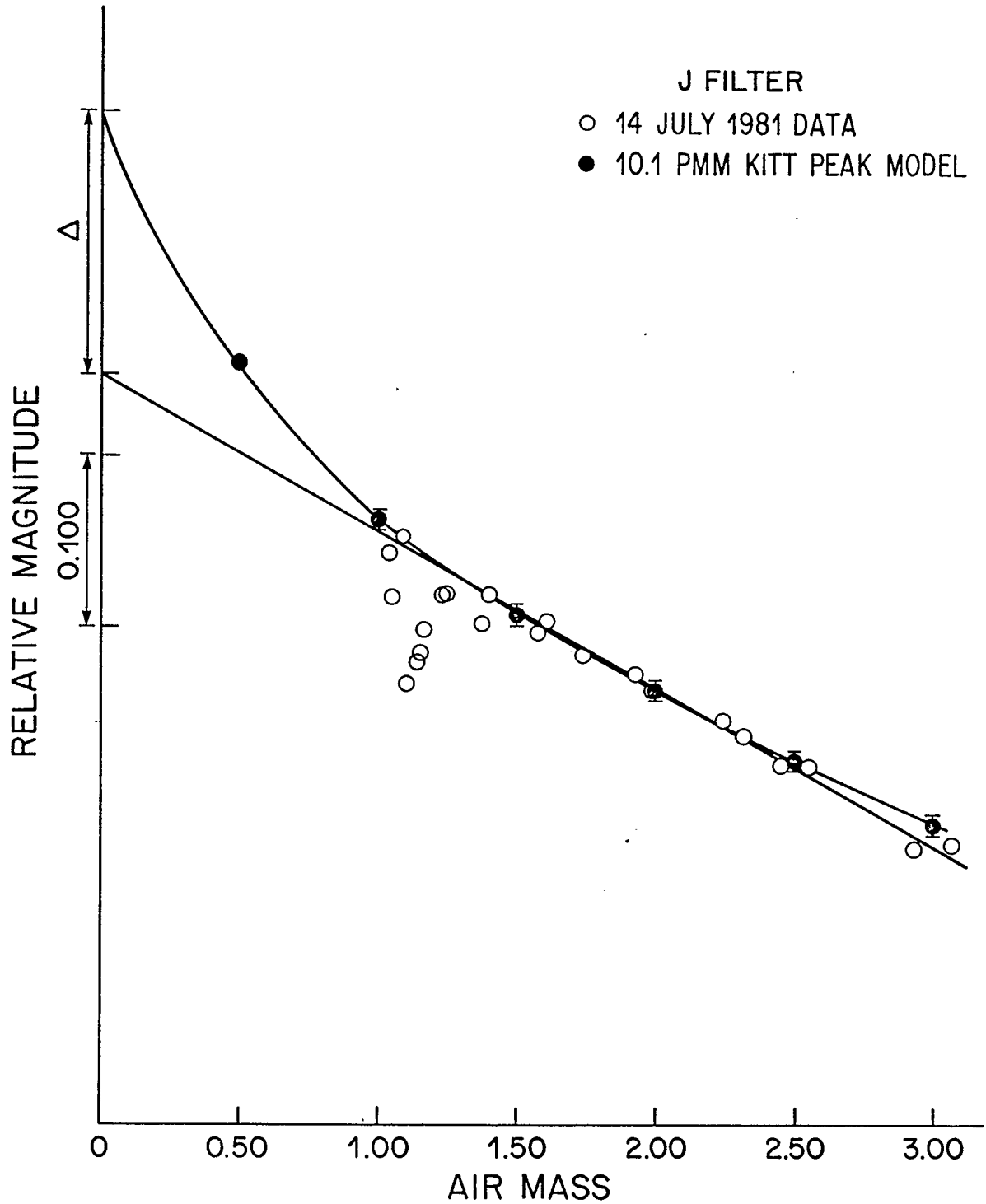


Figure 18- Comparison of the theoretical extinction curve with observational data for the J filter. The theoretical extinction curve was normalized to the data at $X=2.00$. The zero point error Δ predicted by the model calculations is illustrated.

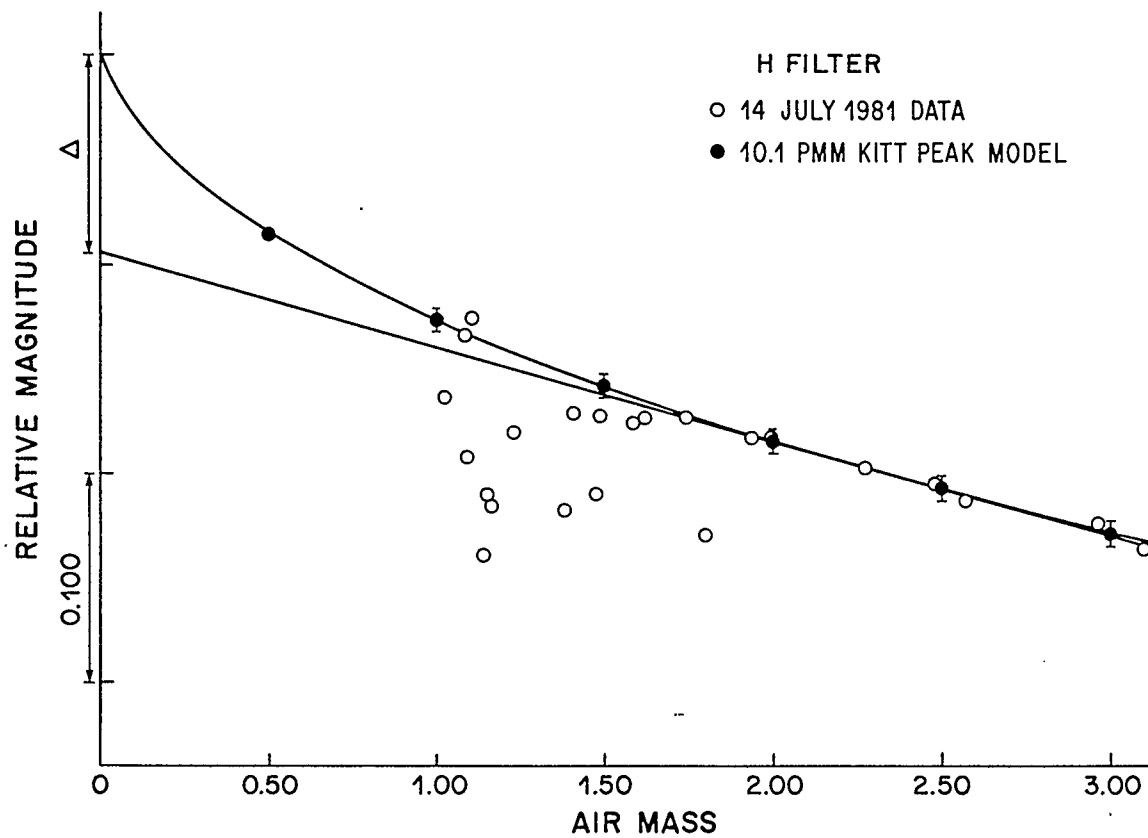


Figure 19- Comparison of the theoretical extinction curve with observational data for the H filter. The approach is as in Figure 18.

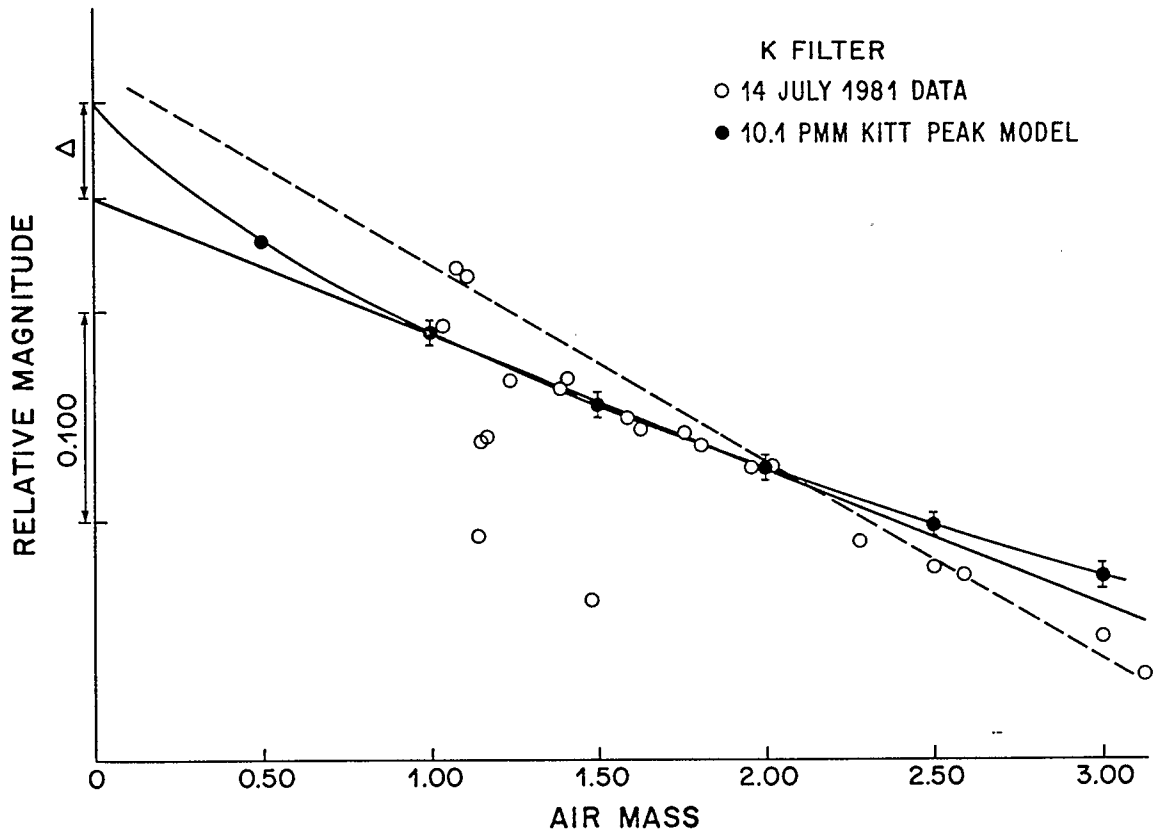


Figure 20- Comparison of the theoretical extinction curve with observational data for the K filter. The approach is as in Figure 18. In this case the linear fit is not clear so two possibilities are shown.

internal error value.

The fit of the theoretical curves to the data is very good for the J and H filters, while the K filter results are somewhat ambiguous. In the case of the J and H filters the data is quite consistent with the theoretical curves. Unfortunately, the scatter of points near 1.00 air masses makes it impossible to decide between the fit of the linear model and that of the theoretical curve. The differences at air mass 0.00 are quite large even though there is no way to tell which of the curves fits the data better.

The K filter results are a problem. The theoretical curve appears to fit well below 2.00 air masses, save for two points near 1.10 air masses, but does not fit the data beyond 2.00 air masses which shows a steeper decline. If the points at 1.10 air mass are trustworthy, either the model fails completely for this filter or anomalous absorption is present for most of the points. However, a linear fit is not all that satisfactory either. The K filter results may indicate a problem with the theory, but the data does not appear to support any stronger statement than that.

It is interesting that the model calculations fit so well, considering the limited number of models available. If the scatter among the points were reduced, observations could be able to detect the curvature in the extinction curves, if any, between

1.00 and 3.00 air masses. Beyond 3.00 air masses the error in the observations becomes large quite rapidly, so extending the observations to higher air masses where the theoretical extinction curves flatten out even more is probably self-defeating. Even for a bright source the air mass would change by a significant amount during an observation when viewed at very high air masses, and more problems are encountered due to atmospheric turbulence and horizontal inhomogeneities.

The alternative to the square-root law is the linear extinction law with a Δ correction. This would require a re-examination of the standard star magnitudes for each site, in order that a Hardie-style method could be used to derive the extinction corrections. It would also require calculations to produce an accurate $\Delta + E$ versus E graph for each site. The curves in Figures 16 and 17 are very nearly linear, which would be very useful if it is true of sites in general. This type of correction process requires accurate input parameters for the calculations and adjustment for any systematic errors is the process of calculation. Under these circumstances it becomes more important to account for the discrepancy between the calculations done here and those of MB.

The differences between IRTRANS and MC, noted in Chapter 4, were considered and found to be small

effects. In some cases the multiple layer model/single layer model comparison confirmed this. In retrospect it was a mistake not to have carried out calculations using the Johnson H and K filters for comparison with the MB results. This would have allowed a better evaluation of the magnitude of this particular source of disagreement. The other contributing factors are the difference in the stellar models which were used, the difference in photometer response functions, the different range of line core integration, the line wing cut-off and the centering of spectral lines in IRTRANS. These are in order of increasing expected effect upon the final results. The comparison of the multiple layer results to the equivalent single layer results showed weak line absorption between the minimum line intensity of MC and that of IRTRANS to be a small effect. This also implies that the line wing cut-off problem is a small effect. In the multiple layer model any line wing cut-off problems will be increased because of the lower layers where the α value is large. There was very little change between the single layer results and the multiple layer results compared to the change between either of these and the MB results. It seems, then, that the difference in filters is the main cause of the discrepancy. The other potential systematic effects appear to be small.

The problem of how all this affects the standard

star magnitudes is not considered by MB. If the value of Δ for each filter were constant, it would simply be absorbed into the detector zero point when these values were set by assigning magnitude values to the primary standard. If the spectrum of this primary standard was known in absolute terms, the flux value derived from the zero air mass magnitude would be slightly less because of the zero point error and the Δ values could be directly measured. When the absolute calibration is done using an assumed stellar spectrum this problem is more difficult to detect because the model is chosen to fit the zero air mass magnitudes rather than the reverse. Under these conditions, changes in Δ would most likely be attributed to changes in the detector response.

Fluctuations in Δ should be observable as changes in the zero air mass magnitude, provided that a comparison source were to be used to provide calibration of the detector. Absolute calibration would not have to be done as long as any relative response variations were removed. The J filter would show this most clearly. The H_2O column density could be monitored by a water vapor meter equivalent to that described by Landau (1982), if observations were made at a single site. It would be better to make observations at two or more sites with altitudes which differ by as large an amount as possible. To avoid

questions of stellar variability, such observations would best be done simultaneously. Kitt Peak and Mount Lemmon offer one possible pair of sites for this type of observation. If a lower altitude observatory is present on Mauna Kea that would be even better.

The standard star magnitudes may be subject to systematic errors because of changes in the Δ values during the initial period of observation which set up the standard system. This is very difficult to evaluate, because it depends upon the observing techniques used as well as the weather conditions. As long as all the magnitudes are always measured relative to the primary standard (Vega in general), either directly or indirectly via secondary standards, the errors should be of the same order as δ for each comparison provided that the observing conditions are good. The Δ fluctuations from one night to another would then produce no direct errors. In effect, this is like defining the magnitude zero point each night. If, however, the photometer output is converted directly to magnitudes on the basis of a set zero point for each filter there will be night-to-night systematic errors in the standard magnitudes. In the early 1960's the accuracy of the photometry may have been low enough that these fluctuations were masked by other factors. This is a matter which needs clarification so that a unified and accurate set of standard magnitudes can be

defined.

A few more comments about the intercomparison of sites is in order here. It is clear from the values in Table 13 that the extinction and the zero point errors are sensitive to the altitude, an effect which becomes much stronger as lower altitudes are considered. This is to be expected, but it is surprising to see how fast this change occurs. The change in extinction is such that for a given air mass Kitt Peak is subject to about 20% more extinction in the J filter than Mount Lemmon, and Calgary experiences about 20% more extinction yet in the J filter. For the H filter the changes are about 25% and 30% respectively, while for the K filter the changes are about 20% and 25% respectively. Although the changes in pressure from Calgary to Mount Lemmon to Mauna Kea are similar, the changes in extinction are very different. This emphasizes the effect of water vapour once again. At Calgary, the J filter is subject to nearly 0.25 magnitudes of extinction at the zenith, which is becoming sufficiently large as to be difficult to handle properly. Most nights there are fluctuations in the atmospheric extinction, which will limit the attainable accuracy of photometry. At present, an accuracy of the order of 0.01 magnitudes is considered good so fluctuations of a few percent will be tolerable. When photometry at the better sites reaches an accuracy of

the order of 0.001 magnitudes, this will no longer be acceptable. Any site which is much lower than Calgary would probably be unsuitable for good infrared photometry.

Much more work must be done before the results can be considered as definitive. Calculations carried out at higher resolution, so that the line core integration is not needed, is one obvious line of refinement. It would also be useful to perform some calculations with a much larger line wing cut-off in order to be sure that there is no significant systematic effect from the truncation of the line wings. Use of more accurate atmospheric data, if this is available, and perhaps a multiple layer model with more layers would also be useful. There is little change from the single layer model to the multiple layer model results, but an expanded multiple layer model would allow a greater range of site altitudes to be modelled. Using the University of Calgary Multics computer system a limit of roughly 20 layers in a multiple layer model would be set by the computer resources needed for the calculation.

The extinction problem could also be approached by carrying out a direct absolute calibration of the JHK filters. It might be possible, for example, to use a balloon to carry a small telescope with JHK filters and a standard calibration source to high altitudes, in

order to measure directly the $m(0)$ values for a series of stars under controlled conditions. Direct observation of the absolute spectrum of Vega at high altitudes using in flight absolute calibration would be even better, provided that the data was accurate to about 0.1%, but would also be much more difficult to do. If a re-definition of the standard star system is ever done, it would be wise to replace Vega as the primary standard because it is a variable star.

It is now clear that infrared extinction is not nearly as simple as it seems at first glance. Infrared photometry, as with many areas of physics, must be carefully standardized in order that the data so taken have meaning. The entire process of producing a standard system of magnitudes must be re-evaluated, if for no other reason than the changes in the filters and detectors which have occurred in the last 20 years. The basic data reduction process should not be an area of near silence in the literature. It seems ironic to see a paper in which great care was taken in the observation of standard and the data reduction procedure so as to reduce the systematic errors, but which does not even mention how the JHKLM extinction was dealt with (for example, Castor and Simon, 1983) and apparently ignores the MB results. It seems almost as if each group of infrared astronomers is left to work by hearsay, to develop their own magnitude system,

each subtly different than the others. Neither this thesis nor MB were able to find a satisfactory data reduction algorithm for infrared photometry. The whole problem of the standard zero air mass magnitudes and the corresponding absolute intensity values must be resolved in some systematic manner. It is to be hoped that in the near future this problem will be addressed and satisfactorily resolved.

List of References

- Allen, C.W., 1963, Astrophysical Quantities [second edition], (London: Athlone Press).
- , 1981, Astrophysical Quantities [third edition reprint], (London: Athlone Press).
- Becklin, E.E. and Neugebauer, G., 1968, *Ap. J.*, 151, 145-161.
- Bell, R.A. and Gustafsson, B., 1979, *Astr. Asph. Supp.*, 34, 229-240.
- Burch, C.B., Gryvnak, D.A., Patty, R.R. and Bartky, C.F., 1969, *J. Opt. Soc. Am.*, 59, 267-280.
- Castor, J.I. and Simon, T., 1983, *Ap. J.*, 265, 304-324.
- Cohen, J.G., Frogel, J.A. and Persson, S.E., 1978, *Ap. J.*, 222, 165-180.
- Dreiling, L.A. and Bell, R.A., 1980, *Ap. J.*, 241, 736-758.
- Fernie, J.D., 1981, *Pub. Astr. Soc. Pac.*, 93, 333-337.
- Gehrz, R.D., Hackwell, J.A. and Jones, T.W., 1974, *Ap. J.*, 191, 675-684.
- Goody, R.M., 1964, Atmospheric Radiation (Oxford: Clarendon).
- Gutierrez-Moreno, A., Moreno, H. and Cortes, G., 1981, *Pub. Astr. Soc. Pac.*, 93, 97-104.
- Hardie, R.H., 1962, Chapter 8 of Astronomical Techniques, W.A. Hiltner (ed.), (Chicago: University of Chicago Press).

- Harris, W.E., Fitzgerald, M.P. and Reed, B.C., 1981, Pub. Astr. Soc. Pac., 93, 507-510.
- Hayes, D.S., 1970, Ap. J. 159, 165-176.
- Hayes, D.S., Latham, D.W. and Hayes, S.H., 1975, Ap. J., 197, 587-592.
- Hayes, D.S. and Latham, D.W., 1975, Ap. J. 197, 593-601.
- Jamieson, J.A., McFee, R.H., Plass, G.N., Grube, R.H. and Richards, R.G., 1963, Infrared Physics and Engineering (New York: McGraw-Hill).
- Johnson, H.L., 1962, Ap. J., 135, 69-77.
- , 1965a, Comm. Lun. Planet. Lab., 3, 67-71.
- , 1965b, Comm. Lun. Planet. Lab., 3, 73-77.
- , 1965c, Ap. J., 141, 923-942.
- Johnson, H.L., Coleman, I., Mitchell, R.I. and Steinmetz, D., 1968, Comm. Lun. Plan. Lab., 7, 83-103.
- Johnson, H.L. and Morgan, W.W., 1953, Ap.J., 117, 313-352.
- Joyce, R.R., 1982, private communication.
- Kleinmann, S.G., Gillett, F.C. and Joyce, R.R., 1981, Ann. Rev. Astr. Asph., 19, 411-456.
- Kyle, T.G., 1968, J. Opt. Soc. Amer., 58, 192-195.
- Landau, R., 1982, Pub. Astr. Soc. Pac.; 94, 600-604.
- Manduca, A. and Bell, R.A., 1979, Pub. Astr. Soc. Pac., 91, 848-854.
- McClatchey, R.A., Fenn, R.W., Selby, J.E., Volz, F.E. and Garing, J.S., 1972, Optical Properties of the Atmosphere, AFCRL 72-0497, Bedford, Mass.

- McClatchey, R.A., Burch, D.E., Rothman, L.S., Benedict, W.F., Calfee, R.F., Garing, J.S., Clough, S.A. and Fox, K., 1973. AFCRL Atmospheric Absorption Line Parameters Compilation, AFCRL-TR-73-0096, Bedford, Mass.
- Oke, J.B. and Schild, R.E., 1970, Ap. J., 6, 1015-1023.
- Pilachowski, C.A., 1978, Ap. J., 224, 412-416.
- Sinton, W.E. and Strong, J., 1960, Ap. J., 131, 470-490.
- Stecker, D.W., Erickson, E.F. and Witteborn, F.C., 1979, Ap. J. Suppl., 41, 501-512.
- Traub, W.A. and Stier, M.T., 1976, Ap. Opt., 15, 364-377.
- U.S. Standard Atmosphere, 1962, NASA, USAF, USWB
(Washington, D.C.: U.S. Government Printing Office).
- _____, 1976, NASA, USAF, USWB
(Washington, D.C.: U.S. Government Printing Office).
- Wing, R.F. and Rinsland, C.P., 1979, A. J., 84, 1235-1243.
- Young, A.T., 1974, Chapter 3 of Methods of Experimental Physics, Vol. 12a, N. Carleton (ed.), (New York: Academic Press).